# Development of methods to determine biologically-weighted UV exposure of humans in different environments

Von der Fakultät für Mathematik und Physik
der Gottfried Wilhelm Leibniz Universität Hannover
zur Erlangung des Grades

Doktor der Naturwissenschaften
Dr. rer. nat.
genehmigte Dissertation
von

Dipl.-Met. Michael Schrempf

geboren am 4. Mai 1983 in Nürtingen

2018

| | |
|---|---|
| Referent: | Prof. Dr. Gunther Seckmeyer (Leibniz Universität Hannover) |
| Korreferent: | Prof. Dr. Günter Groß (Leibniz Universität Hannover) |
| Korreferent: | Prof. Dr. Armin Zittermann (Ruhr-Universität Bochum) |
| Tag der Promotion: | 15. Januar 2018 |

# Kurzfassung

Es wurde ein Expositionsmodell zur Berechnung der solaren ultravioletten (UV)-Exposition eines Menschen weiterentwickelt und eine operationelle Version des Models erstellt. Ein solches Expositionsmodell ist notwendig, um die Auswirkungen der Vitamin-$D_3$-Produktion in der menschlichen Haut einerseits und die schädlichen Auswirkungen der Sonnenstrahlung auf den Menschen wie chronische Hautschäden, Sonnenbrand und Hautkrebs andererseits zu beurteilen. Das Expositionsmodell basiert auf einem dreidimensionalen Voxelmodell eines Menschen und auf der spektrale Strahldichte, welche die Winkelabhängigkeit des Strahlungsfeldes berücksichtigt. Das Modell wurde angepasst um die reflektierte, aufwärtsgerichtete Strahlung und den Einfluss verschiedener Albedowerte des Bodens mit einzubeziehen. Darüber hinaus wurde das Modell erweitert, um die Auswirkungen von Hindernissen (z. B. Vegetation, Gebäude) zu berücksichtigen, die Strahlung aus verschiedenen Richtungen blockieren. Diese Hindernisse wurden aus hemisphärischen Bildern abgeleitet, die von einem mobilen Kamerasystem mit Fischaugenobjektiv aufgenommen wurden. Für die Berechnung der UV-Exposition zu verschiedenen Jahreszeiten kann das menschliche Modell verschieden bekleidet werden, was unter anderem typische Winter- oder typische Sommerkleidung beinhaltet.

Bisher wurden Berechnungen der biologisch gewichteten UV-Exposition eines Menschen basierend auf der globalen Bestrahlungsstärke durchgeführt. Des Weiteren wird der UV-Index, welcher aus der erythemgewichteten Bestrahlungsstärke auf eine horizontale Oberfläche abgeleitet wird, häufig als Indikator für die Exposition verwendet. Die Bestrahlungsstärke berücksichtigt jedoch nicht das komplexe Strahlungsfeld und die Geometrie eines Menschen. Durch die Anwendung des neuen Expositionsmodells konnte gezeigt werden, dass der UV-Index kein guter Indikator für Expositionsbestimmungen ist, da die Exposition sowohl von der Orientierung des Körpers als auch von dessen Haltung abhängt.

Das Expositionsmodell wurde des Weiteren bei Vitamin $D_3$-gewichteten und erythemgewichteten Untersuchungen angewendet. Beispielsweise wurde die menschliche Exposition auf einem schneebedeckten Bergplateau mit der Exposition in einem schneefreien Tal verglichen. Die Untersuchung ergab, dass im Gegensatz zur Bestrahlungsstärke, die um etwa 3 % pro 100 m zunimmt, die Zunahme der erythemgewichteten UV-Exposition mit der Höhe etwa 10 % pro 100 m beträgt. Dies stellt eine mögliche Erklärung für die Zunahme der Melanominzidenz mit der Höhe dar, welche bis zu 30 % pro 100 m beträgt.

Um den Einfluss einer städtischen Umgebung auf die Vitamin-$D_3$-Produktion zu untersuchen, wurde die Vitamin-$D_3$-gewichtete Exposition eines Menschen für mehrere Standorte und entlang zweier Strecken in Hannover, Deutschland berechnet. Das Ergebnis zeigte, dass im Durchschnitt etwa 50 % der Hemisphäre von Hindernissen bedeckt ist und dass im Winter und im Frühjahr (ohne Belaubung) sowohl die Vegetation als auch Gebäude einen vergleichbaren Einfluss auf die Exposition haben, die im Durchschnitt um 40 % reduziert wird. Weiterhin hängt die Vitamin-$D_3$-gewichtete Exposition des Menschen von der Orientierung des menschlichen Körpers zur Sonne ab und variiert beispielsweise vor dem Institut für Meteorologie und Klimatologie um 25 %.

Um die Exposition eines Menschen unter tatsächlichen atmosphärischen Bedingungen zu bestimmen, wurde die spektrale Strahldichte von November 2014 bis April 2015 in hoher zeitlicher Auflösung mit dem neuartigen multidirektionalen Spektroradiometer MUDIS gemessen. Dieses Gerät ist in der Lage, innerhalb von Sekunden Messungen in 113 Richtungen simultan durchzuführen. Aufgrund der Unsicherheiten im Wellenlängenbereich unterhalb von 320 nm wurde eine Methode entwickelt, um die Daten aus dem höheren Wellenlängenbereich in den UVB Wellenlängenbereich zu extrapolieren. Die Methode wurde erfolgreich von einem scannenden Doppelmonochromator Spektroradiometer validiert, das als mobiler Standard für das Network for the Detection of Atmospheric Composition Change zertifiziert ist. Die Ergebnisse bestätigten die in der Literatur beschriebenen Aussagen, dass Menschen mit realistischer Winterkleidung selbst dann nicht im Winter genug Vitamin $D_3$ produzieren können, wenn die Exposition auf den ganzen Tag ausgedehnt werden würde. Zusätzlich zeigen die Messungen, dass der März der erste Monat im Jahr ist, in dem an ein paar Tagen ein ausreichender Vitamin-$D_3$-Status durch Exposition mit Winterkleidung zwischen 12:00 und 13:00 Uhr Ortszeit erreicht werden kann.

**Schlagworte:** Strahldichte, UV-Strahlung, menschliche Exposition, Vitamin D, urbane Umgebungen

# Abstract

An exposure model to calculate solar ultraviolet (UV) exposure of humans was further developed and an operational version was established. Such a model is needed to assess two different effects on humans, the vitamin $D_3$ production in the human skin as well as detrimental effects of solar radiation like chronic skin damage, sunburn and skin cancer. The exposure model is based on a three-dimensional voxel model of a human and the physical quantity spectral radiance that takes into account the angular dependence of the radiation field. The model was adjusted to include upwelling radiation and the effect of different ground albedo values. In addition, the model was extended to consider the effect of obstructions (e.g. vegetation, buildings), which block radiation from various directions. These obstructions have been derived from hemispherical images taken by a mobile camera system equipped with a fisheye lens. For the calculation of the UV exposure in different seasons, the human model can be clothed in various ways, e.g. with typical winter or typical summer clothing.

In the past, calculations of the biologically-weighted UV exposure of a human have been performed based on the global irradiance. Further, the UV index, calculated from erythemally-weighted irradiance falling on a horizontal surface, is often used as an indicator for the exposure. However, the physical quantity irradiance does not take into account the complex radiation field and the geometry of a human. By the application of the new exposure model, it could be shown that the UV index is not a good indicator for exposure determinations because the exposure depends on the orientation of the body as well as on the posture.

The exposure model has further been applied in vitamin $D_3$-weighted and erythemally-weighted investigations. For example, the human exposure on a snow-covered mountain plateau has been compared to the exposure of a snow-free valley. The result showed that in contrast to the irradiance, which increases by about 3 % per 100 m, the increase in erythemally-weighted UV exposure with altitude is about 10 % per 100 m and therefore provides a possible explanation of the increase in melanoma incidence with altitude, which is found to increase by as much as 30 % per 100 m.

To investigate the impact of an urban environment on the vitamin $D_3$ production, the vitamin $D_3$-weighted human exposure was calculated at several locations and along two routes in Hannover, Germany. The result demonstrated that on average about 50 % of the hemisphere is covered by obstructions and that in winter and early spring (without foliage) both, vegetation and buildings, have a comparable impact on the exposure, which is reduced on average by 40 %. Further, the vitamin $D_3$-weighted human exposure depends on the orientation of the human body to the sun and varies for example in front of the Institute of Meteorology and Climatology by 25 %.

In order to determine the exposure of a human under actual atmospheric conditions, rather than using simulated radiation as input in the exposure model, the spectral radiance was measured with high temporal resolution from November 2014 to April 2015 by the novel multidirectional spectroradiometer MUDIS. This instrument is able to simultaneously perform measurements in 113 directions within seconds. Due to the uncertainties for UV wavelengths below 320 nm, a method was developed to extrapolate the data from longer wavelengths into the UVB. The method was successfully validated by a scanning double monochromator spectroradiometer, which is certified as a travelling standard for the Network for the Detection of Atmospheric Composition Change. The results confirmed findings described in the literature that in winter humans with realistic winter clothing cannot produce enough vitamin $D_3$ even if the exposure was extended to all daylight hours. In addition, the measurements indicated that March is the first month in the year with just a few days, where a sufficient vitamin $D_3$ status could be obtained by exposure with winter clothing during 12:00 - 13:00 local time.

**Keywords:** radiance, UV radiation, human exposure, vitamin D, urban environments

# Contents

# List of Figures



# List of Tables

# List of Symbols

## Abbreviations

| | |
|---|---|
| 3D | three-dimensional |
| CCD | Charged Coupled Device |
| DGE | German Nutrition Society |
| DNI | Direct Normal Irradiance |
| DU | Dobson Units |
| HSI | Hemispherical Sky Imager |
| IMuK | Institute of Meteorology and Climatology |
| MUDIS | MUltiDIrectional Spectroradiometer |
| NDACC | Network for the Detection of Atmospheric Composition Changes |
| SCCD | Scanning CCD spectroradiometer |
| IU | International Units |
| UTC | Universal Time Coordinated |
| UV | UltraViolet |
| UVA | UltraViolet radiation between 315 - 380 nm |
| UVB | UltraViolet radiation between 280 - 315 nm |
| UVC | UltraViolet radiation between 100 - 280 nm |

## Greek symbols

| | |
|---|---|
| $\alpha$ | Angle to the normal of an area element d$A$ |
| $\varepsilon$ | Incident angle |
| $\varphi$ | Azimuth angle |
| $\lambda$ | Wavelength |
| $\theta$ | Zenith angle |
| $\Omega$ | Solid angle |

## Latin symbols

| | |
|---|---|
| $A$ | Area |
| $a$ | Albedo |
| $A_{proj}$ | Geometric factor/projection area |
| $E$ | Irradiance |
| $Ex$ | Human exposure |
| $L$ | Radiance |

| | |
|---|---|
| $obs$ | Obstruction parameter |
| $Q$ | Radiant energy |
| $R$ | Radius |
| $S$ | Biological action spectrum |
| $SWE$ | Starting Wavelength of Extension method |
| $t$ | time |

### Indices applied on a variable $\Psi$

| | |
|---|---|
| $\Psi_{\lambda}$ | Spectral component |
| $\Psi_{\text{weighted}}$ | Biologically-weighted component |
| $\Psi_{\text{upwelling}}$ | Upwelling component |
| $\Psi_{\text{downwelling}}$ | Downwelling component |

# 1 Introduction

The solar radiation originating from the sun is in direct and indirect ways an omnipresent part of human lives. The exposure to either the direct beam of the sun, the scattered diffuse radiation from the upper hemisphere or the reflected radiation from the ground is possibly the most obvious direct interaction of a human with solar radiation. The investigation of this interaction and the resulting implications on a human depend on various parameters, for example human behavior, time, environment and radiation field, to name a few. The latter is the result of the interaction of radiation with all constituents of the Earth's atmosphere, in form of scattering and absorption processes. The radiation field can therefore be very complex, with high spatial, temporal and spectral variations. Multiple different physical quantities exist to describe radiation processes and the radiation field. In this thesis mainly the two quantities *radiance* and *irradiance* are used. Almost the entire energy of the solar radiation reaching the Earth's surface is transported by the three wavelength regions ultraviolet (7 %), visible (46 %) and infrared (47 %) (Häckel, 2008). Solar UV radiation reaching human skin can have both positive and negative effects. Two well known effects are for example the occurrence of erythema (also called sunburn) and the production of vitamin D, which plays a particularly important role in human health. To investigate these effects, a novel exposure model was developed within the framework of this thesis. Since the erythemally-weighted or vitamin D-weighted human exposure is only affected by the ultraviolet (UV) wavelength range of the solar spectrum, only the UV part of the solar spectrum will be further discussed in this thesis.

Section 1.1 contains a general overview of the physical quantities used to describe the solar radiation in this thesis. The different biological action spectra are introduced in Section 1.2. The current state of research in the field of vitamin D exposure, as well as of the current exposure models is given in Section 1.3. The scope of this thesis and the underlying research questions are presented in Section 1.4.

## 1.1 Radiation quantities

As mentioned in the previous section, solar radiation originating from the sun interacts with all constituents of the Earth's atmosphere, resulting in a highly complex radiation field at the ground, which varies spatially, temporally and spectrally. To characterize this radiation field, the two quantities *radiance* and *irradiance* are used in this thesis. In Seckmeyer et al. (2010), the spectral radiance $L_\lambda$ is defined as "[...] the radiant energy $\mathrm{d}Q$ per time interval $\mathrm{d}t$, per wavelength interval $\mathrm{d}\lambda$, per area $\mathrm{d}A$, and per solid angle $\mathrm{d}\Omega$ on a receiver orientated normal to the source":

$$L_\lambda = \frac{\mathrm{d}Q}{\mathrm{d}t \cdot \mathrm{d}\lambda \cdot \mathrm{d}A \cdot \mathrm{d}\Omega}, \quad \left[\frac{\mathrm{W}}{\mathrm{m}^2\ \mathrm{nm}\ \mathrm{sr}}\right]. \tag{1.1}$$

For a receiver that is not orientated normal to the source, the area element $\mathrm{d}A$ must be weighted with the cosine of the angle between the direction of the beam and the normal to the area $\mathrm{d}A$ (WMO, 2008; CIE, 2011). This angle is denoted here by $\alpha$ and can also be seen in the schematic diagram in Figure 1.1. The equation is then given as:

$$L_\lambda = \frac{\mathrm{d}Q}{\mathrm{d}t \cdot \mathrm{d}\lambda \cdot \mathrm{d}A \cdot cos\,\alpha \cdot \mathrm{d}\Omega}, \quad \left[\frac{\mathrm{W}}{\mathrm{m}^2\ \mathrm{nm}\ \mathrm{sr}}\right]. \tag{1.2}$$

The radiance can be a source or a receiver based quantity. However, in this thesis the radiance is used as a receiver based quantity only. This can be best visualized by a reversed cone with the given solid angle $\mathrm{d}\Omega$ as its base and the vertex on the area $\mathrm{d}A$. This is shown in a schematic diagram of the radiance in Figure 1.1.

The spectral irradiance $E_\lambda$ is defined as the radiant energy $\mathrm{d}Q$ arriving per time interval $\mathrm{d}t$, per wavelength interval $\mathrm{d}\lambda$ and per area $\mathrm{d}A$ from any origin incident onto a horizontally oriented area element (Seckmeyer et al., 2010) and can be expressed as:

$$E_\lambda = \frac{\mathrm{d}Q}{\mathrm{d}t \cdot \mathrm{d}\lambda \cdot \mathrm{d}A} = \int_{2\pi} L_\lambda \cdot cos\,\alpha \; \mathrm{d}\Omega\,, \quad \left[\frac{\mathrm{W}}{\mathrm{m}^2\ \mathrm{nm}}\right]. \tag{1.3}$$

Equation (1.3) shows that the irradiance can also be derived by integrating the radiance over all solid angles of the upper hemisphere, which is indicated by the integral subscript $2\pi$ (CIE, 2011). It should be noted that for horizontally oriented $\mathrm{d}A$ with an area normal towards the zenith, the angle $\alpha$ represents the zenith angle.

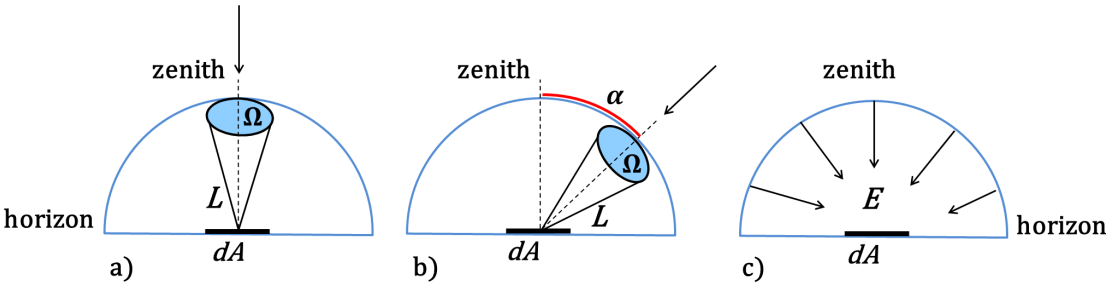


**Figure 1.1:** Schematic diagram of the quantities *radiance* (a) and (b) and *irradiance* (c). In (a) the receiving area $\mathrm{d}A$ is oriented normal to the source, while in (b) the angle $\alpha$ between the normal of the area and the incident beam is 45°. The diagram (c) visualizes the *irradiance*, where radiation of any origin is received by the area element $\mathrm{d}A$.

## 1.2 Biological action spectra

UV radiation can be divided in the three wavelength regions UVA (315 - 380 nm), UVB (280 - 315 nm) and UVC (100 - 280 nm) (Häckel, 2008). UVC radiation is not discussed in this thesis, as it is completely absorbed in the upper atmosphere and therefore, does not reach the ground. In the wavelength region between 380 - 780 nm, the visible part of the solar spectrum is to be found. To investigate the level of biologically-effective UV radiation, the spectral radiance $L_\lambda(\lambda)$ or spectral irradiance $E_\lambda(\lambda)$ are weighted with a biological action spectrum. In this thesis, the action spectra for erythema, defined by the CIE (1998), and for the previtamin $D_3$ synthesis are used. The action spectrum for the previtamin $D_3$ synthesis was derived by MacLaughlin et al. (1982) and ranges until 315 nm. In 2006, based on the data of MacLaughlin et al. (1982), the CIE proposed a standardized action spectrum for the previtamin $D_3$ synthesis in human skin that contains an extrapolation from 315 nm to 330 nm (CIE, 2006). These three action spectra are shown as a function of wavelength in Figure 1.2. Although the term *previtamin $D_3$* expresses correctly the initial photochemical reaction in the human skin, the more general expression *vitamin $D_3$* is used in the following thesis. It should be noted that for vitamin $D_3$ related investigations, only the CIE (2006) action spectrum was used in this thesis.

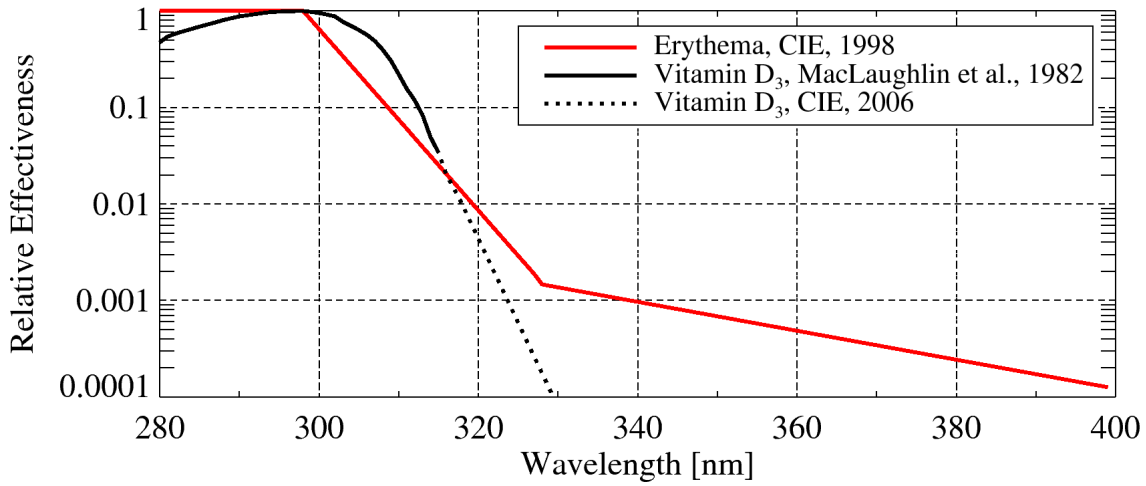


**Figure 1.2:** Biological action spectra for erythema by the CIE (1998) (red line), for previtamin $D_3$ synthesis by MacLaughlin et al. (1982) (black line) and the extrapolated data by the CIE, (2006) (black dotted line).

## 1.3 Current state of research

### 1.3.1 Vitamin D and erythema

Ultraviolet radiation from the sun causes a considerable global disease burden including acute and chronic health effects on the skin, the eyes and the immune system (Seckmeyer et al., 2012). Worldwide up to 60 000 deaths per year are estimated to be caused by ultraviolet radiation, most of which are due to malignant melanoma (Lucas et al., 2008). Other negative effects of an increased UV exposure are for example erythema, sunburn and keratitis (Moukayed and Grant, 2017; Juzeniene et al., 2011). In addition, UV radiation is a fundamental parameter in the genesis of skin cancer (Lucas et al., 2006; Haluza et al., 2014). On the other hand, UV is essential for the vitamin $D_3$ production of humans (Seckmeyer et al., 2012; WHO, 2008). In the following, *vitamin D* is used as a general term, whereas the expression *vitamin* $D_3$ is used to describe UV related issues. There is evidence that suggests vitamin D levels could be seen as an indicator of health risk relating to some sorts of cancer, infectious diseases (e.g. dental caries, pneumonia), autoimmune diseases (e.g. diabetes Mellitus Type 1, multiple sclerosis) among others (WHO, 2008). Vitamin D is essential for regulating the calcium metabolism and is important for various intracellular processes and bone health (WHO, 2008). Further, there are established links with musculoskeletal health, Parkinson's disease and rickets (WHO, 2008; Grant, 2016a). Evidence is abundant that UVB exposure, vitamin D intake, and vitamin D concentrations are inversely correlated with many cancers (e.g. breast, lung, ovarian and colorectal cancer) (Moukayed and Grant, 2013; Grant, 2016b; Moukayed and Grant, 2017). The main source of vitamin D for humans is the vitamin $D_3$ synthesis in the human skin due to solar UVB radiation (280 - 315 nm), although radiation between 280-290 nm is almost completely absorbed by ozone in the atmosphere. Dietary intake contributes only a small percentage (10 %) to the necessary supply (Biesalski et al., 2002). There are large seasonal differences in the production of vitamin $D_3$ (Webb et al., 2010; Wabitsch et al., 2011) which are mainly caused by the varying solar zenith angle and the different amount of skin area that is exposed to solar radiation. Although vitamin $D_3$ can be stored in body fat and can be mobilized during winter months when little, if any, vitamin $D_3$ is produced in the skin (Holick, 2004), more than 50 % of the German population has an insufficient vitamin D supply (Zittermann, 2010). Even in summertime the available UVB

irradiance is much smaller than at comparable latitudes in the southern hemisphere (Seckmeyer et al., 2008). Many investigations have been performed including modeling, calculating and measuring the vitamin $D_3$-weighted exposure according to percentage of exposed skin and their seasonal and latitudinal variation (Zittermann, 2010; Diffey, 2010; Holick, 2007; McKenzie et al., 2009; Rhodes et al., 2010; Webb and Engelsen, 2006; Webb et al., 1988, 2011; Wolpowitz and Gilchrest, 2006a). In this context, several studies refer to the so-called "vitamin D winter" which is the period of time where an adequate vitamin D status can not be gained by solar UV exposure. The vitamin D winter for mid-northern latitudes is often stated to range from October to March (Diffey, 2010; Webb et al., 1988, 2011; Zeeb and Greinert, 2010). Insufficient vitamin D levels can not only occur in winter time because of low UV exposure values, but also due to the environment's obstructions (e.g. vegetation or buildings) and an exposure behavior where an exposure to midday sun is prevented (e.g. indoor working population). The calculation of the vitamin $D_3$-weighted human exposure in an urban environment is necessary in order to estimate if sufficient vitamin $D_3$ could be synthesized and a threshold for an optimal vitamin D status could be reached in everyday situations. This threshold varies from low values (400 IU, international units) to values up to 4000 IU (Wolpowitz and Gilchrest, 2006a). The German Nutrition Society for example suggests 800 IU (DGE, 2012). Although there is not yet an agreed minimum, a consensus opinion could be 1000 IU (Holick, 2007; McKenzie et al., 2009; Bischoff-Ferrari et al., 2006; Chel et al., 1998; Vieth et al., 2007; Wolpowitz and Gilchrest, 2006b), which is equivalent to 25 $\mu$g per day (Zittermann, 2010). The threshold of 1000 IU was also used in this thesis. It should be noted that parts of this section have been adopted from Article A and Article D.

### 1.3.2 Exposure models

Earlier exposure investigations (e.g., by Diffey (2010) and McKenzie et al. (2009)) were based on the irradiance incident on horizontal or vertical surfaces. However, for the calculation of optimal exposure times of human bodies it is insufficient to simplify the body to a flat surface. To better represent the UV dose of a human Godar et al. (2011, 2012) and Pope and Godar (2010) converted the weighted irradiance of a horizontal plane into that of a cylinder by using geometric conversion factors. A better approximation than both approaches is a human body modeled by small tilted surfaces. For example, Oppenrieder et al. (2005) and Höppe et al. (2004) visualized the UV exposure of a human body by combining the measured UV irradiance of inclined surfaces with a virtual human surface model. Their visualization shows a distribution of erythemally-weighted irradiance on the human body. Similar calculations were performed by Vernez et al. (2011, 2012), who calculated erythemally-weighted dose and distribution of UV exposure of a 3D human model using radiative transfer models. However, these theoretical estimations were performed for an unobstructed location only. Kawanishi (2010) used hemispherical images to estimate the shadowing of the sky by sunscreens, though the subject of his study was the protection against erythemally-weighted radiation on a horizontal plane. Parisi et al. (2000) included the shadowing of the sky by trees in their study of the UV exposure. For their investigations they used UV dosimeters on rotating mannequins, which match the statue of an average human. The instruments were distributed over the entire mannequin surface to measure the radiation on as much body surface areas as possible. In a recent study, Parisi et al. (2012) attached dosimeters at the vertex and forehead of a mannequin head and compared measurements conducted under different shade structures and in direct sun. However, instead of the vitamin $D_3$-weighted human exposure, erythemally-weighted doses were investigated in these studies. In addition, one single location may not be representative for an urban environment, because obstructions at different locations differ in shape and size and therefore cover different parts of the sky. As a consequence, the irradiance on a horizontal surface should not be used for exposure

calculations because the angular distribution of the radiation field of the sky would have to be described by a single number only, which does not reflect the complex reality. Instead, the quantity radiance should be used (describing the radiant energy per unit solid angle and per unit area), thus taking into account the complex radiation field. Seckmeyer et al. (2013) developed an exposure model that is based on the radiance in combination with a 3D-voxel model of a human. With this novel method the biologically-weighted human exposure can be calculated by integrating the incident solar spectral radiance over all relevant parts of the human body. Since most surfaces show a very low reflectivity in the UV, the radiance from obstructed directions can be neglected. This also enables the determination of the exposure of a human in an obstructed environment by calculating the multidirectional downwelling radiance originating from unobstructed directions. It should be noted that parts of this section have been adopted from Article A and Article D.

## 1.4 Scope of this thesis

As mentioned in the previous sections, the calculation of human exposure can be highly complex and depends on multiple important parameters (e.g. radiation field, latitude, time, environment, human behavior, skin type). Therefore, the biologically-weighted actual human exposure cannot simply be derived from the UV-Index or global broadband radiation measurements (which detect radiation of the hemisphere on a horizontal surface). Furthermore, the derived exposure of one specific location is in most cases not representative for a larger area, especially if it was calculated for an obstructed environment. The entire complexity of the exposure calculation and the biological implication (e.g. on the production of vitamin $D_3$) is to date not sufficiently understood. This fact builds the motivation for the framework of this thesis, wherein the determination of human exposure was studied for different scenarios starting with the development of novel methods to calculate solar UV exposure.

The novel developed model takes into account the complex radiation field as well as the complex geometry of a human. The latter is achieved by using a three-dimensional voxel model of a human, which was segmented from data of a whole-body computed tomography scan of a patient. The human model can wear various clothing and be orientated in different directions in an upright and a horizontal posture. Before exposure calculations were performed, specific scenarios from different seasons and with different atmospheric conditions have been defined, which were also widely used in literature. With a dataset of different radiation simulations and clothing types, the novel exposure model enables diverse detailed investigations of actual human UV exposure. Besides of the presentation of the novel method, **Article A** focused on three main objectives:

- Comparison of vitamin $D_3$-weighted human exposure (energy per time, received by the human body) and vitamin $D_3$-weighted irradiance (energy per time, received by a horizontal surface).
- Calculation of vitamin $D_3$-weighted human exposure for different scenarios in high temporal resolution.
- Comparison of vitamin $D_3$-weighted human exposure with literature values.

In all previous calculations only radiation form the upper hemisphere was factored. Radiation from the ground was neglected due to the assumed low albedo in Article A. To investigate environments with a higher albedo (e.g snow-cover), the exposure model was extended to include upwelling radiation from the ground, which is described in **Article B**. In this study, the human exposure of two hypothetical locations, a snow-free valley and a snow-covered mountain plateau, in the mountainous region of the Austrian Alps was calculated. The main

objective was to investigate if the high increase of erythemally-weighted UV exposure of a human with altitude could explain the increase of melanoma incidence rates with altitude.

After the inclusion of upwelling radiation in the model, the research proceeded to the next step, namely towards calculating the human exposure in obstructed environments. In order to do so, the exposure model was further developed to take into account obstructions that are covering parts of the sky. Due to the low reflectivity of most surfaces in the UV range, the radiance from obstructed sky regions can then be neglected. Obstructions of real locations are derived from hemispherical sky images, taken by a digital camera equipped with a fisheye lens. This further extended model was used to investigate the human exposure in an urban environment. The investigation was separated into two parts: the impact of obstructions on the human exposure calculation (**Article C**), and the impact of the orientation of a human on the exposure calculation (**Article D**). The research questions answered in **Article C** are:

- To what extent do obstructions of different locations affect the vitamin $D_3$-weighted human exposure?
- Can obstructions of an urban environment, used for the human exposure calculation, be described by one number?

The research objectives of **Article D** were:

- Calculation of the human exposure in an urban environment for different orientations.
- Comparison of derived exposure of a moving human for two different routes.
- Impact of season on the exposure of a moving human for two different routes.
- Calculation of the vitamin $D_3$ doses, accumulated on the two routes to the university cafeteria during lunch break, for different seasons.

In order to analyze these research objectives, hemispherical sky images have been recorded at several locations and along two routes in the area of "Hannover Nordstadt" in winter (without foliage) and summer (with foliage). The derived obstructions of the collected data have then been used in the calculation of the human exposure.

Because measurements of sky radiance are complex and extensive, all investigations presented so far in the Articles A-D are based on simulated radiances. In order to derive the human exposure of actual atmospheric conditions, sky radiance measurements have been performed within a winter measurement campaign from November 2014 to April 2015 at the Institute of Meteorology and Climatology (IMuK). Beside of the campaign description, **Chapter 4** focuses on three main objectives:

- Development of an extension method to enhance radiance measurements by extrapolation from longer wavelengths into the UVB.
- Validation of extension method.
- Vitamin $D_3$-weighted human exposure calculations based on measurements.

The following part of this thesis is structured as follows: Chapter 2 contains a description of the applied exposure model, as well as of the applied formula for the radiance integration. The Chapters 3 and 4 present the research Articles A-D and the results of the measurement campaign. The conclusions and an outlook for further investigations will be given in the Chapters 5 and 6.

# 2 Methods

For the investigation of the biologically-weighted UV exposure of a human, the novel developed exposure model by Seckmeyer et al. (2013) and its embedded new algorithms by Schrempf et al. (2016, 2017a,b) for different environmental scenarios were applied. In Section 2.1, an overview of the simplified exposure model equations and parameters is given. A more detailed description of the exposure model, including a full derivation of the model equations and the model assumptions and limitations, is given in Article A of this thesis. In Section 2.2, the method of the radiance integration is described.

## 2.1 3D-human exposure model

Seckmeyer et al. (2013) (Article A) defined the spectral exposure $Ex_\lambda$ [J] as the spectral radiant energy received by exposed body surfaces of a human who stands on a horizontal plane.

### 2.1.1 Radiation field - sky radiance distribution

$Ex_\lambda$ can be calculated by integrating the spectral radiance

$$L_\lambda(\varepsilon, \varphi, t, \lambda) \;=\; \frac{\mathrm{d}Q}{\mathrm{d}t \cdot \mathrm{d}\lambda \cdot \mathrm{d}A \cdot cos\,\alpha \cdot \mathrm{d}\Omega}, \quad \left[\frac{\mathrm{W}}{\mathrm{m}^2\ \mathrm{nm}\ \mathrm{sr}}\right] \tag{2.1}$$

which depends on the wavelength $\lambda$, the time $t$, the azimuth angle $\varphi$ and the incident angle $\varepsilon$, which is defined as the angle between incident light beam and horizontal plane. In addition, $\mathrm{d}Q$ represents the radiant energy, $\mathrm{d}A$ the area element and $\mathrm{d}\Omega$ the solid angle. The equation of the spectral radiance defined in Equation (1.2) in Section 1.1 is shown here again for the derivation of the exposure model equation. The spectral radiance must be derived either by simulations or measurements. Due to the many dimensions of the radiance (i.e. azmimuth angle, incident angle, time, wavelength), measurements are complex and extensive. Therefore, the radiation field of the upper hemisphere was simulated for most investigations. The simulations were performed by the DISORT code of the UVSPEC model in the libRadtran package (Mayer and Kylling, 2005) with a spatial resolution of 5° in the direction of both azimuth and incident angle. If the reflected radiation from the ground cannot be neglected, due to a high ground albedo, the upwelling radiance $L_{\mathrm{upwelling}}(\lambda)$ is calculated assuming a Lambertian surface and therefore a constant $L_{\mathrm{upwelling}}(\lambda)$. In Schrempf et al. (2016) (Article B) the equation for calculating the upwelling radiance is given as:

$$L_{\mathrm{upwelling}}(\lambda) \;=\; \frac{E_{\mathrm{downwelling}}(\lambda) \cdot a}{\pi}, \quad \left[\frac{\mathrm{W}}{\mathrm{m}^2\ \mathrm{nm}\ \mathrm{sr}}\right] \tag{2.2}$$

where $a$ is the effective albedo of the investigated environment and $E_{\mathrm{downwelling}}(\lambda)$ is the downwelling irradiance, which is defined in Section 1.1 in equation (1.3).

In order to calculate the biologically-weighted human exposure $Ex_{\mathrm{weighted}}$, the spectral radiance $L_\lambda$ is weighted with a biological action spectrum $S(\lambda)$. In Figure 2.1, the simulated radiance weighted with the vitamin $D_3$ action spectrum is shown for Hannover on 21 March at solar noon. The radiance in Figure 2.1 is visualized as a polar plot, where the zenith

is located in the center and the azimuth angles are marked around the plot. It should be noted, that similar to an astronomical map, the directions of east and west are inverted. The

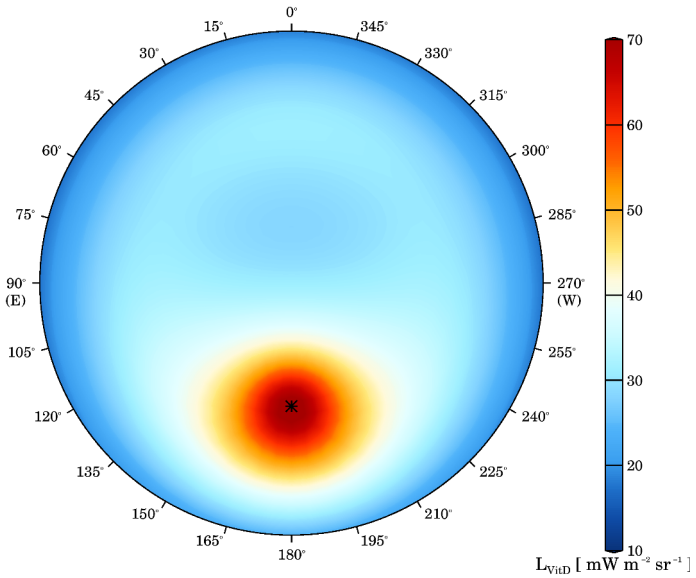


**Figure 2.1:** Distribution of vitamin $D_3$-weighted sky radiance in Hannover on 21 March at solar noon. The position of the sun is marked with a black asterisk. Please note that the high values around the sun are caused by the high diffuse (scattered) radiation.

complete equation of $Ex_{\text{weighted}}$, considering all dependencies, is complex and the calculation can be quite demanding. Therefore, multiple simplifying assumptions have been made, which will not be discussed at this point. However, they are described in detail in Article A and are listed in Section 2.1.5.

In Article A, the simplified equation of $Ex_{\text{weighted}}$ is given as:

$$Ex_{\text{weighted}} = \int_{252\,\text{nm}}^{330\,\text{nm}} \int_{t_1}^{t_2} \left( \int_{\Omega} \int_{A} L_\lambda(\varepsilon, \varphi, t, \lambda) \cdot S(\lambda) \cdot \mathrm{d}A \cdot \cos\alpha \cdot \mathrm{d}\Omega \right) \mathrm{d}t \cdot \mathrm{d}\lambda \,, \tag{2.3}$$

where $\alpha$ is the angle between the incident beam and the normal to the area $\mathrm{d}A$. The solid angle is defined as $\mathrm{d}\Omega = \sin\theta\,\mathrm{d}\theta\mathrm{d}\varphi$, with $\theta$ as the zenith angle.

### 2.1.2 Human geometry - projection area

To further simplify equation (2.3), a geometric factor $A_{proj}(\varepsilon, \varphi)$ is defined as the integral over the projections ($\mathrm{d}A \cdot \cos\alpha$) of all uncovered surface areas $\mathrm{d}A$ of the human. As a result, the biologically-weighted human exposure $Ex_{\text{weighted}}$ is given as:

$$Ex_{\text{weighted}} = \int_{252\,\text{nm}}^{330\,\text{nm}} \int_{t_1}^{t_2} \left( \int_{\Omega} L_\lambda(\varepsilon, \varphi, t, \lambda) \cdot S(\lambda) \cdot \underbrace{\left( \int_{A} \mathrm{d}A \cdot \cos\alpha \right)}_{A_{proj}(\varepsilon,\varphi)} \cdot \mathrm{d}\Omega \right) \mathrm{d}t \cdot \mathrm{d}\lambda \,. \tag{2.4}$$

In the following, the geometric factor $A_{proj}$ will be referred to as projection area. For the calculation of the projection areas a, 3D voxel (volumetric pixel) model, segmented from data of a whole-body computed tomography scan of a patient, is used. The person was 38 years old, 176 cm of height and had a weight of 68.9 kg, thus approximately representing an average male

adult (Valentin, 2002). The projection areas are obtained by a 3D rendering algorithm, which generates a two-dimensional image for a given viewpoint of a three-dimensional scene. From this two-dimensional image the area of the uncovered human skin (considered area elements) can be calculated, which represents the projection area of the corresponding viewpoint. In order to be used in realistic investigations, the human model can wear various types of clothing, which result in different amounts of exposed skin. In Figure 2.2, a two-dimensional projection of the voxel model is shown for three different viewpoints. Additionally, the projection areas of a human with no clothing, summer clothing and winter clothing are visualized as function of the azimuth and zenith angle in form of polar plots.

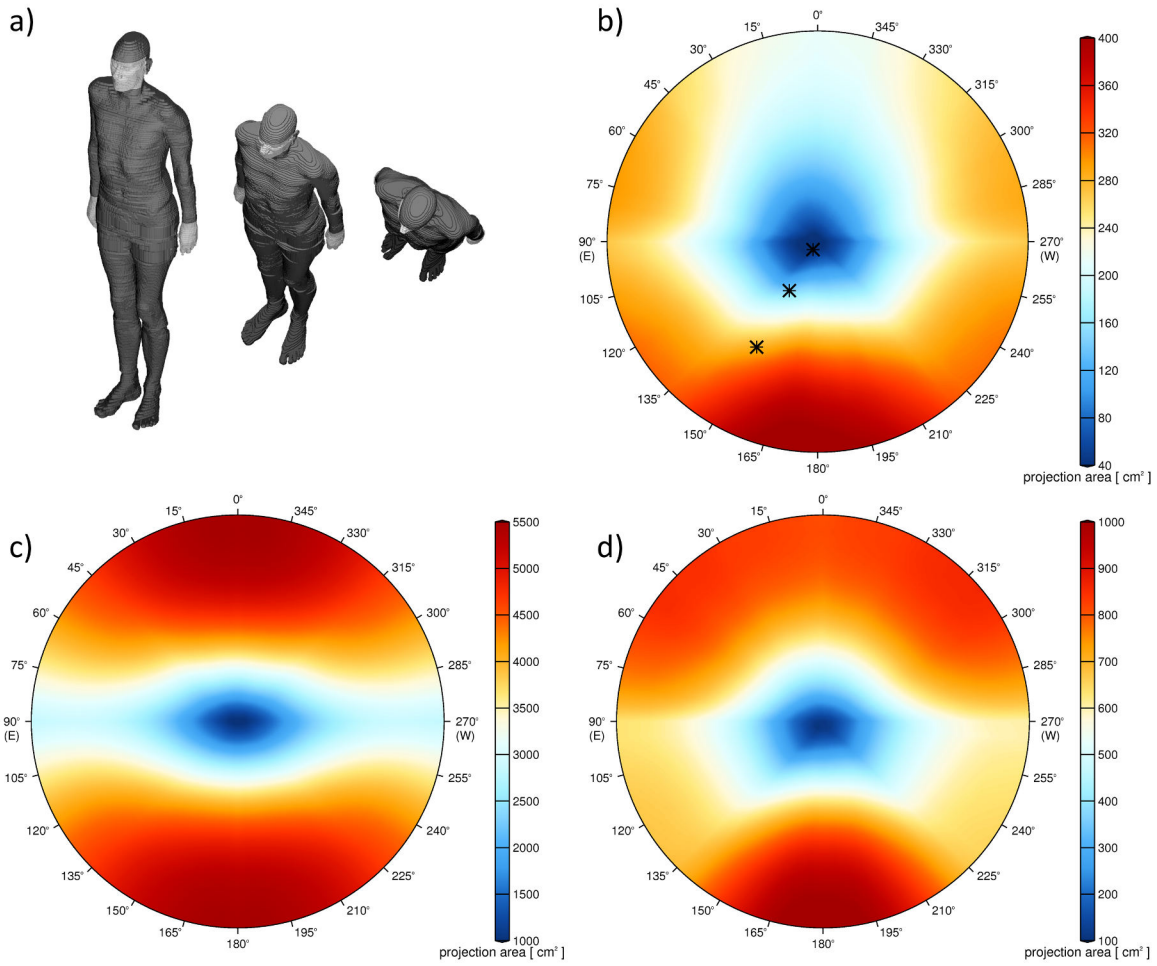


**Figure 2.2:** (a) Projection of the 3D voxel model with winter clothing, visualized for incident angles 30°, 60° and 85°, with the front turned by 30° in azimuth direction. Only hands and face are exposed to UV radiation, which is shown in light gray color and clothing shown in dark gray. (b)-(d) projection areas of the 3D voxel model oriented towards 180°/south, as a function of incident and azimuth angles. The minimal projection area in each plot is located in the middle of each picture, representing a view from the zenith at an incident angle of 90°. (b) Projection area of a human with winter clothing. The three asterisks mark the projections shown in (a). (c) Projection area of a human without any clothing, which results in nearly identical projection areas between the front and back of the human. (d) Projection area of a human with summer clothing, where face, hands, neck and arms are exposed.

### 2.1.3 Exposure calculation in obstructed environments

Equation (2.4) is only valid for calculations in an unobstructed environment, where for example no buildings or vegetation are covering parts of the sky. To calculate the biologically-weighted human exposure in an obstructed environment, the additional parameter obstruction *obs* needs to be included in the equation. $obs(\varepsilon, \varphi)$ depends on the azimuth and incident angle and contains the information to what percentage the sky is visible (unobstructed) for the corresponding solid angle. Due to the low reflectivity of most surfaces in the UV range, it is assumed that the radiance from obstructed sky regions can be neglected. $Ex_{\text{weighted}}$ can then be calculated by:

$$Ex_{\text{weighted}} = \int_{252\,\text{nm}}^{330\,\text{nm}} \int_{t_1}^{t_2} \left( \int_{\Omega} L_\lambda(\varepsilon, \varphi, t, \lambda) \cdot S(\lambda) \cdot A_{proj}(\varepsilon, \varphi) \cdot obs(\varepsilon, \varphi) \cdot \mathrm{d}\Omega \right) \mathrm{d}t \cdot \mathrm{d}\lambda \,. \quad (2.5)$$

The obstruction of the sky is calculated by using hemispherical images taken by a digital camera with a fisheye lens. In previous investigations, the projection function of the fisheye lens was found to be equidistant which provides proper segmentation in equal solid angles (Tohsing et al., 2013, 2014). For the derivation of the obstruction, the mean of the count values of the red, green and blue color of each pixel is compared to a predefined fixed value, which can change depending on the camera settings. Pixels with a mean count value lower than this fixed value are defined as obstructions, the others are identified as unobstructed sky. Obstructions can best be detected in hemispherical images taken under overcast conditions, since the obstructions are relatively dark compared to the sky (Schrempf et al., 2017a,b). Figure 2.3 shows a hemispherical image taken in an urban environment and the derived obstructions from this image.

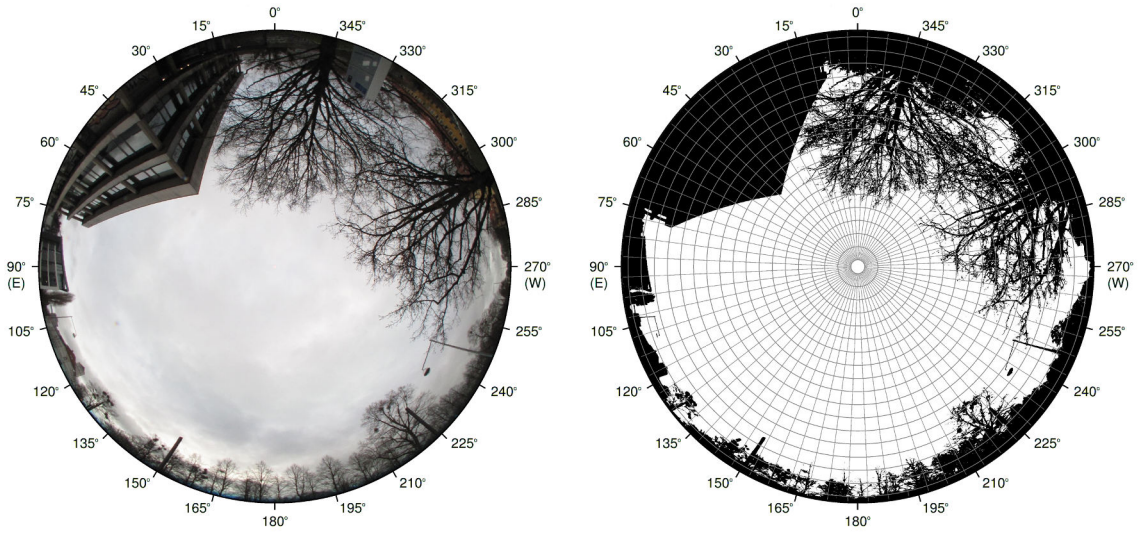


**Figure 2.3:** Hemispherical image taken in front of the Institute of Meteorology and Climatology of the Leibniz Universität Hannover (left) and image with derived obstructions (right), with obstructions covering the sky shown in black and sky in white. The image is segmented by a grid, illustrating the corresponding solid angles.

### 2.1.4 Exposure model summary

The exposure model presented in this chapter calculates the exposure $Ex_{\text{weighted}}$, which is the total biologically-weighted radiant energy received by exposed body surfaces of a human.

When the simplified equation (2.5) is used for the calculation of $Ex_{\text{weighted}}$, five main input parameters are essential:

- the spectral radiance distribution $L_\lambda(\varepsilon, \varphi, t, \lambda)$
- the direct beam of the sun, defined as direct normal irradiance (DNI)
- the biological action spectrum $S(\lambda)$
- the human geometry in form of projection areas $A_{proj}(\varepsilon, \varphi)$
- information of obstructions $obs(\varepsilon, \varphi)$ covering parts of the sky

The calculation can be illustrated by using the polar plots of input parameters presented in Section 2.1.1-2.1.3 and arrange them as an exploded view (see Fig. 2.4). The process of weighting the radiance of each solid angle with the human geometry and the existing obstructions can be easily envisioned by multiplying each value of the top polar plot with the corresponding values below. This is indicated in Figure 2.4 by the red asterisks and the black arrows. To receive $Ex_{\text{weighted}}$, the weighted radiances $L_{\text{weighted}}(\varepsilon, \varphi, t)$ must be

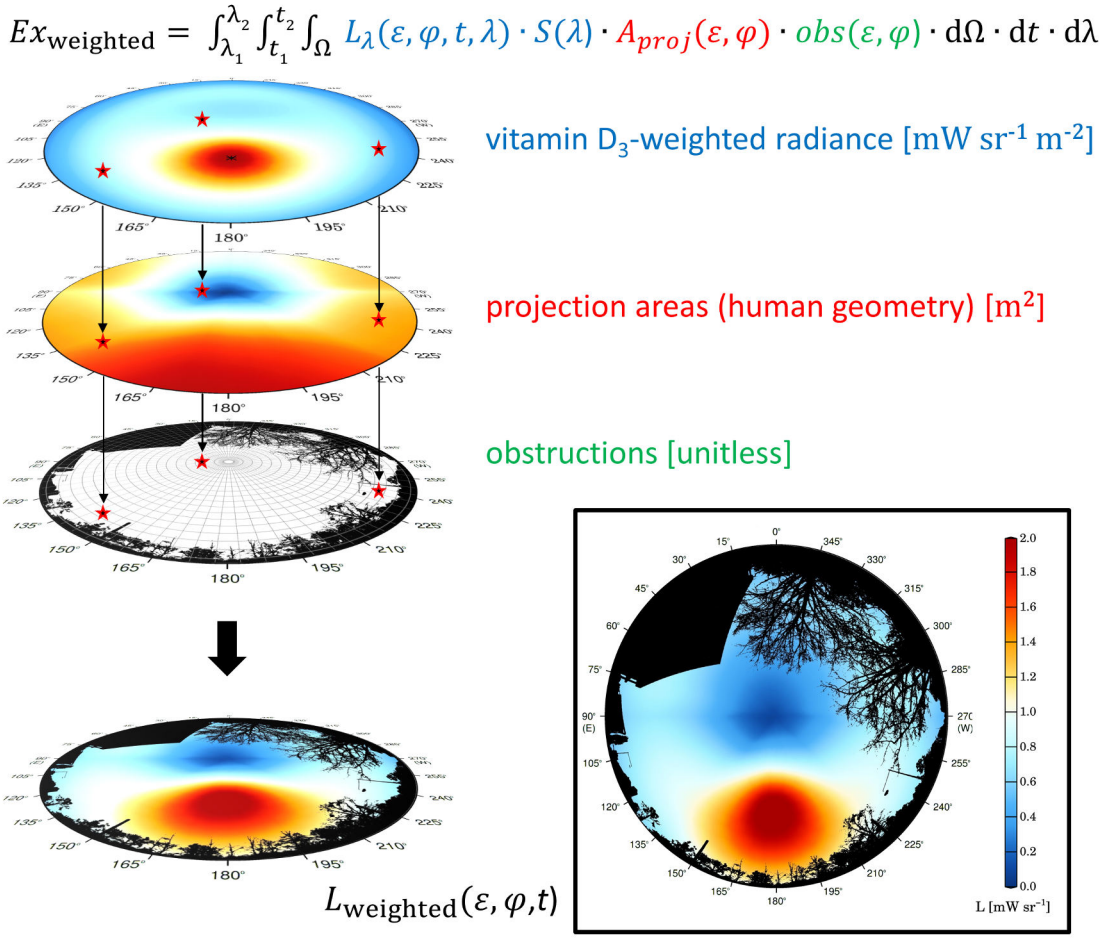


**Figure 2.4:** Visualization of the parameters of the exposure model and the calculation of the human exposure $Ex_{\text{weighted}}$. The red asterisks mark values of exemplary directions and the black arrows indicate the multiplication of these values. The radiances $L_\lambda(\varepsilon, \varphi, t, \lambda)$ weighted with the vitamin $D_3$ action spectrum, the human geometry and the existing obstructions, are shown as function of azimuth and incident angle in the polar plot at the bottom as well as the framed plot labeled with $L_{\text{weighted}}(\varepsilon, \varphi, t)$.

integrated over all directions and the exposure period $t$. The spatial integration is done by summation of the products of $L_{\text{weighted}}(\varepsilon, \varphi, t)$ and $\Omega$. The equations for the calculation of the solid angles $\Omega$ are derived in Section 2.2. At last the biologically-weighted direct normal irradiance multiplied with $A_{proj}(\varepsilon, \varphi)$ of the corresponding sun position is added to $Ex_{\text{weighted}}$. In order to convert the calculated human exposure from Joule into IU, a conversion factor of 70.97 [IU $J^{-1}$] (i.e. IU per Joule of vitamin $D_3$-weighted UV) was defined in Article A.

### 2.1.5 Exposure model assumptions

For the calculation of the biologically-weighted human exposure using the exposure model described in Section 2.1 various assumptions were made. In the following, general assumptions, adopted from Article A-D, are listed. However, it should be noted, that for some specific investigated scenarios additional assumptions were made and stated in the articles, which are not mentioned here.

- The calculated spectral radiance represents the radiation field of the downwelling radiance sufficiently. This may not be the case as the radiative transfer models calculating radiance have not yet been rigorously validated.
- Aerosols have no significant impact on the exposure.
- The exposure from solar radiation of a human in vertical posture experiencing a UV Index of 10 is equivalent to 1000 IU per minute.
- 1000 IU per day are sufficient for a healthy vitamin D status.
- The conversion factor is applicable for all solar zenith angles and ozone values.
- The production of vitamin $D_3$ is proportional to the cosine of the incident angle on all skin areas.
- Different parts of the human skin have the same spectral transmission and the same sensitivity towards the incoming energy.
- The weighting function for vitamin $D_3$ production is correctly described by the CIE weighting function.
- The accumulated vitamin D increases linearly with exposure (a linear dose effect relationship is assumed).
- The investigations in this thesis are done for a skin type II person.
- Aging effects of the human skin do not need to be considered.
- The chosen 3D voxel model represents the human body well.
- In the case of a clothed person, the model wears skintight clothes with no transmission of radiation.
- If not mentioned otherwise, the front-side of the 3D voxel model is oriented to the sun.
- For the Articles A, C, D: The radiation reflected from the ground can be neglected.
- For the Articles A and B: There are no obstructions covering parts of the horizon or the sky.
- For the Articles C and D: The reflectivity of the surface materials of the detected obstructions is low and can be neglected.

## 2.2 Equations for radiance integration

For the calculation of the exposure, the weighted radiances are integrated over all solid angles (see Eq. (2.5)). For this, the area of each solid angle $d\Omega$ on a unit sphere must be calculated. These dimensionless areas have the unit [sr] and can be understood as weighting factors since not all considered solid angles from the different directions have the same size (see also Fig. 2.5). The summation of the radiances, multiplied with the areas of the solid angles of the corresponding directions, yields the final integral. For the calculation of the solid angles the following assumptions are made:

- The hemisphere is divided into segments, which represent the different solid angles (i.e. directions of the radiance data set).
- The radiance data set to be integrated consists of an equidistant array. In this thesis, a spatial resolution of 5° in azimuthal and zenithal direction is used.
- The radiances of the data set originate from the center of each segment (e.g. $\theta = 45°$, $\varphi = 180°$ in Fig. 2.5). An exception of this rule are all segments of the zenith ($\theta = 0° - 2.5°$), the nadir ($\theta = 177.5° - 180°$) and all azimuthal segments next to the horizon, which range from $87.5° - 90°$ for sky segments and $90° - 92.5°$ for ground reflection segments.
- Each radiance value is representative for the entire solid angle (segment).

As a result of this assumptions, three equations with different integration limits must be derived for the zenith and nadir segments, for the segments next to the horizon and for all other segments in between. The schematic diagram in Figure 2.5 shows an exemplary segmented upper hemisphere and the integration limits for the different segments. The different limits are also listed in Table 2.1.

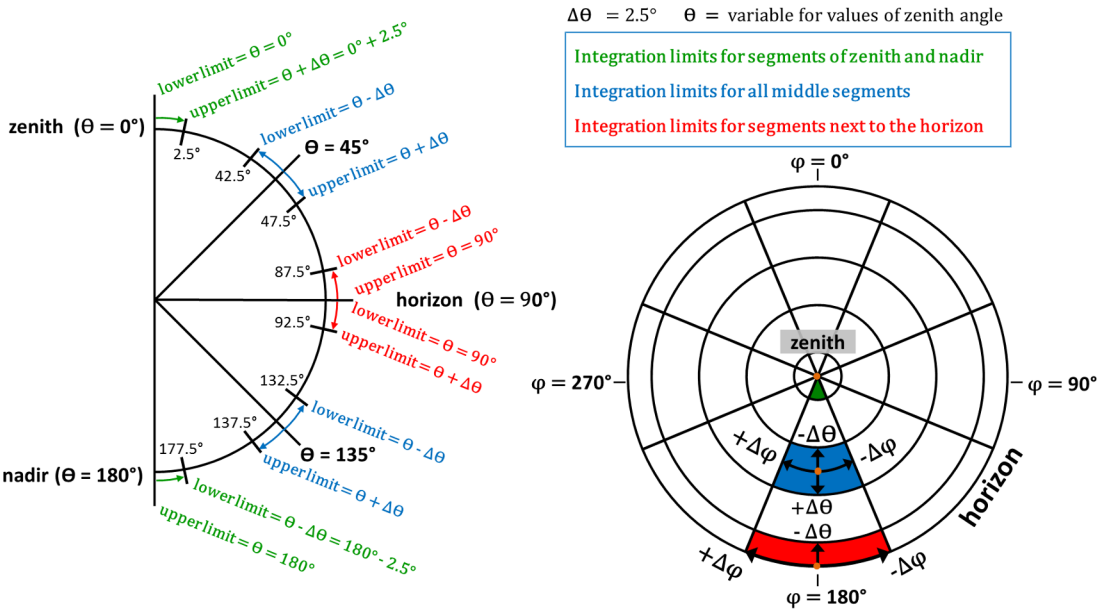


**Figure 2.5:** Schematic diagram of an exemplary segmented upper hemisphere, that visualizes the integration limits for the different segments. The numbers and proportions in the schematic diagram are for demonstration purposes only and do not exactly match the solid angles used in the investigations of this thesis.

The equations used for the computation of the solid angles are based on the equation of an area element $\mathrm{d}A$ on a sphere (Weltner et al., 2008):

$$\mathrm{d}A = R^2 \sin\theta \, \mathrm{d}\theta \mathrm{d}\varphi \; . \tag{2.6}$$

With radius $R = 1$ of a unit sphere the equation is then given by:

$$\mathrm{d}A = \sin\theta \, \mathrm{d}\theta \mathrm{d}\varphi = \mathrm{d}\Omega \; , \tag{2.7}$$

which represents the equation for the area of a solid angle on a sphere (Petty, 2006). The value of the solid angle can then be derived by integrating equation (2.7) over the zenith angle $\theta$ and the azimuth angle $\varphi$. With the lower and upper integration limits of $\theta$ and $\varphi$ the equation can be expressed as:

$$\begin{aligned}
\Omega(\varphi,\theta) &= \int_{\theta_{\text{lower limit}}}^{\theta_{\text{upper limit}}} \int_{\varphi_{\text{lower limit}}}^{\varphi_{\text{upper limit}}} \sin\theta \, \mathrm{d}\theta \mathrm{d}\varphi && (2.8)\\
&= \big[\varphi\big]_{\varphi_{\text{lower limit}}}^{\varphi_{\text{upper limit}}} \cdot \big[-\cos\theta\big]_{\theta_{\text{lower limit}}}^{\theta_{\text{upper limit}}} && (2.9)\\
&= \big[\varphi_{\text{upper limit}} - \varphi_{\text{lower limit}}\big] \cdot \big[-\cos\theta_{\text{upper limit}} + \cos\theta_{\text{lower limit}}\big] && (2.10)
\end{aligned}$$

In Table 2.1 the different integration limits for the zenith and nadir segments, the middle segments and the segments directly above and below the horizon are presented.

**Table 2.1:** List of the different integration limits for the calculation of the area weighting factors, which are used for the integration of radiance data sets in this thesis. Both $\Delta\varphi$ and $\Delta\theta$ have a constant value of 2.5°.

| | lower limit | upper limit | value of $\theta$ or $\varphi$ |
|---|---|---|---|
| limits of $\theta$ for zenith segment | $\theta$ | $\theta + \Delta\theta$ | 0° |
| limits of $\theta$ for nadir segment | $\theta - \Delta\theta$ | $\theta$ | 180° |
| limits of $\theta$ for middle segments (sky) | $\theta - \Delta\theta$ | $\theta + \Delta\theta$ | 5° to 85° |
| limits of $\theta$ for middle segments (ground) | $\theta - \Delta\theta$ | $\theta + \Delta\theta$ | 95° to 175° |
| limits of $\theta$ for horizon segments (sky) | $\theta - \Delta\theta$ | $\theta$ | 90° |
| limits of $\theta$ for horizon segments (ground) | $\theta$ | $\theta + \Delta\theta$ | 90° |
| limits of $\varphi$ for all segments | $\varphi - \Delta\varphi$ | $\varphi + \Delta\varphi$ | 0° to 355° |

These limits are combined with equation (2.10) to derive the final equations used for the calculation of the solid angle $\Omega$. For this purpose, all integration limits are transformed in radiant. This can be done by multiplying the limit given in [°] with $\frac{\pi}{180}$. Because the integration limits of the zenith and the nadir segments lead to the same result, only the equation for the zenith segments is shown (Eq. (2.11) and (2.14)). The same applies for the integration limits of the horizon segments, which also lead to the same result. Here the equation for the segments directly above the horizon is shown (Eq. (2.13) and (2.16)). With equation (2.15) the solid angles for all other segments can be calculated.

$$\begin{aligned}
\Omega_{\text{zenith segments}}(\varphi,\theta) &= \big[(\varphi + \Delta\varphi) - (\varphi - \Delta\varphi)\big] \cdot \big[-\cos(\theta + \Delta\theta) + \cos(\theta)\big] && (2.11)\\
\Omega_{\text{middle segments}}(\varphi,\theta) &= \big[(\varphi + \Delta\varphi) - (\varphi - \Delta\varphi)\big] \cdot \big[-\cos(\theta + \Delta\theta) + \cos(\theta - \Delta\theta)\big] && (2.12)\\
\Omega_{\text{horizon segments}}(\varphi,\theta) &= \big[(\varphi + \Delta\varphi) - (\varphi - \Delta\varphi)\big] \cdot \big[-\cos(\theta) + \cos(\theta - \Delta\theta)\big] && (2.13)
\end{aligned}$$

These equations result in:

$$\Omega_{\text{zenith segments}}(\varphi,\theta) = 2\,\Delta\varphi \cdot \left[1 - \cos\left(\Delta\theta\right)\right] \tag{2.14}$$

$$\Omega_{\text{middle segments}}(\varphi,\theta) = 2\,\Delta\varphi \cdot \left[-\cos\left(\theta + \Delta\theta\right) + \cos\left(\theta - \Delta\theta\right)\right] \tag{2.15}$$

$$\Omega_{\text{horizon segments}}(\varphi,\theta) = 2\,\Delta\varphi \cdot \left[\cos\left(\theta - \Delta\theta\right)\right]. \tag{2.16}$$

When the radiances are multiplied with the corresponding $\Omega$ from equation (2.14) - (2.16), the actinic flux (radiance integrated over all solid angles $\Omega$) can be calculated by summation of these weighted radiances. The same approach applies for the calculation of the human exposure (Eq. (2.17)), which is the sum of the products of $\Omega(\varepsilon,\varphi)$ and the radiance $L_{\text{weighted}}(\varepsilon,\varphi)$, weighted in equation (2.5) with a biological action spectrum, with the human geometry and the existing obstructions. It has to be noted, that the dependence of $L_{\text{weighted}}$ and $Ex_{\text{weighted}}$ from $t$ is not shown in the following equation:

$$Ex_{\text{weighted}} = \int_{\Omega} L_{\text{weighted}}(\varepsilon,\varphi)\ \mathrm{d}\Omega = \sum_{\Omega} \Big( \Omega(\varepsilon,\varphi) \cdot L_{\text{weighted}}(\varepsilon,\varphi) \Big). \tag{2.17}$$

To calculate the irradiance $E$ on a horizontal surface from the radiance data set, the radiance $L(\varepsilon,\varphi)$ of each solid angle $\Omega(\varepsilon,\varphi)$ must additionally be weighted with the cosine of the corresponding zenith angle $\theta$ of the beam, as defined in equation (1.3). The equation to calculate the irradiance can therefore be expressed as:

$$E = \int_{\Omega} L(\varepsilon,\varphi) \cdot \cos\theta\ \mathrm{d}\Omega = \sum_{\Omega} \Big( \Omega(\varepsilon,\varphi) \cdot L(\varepsilon,\varphi) \cdot \cos\theta \Big). \tag{2.18}$$

# 3 Research articles of this cumulative thesis

This chapter contains four peer-reviewed research Articles (A-D), all of which are a result of this PhD project. It should be noted that there might be slight deviations in the notations of variables and parameters among the four articles, as well as between the articles and the introductory words in the Chapters 1 and 2.

**Research Article A** presents a novel method to calculate biologically-weighted UV exposure of humans by integrating the incident solar spectral radiance over all relevant parts of the human body. For the calculation of the exposure, a three-dimensional voxel model of a human was used, which was segmented from data of a whole-body computed tomography scan of a patient. In contrast to earlier investigations, that were based on the irradiance on horizontal surfaces, the quantity *radiance* was used in this investigation, thus taking into account the complex geometry of the radiation field. Two main objectives were pursued in the course of this study: (1) Development of a novel model for the calculation of biologically-weighted UV exposure of humans and (2) calculation of the vitamin $D_3$-weighted exposure of humans for different seasons and atmospheric conditions. The exposure is derived for a human with different clothing in upright and horizontal postures.

In **research Article B** we calculated the human exposure for locations with different ground albedo. For this purpose we extended the exposure model, presented in Article A, to include upwelling radiation reflected from multiple directions of the ground in the calculation of human exposure. We used the extended exposure model in an idealized investigation of two hypothetical locations, a snow-free valley and a snow-covered mountain top, in the mountainous region of the Austrian Alps. In this study, the increase of erythemally-weighted UV exposure of a human with altitude was derived from the calculated exposure values and compared with the increase of irradiance with altitude.

**Research Article C** deals with the exposure calculation in an obstructed environment. For this purpose, new algorithms have been developed to analyze hemispherical sky images, taken by a digital camera with a fisheye lens, and derive obstructions that are covering the sky. A further extension of the exposure model enables the use of derived obstructions as input parameter in the exposure calculation. One objective of this study was to investigate the impact of obstructions on the human exposure calculation. This was done by comparing the exposure of obstructed locations with the exposure of an unobstructed environment.

**Research Article D** is a follow up study to Article C. It investigates the impact of the orientation of a human on the exposure calculation in an urban environment. This is achieved by rotating the three-dimensional model on its upright axis and performing exposure calculations for each direction in two different obstructed environments. Further, the exposure of a walking human along two different obstructed routes to the university cafeteria was calculated for the spring and summer season. For this, the obstructions along the two routes were derived in a high spatial resolution. The results of the accumulated doses were compared to an unobstructed case.

**List of additional publications**

The following list summarizes additional co-authored publications, which have a reference to the thesis. Because the publications are not part of the principal topic, they are not included in this dissertation.

**Tohsing, K., Schrempf, M., Riechelmann, S., Schilke, H., and Seckmeyer, G.**: Measuring high-resolution sky luminance distributions with a CCD camera, Appl. Opt., 52, 1564-1573, 2013.
and
**Tohsing, K., Schrempf, M., Riechelmann, S., and Seckmeyer, G.**: Validation of spectral sky radiance derived from all-sky camera images-a case study, Atmos Meas Tech, 7, 2137-2146, 2014.

A hemispherical sky imager (HSI) system was developed at the Institute of Meteorology and Climatology, which consists of a digital compact camera equipped with an fisheye lens. With this system, images of the complete hemisphere can be acquired, from which different quantities and atmospheric information can be derived. The developed system as well as the derivation of the quantities *luminance* and *radiance* are described in the two above mentioned publications. The HSI system was also used in this thesis and is described in Section 4.1.1.

**Riechelmann, S., Schrempf, M., and Seckmeyer, G.**: Simultaneous measurement of spectral sky radiance by a non-scanning multidirectional spectroradiometer (MUDIS), Meas. Sci. Technol., 24, 125 501, 2013.

This publication was part of the dissertation of Riechelmann (2014) and introduces the novel developed instrument MUDIS. The experience gathered through joint discussions and the assistance in the campaign performed by Stefan Riechelmann for this publication build the basis of the 2014/2015 winter campaign conducted for this PhD project. In this campaign, MUDIS was also used and is described in Section 4.1.1.

**Seckmeyer, G., Mustert, C., Schrempf, M., McKenzie, R. L., Liley, J. B., Kotkamp, M., Bais, A. F., Gillotay, D., Slaper, H., Siani, A. M., Smedley, A. R. D., Webb, A.**: Why is it so hard to gain enough Vitamin D by solar exposure in the European winter?, submitted to Meteorol. Z., in review.

The investigation, described in this manuscript, deals with the difference of UV exposure between the two stations Lauder, New Zealand and Hannover, Germany. This topic was investigated within the Master thesis of Christopher Mustert, which I supervised in most parts. The global irradiance measurements, conducted during the 2014/2015 winter campaign by myself and Christopher, were used in this publication. In addition, a representativity study for this data was performed. It showed that November 2014 is representative for other years, however, the mean irradiance of December 2014 was lower than the average.

## 3.1 Research Article A: A Novel Method to Calculate Solar UV Exposure Relevant to Vitamin D Production in Humans

### 3.1.1 Declaration of my contribution

Gunther Seckmeyer conceived the idea to use the radiance from multiple sky directions in combination with a 3D-voxel model of a human to calculate vitamin $D_3$-weighted exposure. Gunther Seckmeyer and I developed the algorithm of the exposure model. Together with Anna Wieczorek I performed the simulations and analyzed the data. Stefan Riechelmann, Kathrin Graw, Stefan Seckmeyer and Maria Zankl contributed ideas, materials and analysis tools. Based on existing outlines, I wrote a draft of the article and created the visualizations. All authors contributed substantially with comments and revised the manuscript. The quality of the article was further increased by the valuable remarks of the three anonymous reviewers of the article.

### 3.1.2 Published article

This article has been published in Photochemistry and Photobiology. It is printed with kind permission from John Wiley and Sons (license number 4215221030603) as part of this dissertation.
Submitted: 2 August 2012. Accepted: 12 March 2013. Published online: 21 March 2013.

**Seckmeyer, G., Schrempf, M., Wieczorek, A., Riechelmann, S., Graw, K., Seckmeyer, S., and Zankl, M.:** A Novel Method to Calculate Solar UV Exposure Relevant to Vitamin D Production in Humans, *Photochem. Photobiol.*, 89(4), 974-983,
DOI: 10.1111/php.12074., 2013.

Remark: It was noticed that there is a mistake in Equation (1) on page 975. An additional derivative with respect to time is missing. In addition, the unit should be [$W \cdot m^{-2} \cdot sr^{-1} \cdot nm^{-1}$]. Furthermore, there is a mistake in the definition of the solid angle in Equation (4) on page 976, where $\varepsilon$ should be the zenith angle $\theta$. The correct equation of the solid angle is shown in Equation (2.7) in Section 2.2.

Photochemistry and Photobiology, 2013, 89: 974–983

# A Novel Method to Calculate Solar UV Exposure Relevant to Vitamin D Production in Humans

**Gunther Seckmeyer*[1], Michael Schrempf[1], Anna Wieczorek[1], Stefan Riechelmann[1], Kathrin Graw[1], Stefan Seckmeyer[1] and Maria Zankl[2]**

[1]Institute of Meteorology and Climatology, Leibniz University of Hannover, Hannover, Germany
[2]Research Unit Medical Radiation Physics and Diagnostics, Helmholtz Zentrum München, German Research Center for Environmental Health, Munich, Germany

**Received 2 August 2012, accepted 12 March 2013, DOI: 10.1111/php.12074**

## ABSTRACT

**We present a novel method to calculate vitamin $D_3$–weighted exposure by integrating the incident solar spectral radiance over all relevant parts of the human body. Earlier investigations are based on the irradiance on surfaces, whereas our calculated exposure of a voxel model of a human takes into account the complex geometry of the radiation field. Assuming that sufficient vitamin $D_3$ (1000 international units) can be produced within the human body in one minute for a completely uncovered body in vertical posture in summer at midlatitudes (*e.g.* Rome, June 21, noon, UV index of 10), we calculate the exposure times needed in other situations or seasons to gain enough vitamin $D_3$. Our calculations show that the UV index is not a good indicator for the exposure which depends on the orientation of the body (*e.g.* vertical (standing) or horizontal (lying down) posture). Without clothing the exposure is dominated by diffuse sky radiation and it is nearly irrelevant how the body in vertical posture is oriented toward the sun. At the winter solstice (December 21, noon, cloudy) at least in central Europe sufficient vitamin $D_3$ cannot be obtained with realistic clothing, even if the exposure were extended to all daylight hours.**

## INTRODUCTION

Ultraviolet radiation from the sun (1) causes a considerable global disease burden including acute and chronic health effects on the skin, eye and immune system. Worldwide up to 60 000 deaths per year are estimated to be caused by ultraviolet radiation, most of which are due to malignant melanoma (2). On the other hand, UV is essential for the vitamin $D_3$ production of humans. (1,3) In the following vitamin D is used as a general term, whereas we use the expression vitamin $D_3$ to describe UV-related issues. Emerging evidence suggests an association between vitamin D levels as an indicator of health risk (3) relating to some cancers, cardiovascular disease and multiple sclerosis among others, along with the established link with musculoskeletal health. Vitamin D is essential for regulating the calcium metabolism and is important for various intracellular processes and bone health. Prospective observational and cohort studies have shown that the cardiovascular morbidity and mortality risk is around 50% lower with a higher vitamin D supply (4–8). There is also consistent epidemiological evidence that there is an association between a lack of vitamin D and some kinds of cancer (3).

Vitamin D synthesis in the human skin due to solar UVB (280–315 nm) radiation is the main source of vitamin D for humans, whereas dietary intake contributes only a small percentage (10%) to the necessary supply (9), at least according to the present knowledge. Although vitamin D can be effectively produced by UVB radiation, there are large seasonal differences in its production (10,11), mainly caused by the varying solar altitude and the different proportion of skin that is exposed to solar radiation. As a result more than 50% of the German population has an insufficient vitamin D supply, especially during wintertime (12). Even in summertime the available UVB irradiance is much smaller than at comparable latitudes in the southern hemisphere (13).

Many investigations have been performed including modeling, calculating and measuring the vitamin $D_3$–weighted exposure according to percentage of exposed skin and their seasonal and latitudinal variation (12,14–21). Several studies indicated the so-called "vitamin D winter" which is the time when it is not possible to gain an adequate vitamin D status by solar exposure. Often the vitamin D winter for midnorthern latitudes is stated to range from October to March (12,14,19,20,22), whereas other authors suggested that if the commonly assumed action spectrum for vitamin D production is correct, then it should be possible to synthesize vitamin D even in winter (16). However, it would be difficult to gain optimal vitamin $D_3$–weighted UV exposure without a risk of sunburn (16,18). A common "rule of thumb" is that below UV indices (UVI) of 1 to 3 it is impossible to reach an adequate vitamin D status (12,16,18). To ameliorate this problem short exposure times (up to 20 min) are suggested with as most exposed skin as possible (12,16). Some investigations state that the vitamin D status will not be as low as assumed in winter time due to the long lifetime of vitamin D, and the possibility of human body to store vitamin D in body fat (15).

Most of the publications used to date have related the irradiance on surfaces to the UVI and then calculated the time to

*Corresponding author email: seckmeyer@muk.uni-hannover.de (Gunther Seckmeyer)

reach a threshold for an optimal vitamin D. This threshold varies from low values (400 IU, international units) to values up to 4000 IU (21). Although there is not yet an agreed minimum, a consensus opinion could be 1000 IU (15,16,23–26) which is equivalent to 25 $\mu$g (12) per day. The mean daily vitamin D intake by food varies from 1 $\mu$g (40 IU) to 4 $\mu$g (120 IU) in Germany (12).

For the calculation of optimal exposure times of human bodies it is insufficient to assume horizontal or singly tilted surfaces. By a geometric conversion factor Godar and Pope (27–29) estimate the human UV dose by converting the weighted irradiance of a horizontal plane into that of a cylinder. A better approximation is a human body modeled by small elementally titled surfaces. For example, Oppenrieder *et al.* (30) and Höppe *et al.* (31) visualized the UV exposure of a human body by combining the measured UV irradiance of inclined surfaces with a virtual human surface model. Their visualization shows a distribution of erythemally weighted irradiance on the human body. Similar calculations were performed by Vernez *et al.* (32,33) who calculated the dose and distribution of UV exposure of a 3D human model using radiative transfer models. One of the main results of this simulation is that the diffuse part of radiation is quite important for calculations of human exposure and should not be underestimated. They stated that about 80% of annual UV exposure is caused by diffuse radiation and that the direct irradiance is only responsible for UV irradiance peaks around noon, especially in summer and for horizontally oriented parts of the human body. The diffuse irradiance on a horizontal surface, however, does not take into account the complex geometry of the radiation field of the sky for different meteorological conditions. Even if measured UVI values on tilted surfaces are taken into account it is difficult to parameterize the influence by reflections from the ground to sufficient accuracy. Therefore, our goal has been to calculate the vitamin $D_3$–weighted exposure of a human, represented by a 3D voxel model, using estimates of the sky radiance and the direct radiance.

## MATERIALS AND METHODS

The spectral exposure $Ex_\lambda$ [J] may be defined as the spectral radiant energy $Q_\lambda$ [J] falling on a human body which stands on an imaginary horizontal plane.

$Q_\lambda$ can be calculated by integrating the spectral radiance (34)

$$L_\lambda(\varepsilon, \varphi, t, \lambda) = \frac{d^2 Q_\lambda}{d\Omega \cdot dA \cdot \cos\alpha}, \ \frac{W}{m^2 \cdot sr} \tag{1}$$

which depends on the wavelength $\lambda$, the time $t$, the azimuth angle $\varphi$ and the incident angle $\varepsilon$; $dA$ is the infinitesimal area and $\Omega$ is infinitesimal solid angle. We define the incident angle $\varepsilon$ as the angle between incident light beam and the horizontal plane mentioned above (see Fig. 1), also denoted as elevation angle. $\alpha$ is defined as the angle between the normal vector of the area $dA$ and the incident radiation. $Ex_\lambda$ ($\lambda$) may be weighted with a biological action spectrum S($\lambda$,$dA$, $\alpha$, $\varphi$), which may depend on the skin area under consideration as well as on the azimuth angle $\varphi$ and the angle $\alpha$. To assess its biological impact, the exposure is integrated over all relevant wavelengths. In this case, the exposure is no longer a function of wavelength and has the unit Joule (times an arbitrary factor that depends on the normalization of the action spectrum which may be applied).

If different areas of the human body have different biological weightings, $Ex_{\text{weighted}}$ may therefore be calculated by the following formula:

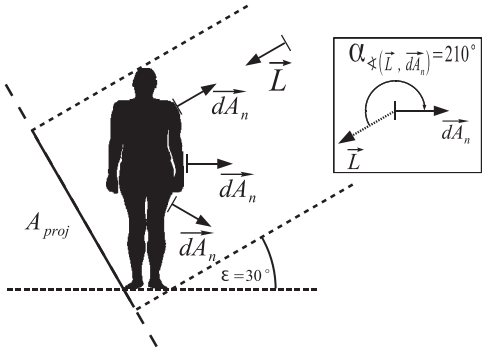


**Figure 1.** Two-dimensional schematic illustration of the relation between the normal vectors $d\vec{A}$ of the surface areas of a human body, the vector of the spectral radiance $\vec{L}_\lambda(\varepsilon, \varphi, \lambda, t)$, the angle between these vectors (framed rectangle) and the projection area $A_{\text{proj}}$ ($\varepsilon$, $\varphi$) for a given solid angle with ($\varepsilon$ = 30°, $\varphi$ = 0°).

$$Ex_{weighted} = \int_{\lambda_1}^{\lambda_2} \int_{t_1}^{t_2} \left( \int_0^{2\pi} \int_{-\pi/2}^{\pi/2} \left( \int_{A(\varepsilon,\varphi)} L_\lambda(\varepsilon, \varphi, t, \lambda) \cdot dA_n \cdot S(\lambda, dA_n, \alpha, \varphi) \cdot \cos(\alpha) \right) \sin(\varepsilon) \cdot d\varepsilon \cdot d\varphi \right) dt \cdot d\lambda, \tag{2}$$

Alternatively, $Ex_{\text{weighted}}$ may be expressed in vector formulation:

$$Ex_{weighted} = \int_{\lambda_1}^{\lambda_2} \int_{t_1}^{t_2} \left( \int_0^{2\pi} \int_{-\pi/2}^{\pi/2} \left( \int_{A(\varepsilon,\varphi)} \vec{L}_\lambda(\varepsilon, \varphi, t, \lambda) \bullet d\vec{A}_n \cdot S(\lambda, dA_n, \alpha, \varphi) \right) \sin(\varepsilon) \cdot d\varepsilon \cdot d\varphi \right) dt \cdot d\lambda, \tag{3}$$

where $t_1$ is the start of the exposure period, $t_2$ the end of the exposure period, $\varepsilon$ the incident angle and $S(\lambda, dA_n, \alpha, \varphi)$ is the weighting function which may depend on wavelength $\lambda$, surface area $dA_n$ (different skin surfaces, noted by the subscript $n$, may have a different sensitivity), incident angle to the surface area normal $\alpha$ and azimuth angle $\varphi$ (1). The deviation of the ideal cosine behavior of lambertian surfaces can be described by the latter three dependencies of $S(\lambda, dA_n, \alpha, \varphi)$. $\vec{L}_\lambda \bullet d\vec{A}_n$ denotes the scalar product between the spectral radiance and the unit area of the human body. To compute the vitamin $D_3$–weighted exposure, the radiance from each sky coordinate is weighted with the action spectrum of a determined biological response to vitamin D and integrated over all relevant wavelengths to assess its biological impact. For the weighting function we use the action spectrum for synthesis of previtamin $D_3$ in human skin of the International Commission on Illumination (35), denoted as $S_{vit\,D}(\lambda)$. The calculation of the exposure by the formula given above can be quite demanding and the following simplifying assumptions have been made: In reality not all radiation is absorbed by the relevant skin layers, but is partly reflected or absorbed by inactive material. The dependence of the incident radiation could be quite complex and may not be well represented by the dependence of a lambertian surface. Therefore, the first assumption is that the areas considered can be treated as a lambertian surface, *i.e.* the energy falling onto any surface under consideration has an angular dependence that follows the cosine of the incident angle. In addition, it is assumed that all areas of the human body have the same sensitivity. In this case the integration over the wavelength can be separated from the calculation of the spectral exposure $Ex_\lambda$.

With the assumptions described above the vitamin D–weighted exposure $Ex_{vitD}$ is then given by

$$Ex_{vitD} = \int_{252\,\mathrm{nm}}^{330\,\mathrm{nm}} \int_{t_1}^{t_2} \left( \int_{\Omega} \int_{A} L_{\lambda}(\varepsilon, \varphi, t, \lambda) \cdot S_{vitD}(\lambda) \cdot dA \cdot \cos\alpha \cdot d\Omega \right) dt \cdot d\lambda, \text{with } d\Omega = \sin\varepsilon \cdot d\varepsilon d\varphi \tag{4}$$

where the radiance is integrated over the relevant areas $dA$ of the human body, integrated over all solid angles $\Omega$ and integrated over the time of exposure. In this context the radiance $L$ and the surface area $dA$ are shown as a result of the scalar product $L_{\lambda}(\varepsilon, \varphi, t, \lambda) \cdot dA \cdot \cos\alpha$. As already mentioned above, $\alpha$ is the angle between the vector $\vec{L}_{\lambda}(\varepsilon, \varphi, \lambda, t)$ and the normal of the surface area $d\vec{A}$ as shown in Fig. 1. In this context relevant areas $dA$ are those where the angle $\alpha$ is $90° \leq \alpha \leq 270°$ and which are not covered by clothing (assuming that clothing has a negligible UV transmission).

Due to the interval [90, 270] of the angle $\alpha$ and the definition of the scalar product, the results of the calculated projections are always negative (see Fig. 1), and absolute values of the projections are used.

As the spectral radiance $L_{\lambda}(\varepsilon, \varphi, \lambda, t)$ is constant for a given time and solid angle, it can be separated from the calculation of the geometric factor $A_{\mathrm{proj}}(\varepsilon, \varphi)$ which is obtained by integrating the projection of all uncovered surface areas $dA$ (see Fig. 1). The vitamin D–weighted exposure $Ex_{vitD}$ is then given by the equation:

$$Ex_{vitD} = \int_{252\,\mathrm{nm}}^{330\,\mathrm{nm}} \int_{t_1}^{t_2} \left( \int_{\Omega} L_{\lambda}(\varepsilon, \varphi, t, \lambda) \cdot S_{vitD}(\lambda) \cdot \underbrace{\left( \int_{A} dA \cdot \cos\alpha \right)}_{A_{proj}(\varepsilon, \varphi)} \cdot d\Omega \right) dt\, d\lambda. \tag{5}$$

In this context, the spectral radiance originates from the sun's direct beam and any scattered components.

The advantage of this formulation is that the determination of geometric factors or projection areas can be accessed independently from the determination of the radiance. To determine these projection areas, a 3D model of a human is required because the amount of radiation that a person receives is assumed to depend only on the exposed skin area.

*3D voxel model:* The 3D voxel (volumetric pixel) model named Golem has been segmented from data of a whole-body computed tomography scan of a patient. The person was 38 years old, 176 cm of height and has a weight of 68.9 kg, thus approximately representing an average male adult (36). Golem consists of approximately 1.9 million voxels with 8 mm height and 2.08 mm × 2.08 mm in-plane resolution. The cuboid voxels are arranged in 256 columns, 256 rows and 220 slices. A total of 121 different organs and tissues have been segmented in this voxel model (37–39).

*Projection area and rendering:* If the radiation falling on a human body originates from one direction only, the exposed skin area of the 3D voxel model would be its projection area from this direction. However, in sunlight the diffuse radiation originates from a wide range of directions, so the projection areas from all directions need to be calculated. This is achieved by a 3D rendering algorithm which generates a two-dimensional image for a given viewpoint of a three-dimensional scene. Rendering methods often use polygons to describe three-dimensional shapes. Therefore, the voxel model is transformed into a polygon model and rendered by a visualization function to generate the two-dimensional projection which represents the projection area. We used the rendering model described in (40). The projection area is minimal when the 3D voxel model is viewed from the zenith (see Fig. 2). If the human body is uncovered and not shaded, the projection areas for an incident angle of 0° and a given azimuth angle will be identical to those from the opposite direction ($\varphi$ + 180°) because the photons will eventually hit the human body from the opposite side. In the case of a clothed person the model wears skintight clothes with no transmission of radiation.

*Relationship between IU and exposure time:* In McKenzie (16), it is stated that "It has been previously estimated […] that a full-body exposure of pale skin under high sun conditions (UVI = 10) produces 1000 IU in less than 1 min." This statement is based on values of Holick (41) and Holick (15).

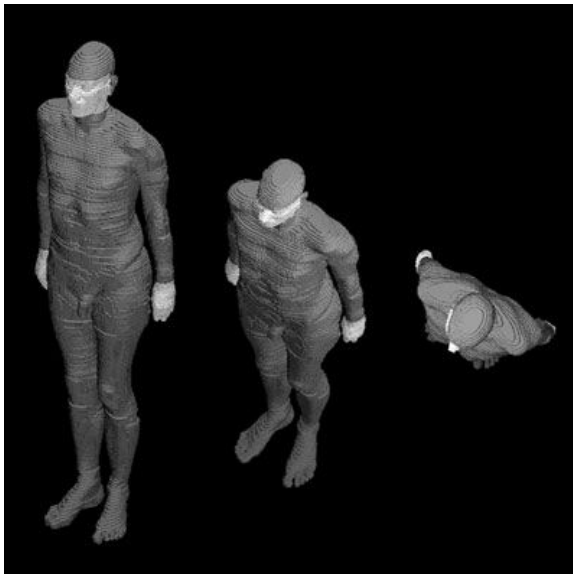

**Figure 2.** 3D voxel model with typical clothing for winter, visualized by the dark gray color. Only hands and face are exposed to UV radiation and shown in white color. The projection of the visualized 3D voxel model is displayed for incident angles 30°, 60° and 90° with the front turned by 30° in azimuth. The projection areas of a person in vertical posture become smaller with an increasing incident angle.

It has been stated in Holick (41) that "Exposure of 6% of the body to 1 minimal erythemal dose is equivalent to taking between 600 and 1,000 IU of vitamin D". One MED equals to 250 $\frac{\mathrm{J}}{\mathrm{m}^2}$ for skin type 2 according to Fitzpatrick (42). A UVI of 10 corresponds to an erythemally weighted irradiance $E_{ery}$ of 250 $\frac{\mathrm{mW}}{\mathrm{m}^2}$ according to the definition of the UVI. The required exposure time for receiving one MED can thus be calculated by:

$$\text{exposuretime}\,[\text{min}] = \frac{\text{MED}}{E_{ery}} \cdot 1/60. \tag{6}$$

The international unit (vitamin D) per minute for a full-body exposure is estimated by the following equation:

$$\frac{\text{IU}}{\text{min}} = \frac{\text{IU}_{\text{literature}}}{\text{exposuretime}} \cdot \frac{100\%}{\text{skin area}\,[\%]} \tag{7}$$

With the literature values from (41) and an exposure time of 16.7 min (see Eq. 7) the statement of McKenzie (16) is confirmed. In Holick (15), it is stated in Table 1 that "Exposure to sunlight (ultraviolet B radiation, 0.5 minimal erythemal dose) equals about 3000 IU of vitamin D3". In the subscripts of this table it is further specified "About 0.5 minimal erythemal dose of ultraviolet B radiation would be absorbed after an average of 5–10 min of exposure (depending on the time of day, season, latitude, and skin sensitivity) of the arms and legs to direct sunlight." Unfortunately, it is not stated whether these numbers are derived by outdoor or indoor experiments, and no details on the spatial distribution of the spectral radiance are provided. Adams et. al. (43) provide more details on the experimental setup and a quite uniform radiance can be assumed. Similar to Holick who applied the values he derived by artificial radiation to outdoor exposure (15), we assume for the following calculations that the estimated value of 1000 IU per minute (Eq. 7) is valid for a human outdoors in vertical posture and an UVI of 10. In any case it appears reasonable that the numbers given above will be in range 10 000–25 000 IU for full-body exposure and 1 MED as stated by Holick (15,41). We therefore believe that current knowledge suggests the maximum

**Table 1.** Parameters for case 5, $R_{eff}$ is the effective radius of the cloud droplet size distributions in $\mu$m, LWC is the liquid water content in g $m^{-3}$ and $z$ is the height of the basis and top of the homogeneous cloudiness in m. Stratocumulus (Sc) ranges from 1300 to 1800 m and Altocumulus (Ac) from 4200 to 4500 m.

| Homogeneous cloudiness of case 5 (Ac & Sc) | | |
|---|---|---|
| $z$ [km] | LWC [g $m^{-3}$] | $R_{eff}$ [$\mu$m] |
| 4.500 | 0.100 | 5.77 |
| 4.200 | 0.100 | 5.77 |
| 1.800 | 0.092 | 4.00 |
| 1.300 | 0.092 | 4.00 |

uncertainty of our assumption (adapted from McKenzie et. al. (16)) to be less than a factor of 2.

## RESULTS

All projection areas are plotted in Fig. 3 as a polar plot in dependence of the azimuth and the elevation angles of incident radiation. The size of the elemental projection areas ranges between 0.09 and 0.55 $m^2$. The upper plots show the model with skin not covered by clothing and the lower plots refer to clothing typical for colder days (see Fig. 2). The calculated percentage of covered skin area to the total skin area is 93%.

### Radiance simulations

Five different cases were chosen (see Table 2), including one for Rome (June 21) and four for Hannover (June 21, March 21 and two simulations for December 21). The summer and winter solstice dates were selected because the sun's noon solar incident angle at solstice is maximal in June and minimal in December. Except for case 5 which was simulated for December 21 in Hannover for homogeneous cloudiness, all cases were simulated for cloudless sky. Rome was selected because simulations have shown that the UVI on June 21 can reach the value 10. A UVI of 10 represents the maximum UVI for northern midlatitudes.

It has been stated that if the UVI is equal to 10, a person can produce 1000 IU vitamin D in one minute, which would result in a sufficient vitamin D status (15,16,41). Some scientists consider even higher values of up to 3000 IU vitamin D concentrations as optimal (R. Scragg, personal communication). In central Europe (*e.g.* Hannover), the UVI is always lower than 10 for cloudless skies.

As mentioned above, the spectral radiance may be determined by measurements or calculated by radiative transfer models. For this study the radiance was calculated by the DISORT code of the UVSPEC model in the LibRadTran package (44). The resolution of the simulated radiance is 5° for both incident and azimuth angles. This resolution results in 1297 different directions and is sufficient for the calculation of the exposure. The different cases and parameters used are listed in Table 2. Common parameters are as follows: radiative solver DISORT, pressure = 1013.0 hPa, ozone dense column = 300 DU and an albedo of 0.02 for Hannover and 0.05 for Rome.

For an albedo of 0.02, which is typical for many surfaces (*e.g.* grass) in the UV (45) in summer, the influence of the reflected spectral upwelling radiance can be neglected. This can be shown by calculating the extra exposure from an isotropic surface reflection, which was found to be smaller than 3% of the exposure from the downwelling radiance for cases 2–5 and 7% for case 1. Compared with the other uncertainties described in the discussion, omitting the reflection from the ground will therefore be a negligible effect, provided the albedo is low. It should be noted that for some artificial surfaces, white sand or snow (46,47), a significant amount of UV exposure originates from the upwelling radiance. For these cases the exposure can be calculated by our method as well if the upwelling radiance is known. However, such cases are not elaborated for this study.

Case 5 represents the great majority of meteorological situations in winter in Germany (48). The radiance for this case has been calculated with the radiative transfer model for homogeneous cloudiness with the parameters given in Table 1. The resulting irradiance on a horizontal surface deviates by less than 15% from measurements of the spectral irradiance performed by the NDACC mobile reference instrument (49) for wavelengths between 310 and 400 nm and for solar zenith angles of 75°±1°.

The vitamin $D_3$–weighted sky radiance for the downwelling radiance has been calculated for summer conditions in Rome (case 1) and is shown in Fig. 4. In this case the highest values of sky radiance can be recognized around the solar disk.

The weighted radiance and the projection surfaces were multiplied for all incident and azimuth angles. The direct beam contributes to the exposure as well. For the calculation of this contribution the projection areas (determined for the sky radiance resolution of 5°) were interpolated to a resolution of 0.1°. A typical result for case 1 and the 3D voxel model in vertical posture is shown in Fig. 5.

The components direct, diffuse and "global" of vitamin $D_3$–weighted exposure per second in Rome on June 21 at solar noon are shown in Fig. 6 as a function of orientation of the 3D voxel model to the sun. Although both the direct and the diffuse component depend on the orientation of the 3D voxel model with respect to the sun, the dominating diffuse component remains relatively constant. Therefore, the maximum variation in the exposure is less than ±4%. This is probably negligible compared with other uncertainties in determining the exposure. However, the variation with orientation of a human in vertical posture must be taken into account in the case of the chosen clothing, which covered 93% of the total skin area. For all following results the front side of the 3D voxel model was orientated with respect to the sun over the day.

Assuming that a human in upright position would be able to produce 1000 IU vitamin D by the exposure as described for case 1 and assuming a linear dose effect relationship, the exposure may also be expressed in IU. For this purpose the conversion factor was determined by setting the calculated vitamin $D_3$–weighted exposure of 1 min for solar noon of case 1 (14.09 J) equivalent to 1000 IU, which results in a conversion factor of 70.97 [IU $J^{-1}$ (*i.e.* IU per Joule of vitamin D–weighted UV)] for case 1 for example. With the assumption that the vitamin $D_3$–weighted irradiance at solar noon corresponds to 1000 IU per minute, the corresponding conversion factor is 33.51 [IU$m^2$ $W^{-1}$]. Diurnal variations are illustrated by showing vitamin $D_3$–weighted power versus time, *e.g.* exposure per minute versus time of day. The resulting seasonal and diurnal variations are so large that it was necessary to use a logarithmic ordinate scale.

Figure 7 shows diurnal variation in the vitamin $D_3$–weighted irradiance and the vitamin $D_3$–weighted exposure for a vertical and horizontal posture for case 1 (Rome, noon, June 21,

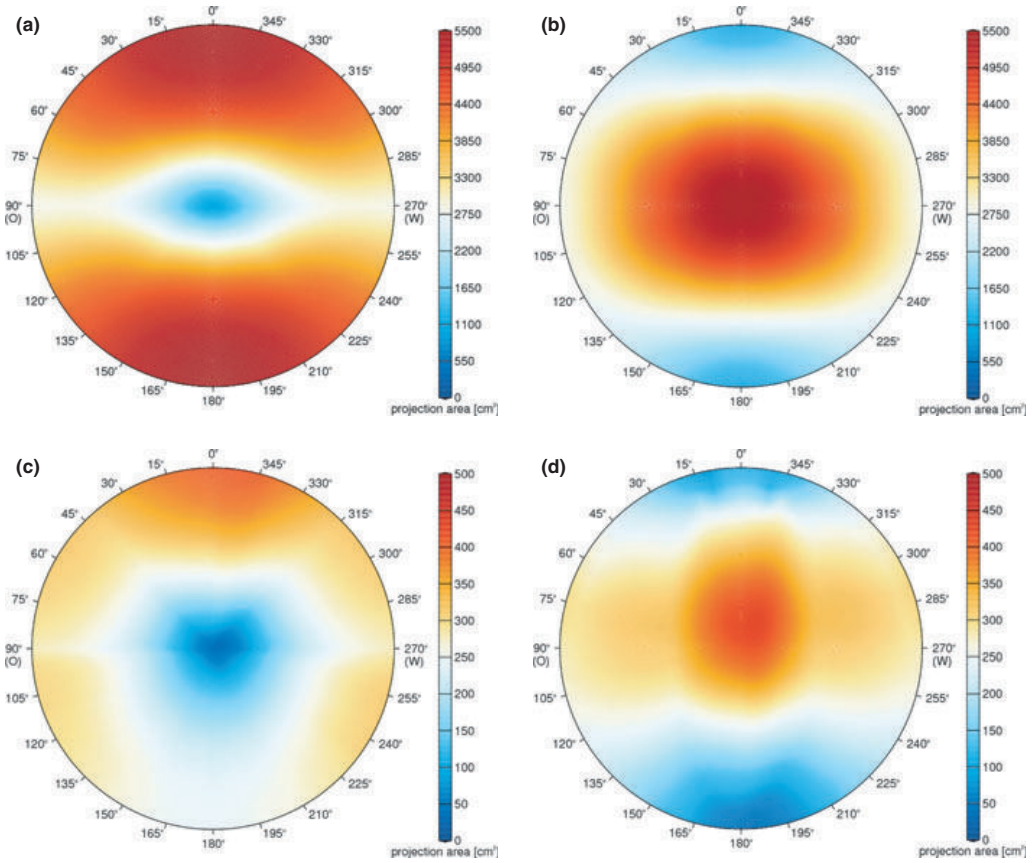


**Figure 3.** 3a (left upper plot): Projection areas of the 3D voxel model in vertical posture, oriented toward 0°/North, as a function of elevation and azimuthal angles. The minimal projection area is located in the middle of this picture, representing the zenith at an elevation angle of 90°. The front and back of this model with a maximum projection area of 0.55 m² can be recognized at azimuth angles of 0° and 180° respectively (elevation angle = 0°), whereas the side projections are smaller (90° and 270°). 3b (right upper plot): Distribution of projection area of the 3D voxel model in horizontal posture (sole of foot is directed to 0°/North). As expected the largest projection area occurs in the middle of the plot, at an elevation angle of 90°. 3c (left lower plot): Projection areas for the 3D voxel model in vertical posture oriented toward 0°/North with only face and hands exposed. As expected the projection areas become much smaller. 3d (right lower plot): Projection areas for the 3D voxel model in horizontal posture (sole of foot is directed to 0°/North) with only face and hands exposed.

**Table 2.** Exposure and estimated times to gain 1000 IU vitamin D for five different cases and exposure areas. For all realistic conditions there is not enough daily vitamin D production at the beginning of winter in central Europe even if the exposure times are extended to all daylight hours.

| | | Case 1 | Case 2 | Case 3 | Case 4 | Case 5 |
|---|---|---|---|---|---|---|
| Place | | Rome | Hannover | Hannover | Hannover | Hannover |
| Latitude | | 41.8833 | 52.3914 | 52.3914 | 52.3914 | 52.3914 |
| Date | | June 21 | June 21 | March 21 | December 21 | December 21 |
| SZA at solar noon | | 18.4385 | 28.9465 | 52.2699 | 75.8086 | 75.8086 |
| Cloudiness | | None | None | None | None | Homogeneous |
| UVI | | 10 | 8 | 3.3 | 0.4 | 0.04 |
| Daily production in IU, human in vertical posture with full-body exposure | | 440000 | 398000 | 134000 | 5400 | 470 |
| Exposure in J per minute at noon, human in vertical posture with full-body exposure | | 14.09 | 12.62 | 6.11 | 0.36 | 0.03 |
| Required Exposure time with full-body exposure | Vertical posture | 1.0 min | 1.1 min | 2.3 min | 39 min | 2.1 days |
| | Horizontal posture | 0.7 min | 0.9 min | 2.4 min | 38 min | 1.9 days |
| Required exposure time with clothing | Vertical posture | 17 min | 18 min | 37 min | 3.0 days | 35 days |
| | Horizontal posture | 10 min | 12 min | 30 min | 2.4 days | 25 days |

cloudless, UVI = 10, unclothed). In this case the horizontal posture will synthesize more IU per minute than the vertical posture at almost all times of the day. At noon the exposure of the human body in horizontal posture is 35% larger than the human body in vertical posture. The increase is not caused by the direct component of the sun. For case 2 (June 21, noon, Hannover,

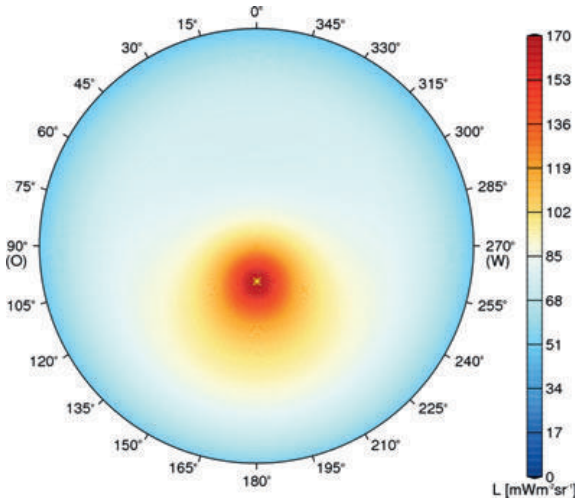


**Figure 4.** Distribution of vitamin $D_3$–weighted sky radiance in Rome on June 21 at solar noon. The position of the sun is marked with a yellow asterisk. Please note that the high values around the sun are caused by the high diffuse (scattered) radiation, which is centered around the sun for this case. The sky radiance is a major input for the calculation of the exposure (Eq. 5) and changes significantly for other solar zenith angles (not shown here).

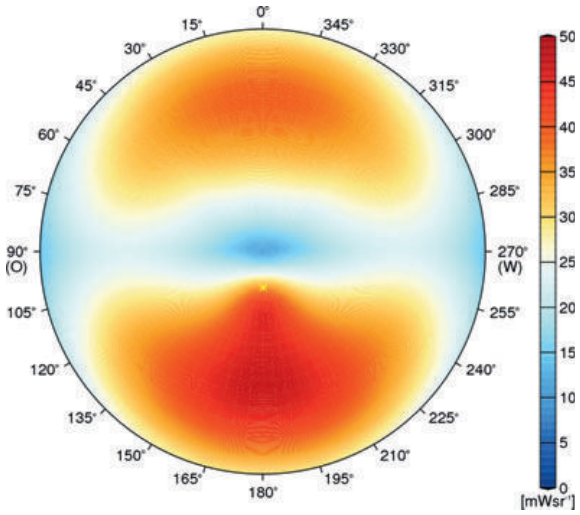


**Figure 5.** Distribution of vitamin $D_3$–weighted radiance multiplied with the projection areas for a cloudless sky in Rome on June 21 at solar noon. The face of the 3D voxel model is oriented south toward the sun (180° azimuth angle).

UVI = 8), the person in horizontal posture has a higher exposure than the person in vertical posture as well. However, in this case the increase is only 19%. The differences between a person in vertical and horizontal posture depend strongly on season even without taking account of seasonal differences in attire: In March a person in horizontal posture receives a lower exposure than a person in vertical posture (case 3), and in December at noon there is no remarkable difference in exposure times between a person in vertical and horizontal posture. The main parameters

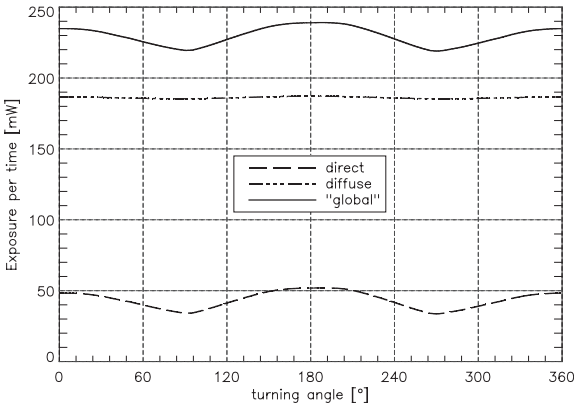


**Figure 6.** Exposure as a function of azimuthal rotation angle of the upright 3D voxel model in vertical posture at solar noon for clear skies. The abscissa shows the rotating angle of the model, the ordinate shows the direct (dashes), diffuse (dashed-dot-dot) and the "global" (line) component of vitamin $D_3$–weighted exposure per second. At the turning angle of 0° the voxel model is facing south (180° azimuth angle). The values for the "global" component vary by less than ±4%.

for the different cases and the resulting exposure times are summarized in Table 2. For short exposure times (*e.g.* 1 min) the times refer to local noon. For longer exposure times, the integral under the graph with its center at solar noon has been calculated with limits chosen so that 1000 IU are reached. If all daylight hours are not sufficient to reach 1000 IU, the number of days required to reach 1000 IU is given. If more than all daylight hours are necessary, it can be concluded that a sufficient vitamin D status can no longer be reached because the requirement has been for 1000 IU on each day. The extreme case occurs for December 21 under cloudy conditions with clothing, when less than 3% of the daily requirement can be synthesized. It is thus impractical to obtain the required UV exposure at the winter solstice (December 21).

Often it is argued that the vitamin $D_3$–weighted exposure can be estimated from the UVI (16,18). However, we found that the UVI is not a good indicator to represent the real exposure. This is demonstrated by the example shown in Fig. 9, which illustrates the ratio of exposure per minute over UVI as a function of UVI for the person in vertical and horizontal posture. For comparison the ratio between vitamin $D_3$–weighted irradiance and UVI is plotted as well, assuming that 1000 IU will result from the vitamin $D_3$–weighted irradiance with an UVI of 10. We consider the variation in exposure with respect to UVI as too large to derive the exposure from the UVI. Even if the body in horizontal posture is scaled to the irradiance on horizontal planes there would be a difference between vertical and horizontal postures.

## DISCUSSION

We have calculated the exposure by integrating the spectral radiance weighted with the projection areas of a 3D voxel model of their human form. The following assumptions were made:

1. The exposure from solar radiation of a human in vertical posture experiencing a UVI of 10 is equivalent to 1000 IU per minute

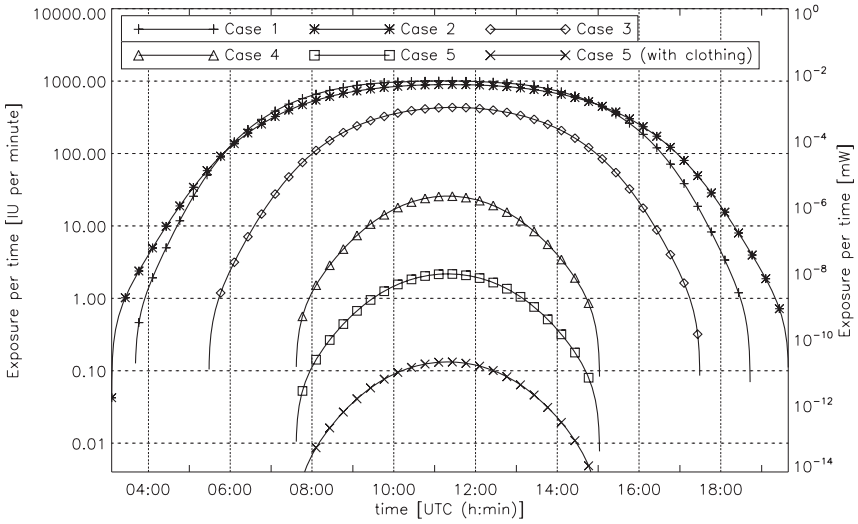


**Figure 7.** Diurnal variation for vitamin $D_3$–weighted exposure for a completely uncovered human body for different cases. At the beginning of winter it is practically impossible to gain enough vitamin D.

2. 1000 IU per day are sufficient for a healthy vitamin D status
3. The radiation reflected from the ground can be neglected (*e.g.* no white sand or snow at the ground)
4. The calculated spectral radiance represents the radiation field of the downwelling radiance sufficiently. This may not be the case as the radiative transfer models calculating radiance have not yet been rigorously validated.
5. Aerosols have no significant impact on the exposure
6. No shading by obstruction of the horizon occurs (*e.g.* no buildings)
7. The production of vitamin D is proportional to the cosine of the incident angle on all skin areas
8. Different parts of the human skin have the same spectral transmission and the same sensitivity toward the incoming energy
9. The weighting function for vitamin D production is correctly described by the CIE weighting function
10. The accumulated vitamin D increases linearly with exposure (a linear dose effect relationship is assumed)
11. The investigation was done for skin type II person. Different pigmentations of the skin do not need to be considered
12. Aging effects of the human skin do not need to be considered
13. The chosen 3D voxel model represents the human body well
14. The front-side 3D voxel model is (except in the calculations of Fig. 6) oriented to the sun

In reality none of these assumptions are probably strictly fulfilled. Therefore, our exposure times should be treated with caution. Some of the assumptions can easily be adjusted if new knowledge is gained. This is particularly true for the statement that a person can synthesize 1000 IU in one minute with an UVI of 10 (15,16,41). The posture of the person has not been specified in these publications. However, it appears reasonable to assume that persons are mostly in vertical posture outdoors. Some scientists consider 1000 IU as not sufficient, but request about 3000 IU per day (R. Scragg, personal communication); in this case, the necessary exposure times would be three times greater. Other assumptions impose greater difficulties, such as a nonlinear dose effect relationship; an example for such a nonlinear effect is that an intoxication of vitamin D cannot be caused by excessive exposure to sunlight because any excess of vitamin D is destroyed within the human body (15,50). Concerning the spectral transmission of human skin Meinhardt-Wollweber and Krebs (51) calculated different sensitivities at different parts of the human body. This is, for example, demonstrated by the optical properties of thick horny layer of thumbs compared with the inner side of the forearm. Especially on colder days the pigmentation of (sun-exposed) skin might lead to an elevated risk of vitamin D deficiency (21) because the needed exposure time could increase by a factor 6 (12). Fig. 8.

Previous studies estimated the exposure to UV radiation by use of the spectral or weighted irradiance on a horizontal surface (12,14–21). However, even if the measured irradiance on tilted surfaces is considered (30,32,33), there is always the difficulty that the effects of reflections from the ground are difficult to parameterize and will influence the measured irradiance of the tilted surfaces. According to Diffey (14) important dependences of vitamin D–weighted exposure are the posture, the orientation with respect to the sun and the influence of nearby shade. Our results confirm the importance of posture, but we found that for a human body in vertical posture the importance of orientation toward the sun depends on clothing, whereas for an unclothed person it is nearly irrelevant. Although we did not consider any shading obstructions, we agree on the importance of this factor for the calculation of a realistic exposure. There is also concern about the correctness of the CIE weighting function for previtamin $D_3$ production (52). As our investigations consider spectral radiance, rather than weighted irradiance (*e.g.* with erythema), the calculations can easily be repeated for other vitamin D action spectra.

In the following we compare the exposure times needed to gain an adequate vitamin D status with some results found in literature. Compared with the exposure calculated on the basis of vitamin D–weighted horizontal irradiance (see asterisks in Fig. 9), we find an exposure that is about 40% higher for an UVI of 2, both for the human body in vertical and horizontal posture. As the analysis of McKenzie *et al.* (16) is based on

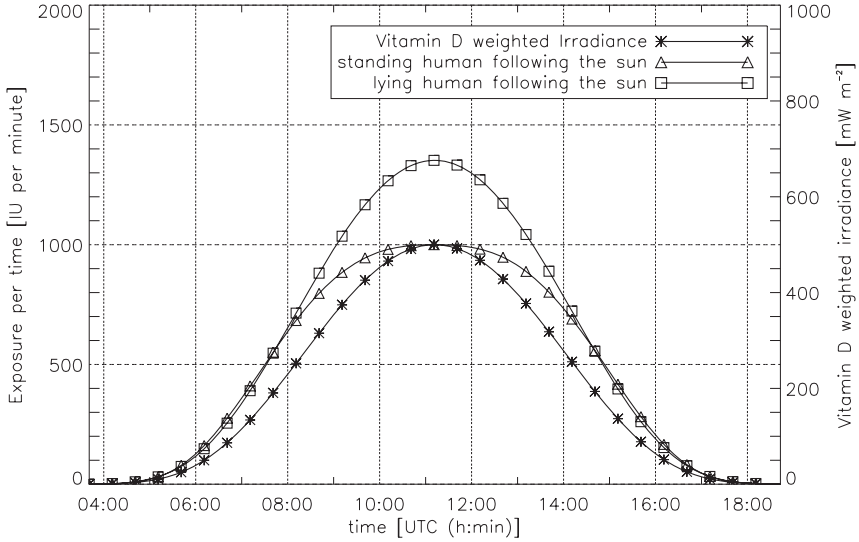


**Figure 8.** Diurnal variation in exposure (left ordinate), for different postures, compared with vitamin $D_3$–weighted irradiance (right ordinate) for Rome with cloudless sky on June 21. Under these conditions the vertical posture has a lower exposure than the horizontal posture.

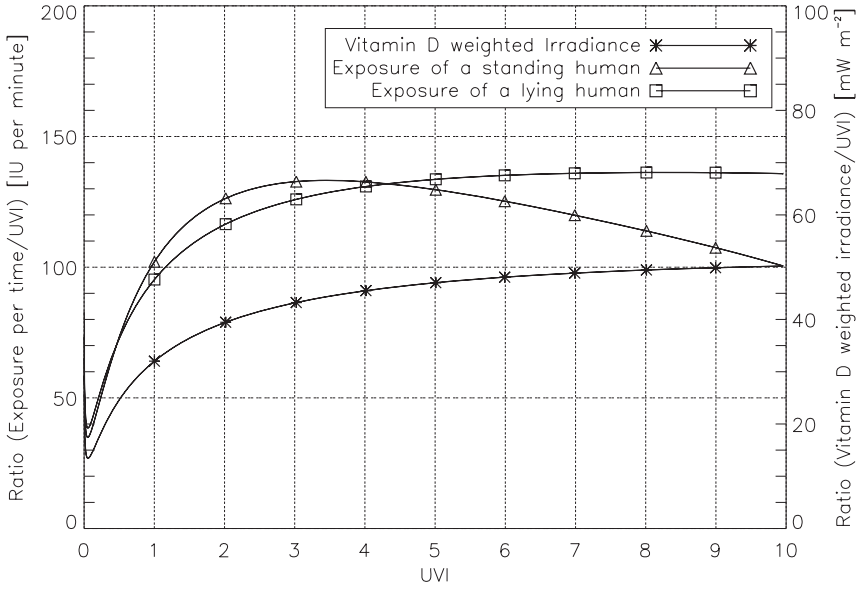


**Figure 9.** Ratio of exposure per time interval and UVI (left ordinate) and ratio of vitamin $D_3$–weighted irradiance and UVI (right ordinate) for midsummer conditions in Rome (case 1). It can be concluded that the UVI is not a good indicator for the vitamin $D_3$–weighted exposure of a human.

irradiance on horizontal surfaces, we conclude that the real exposure will be underestimated in cases of low UVI when only irradiance is taken into account. This result is in accordance with the results of Höppe *et al.* (31) that assessed an underestimation of the UV exposure for horizontal planes. McKenzie *et al.* (16) stated a ratio of vitamin D–weighted irradiance between winter and summer of approximately 5% at 45°S. Our results (for 50°N) indicate a ratio of 1% between winter and summer for a person in horizontal posture. It should be noted that this ratio corresponds to a low UVI, which is quite typical for the European midwinter. Our results cannot confirm statements that the "vitamin D winter" lasts from October to March (12,14,19,20,22). Instead the exposure times required at the end of winter (March 21) are only about half an hour for cloudless skies, even if just face and hands are exposed.

Webb *et al.* (19) estimated the time to gain an adequate vitamin D status during midsummer sunlight for a person in vertical posture, with 35% skin exposed, to be 22 min and for a person in horizontal posture to be 13 min at 53.5°N on a cloudless day. With 13 min exposure time for the same location on June 21, Rhodes *et al.* (17) obtained similar results, assuming a 35% skin exposure. In contrast we calculated

exposure times of about 4 min for a person in vertical posture and about 3 min for a person in horizontal posture with minor differences in skin area (32%) and latitude of 52.4°N. We conclude that at least in summer there are significant differences in the estimated exposure times. It must be emphasized, however, that the method to determine the exposure times is quite different from our approach. In addition, Webb *et al.* (19) assume 2000 IU $\pm$ 600 IU to be sufficient for an adequate vitamin D status, whereas we assume 1000 IU to be sufficient in accordance with Holick (15,41) and McKenzie *et al.* (16). Summarizing the exposure times calculated by McKenzie *et al.* (16) are found to be in better agreement with our calculations than the results of Rhodes *et al.* (17). Nevertheless, there remains a remarkable difference in the estimated exposure times required to obtain a sufficient Vitamin D level.

## CONCLUSION

Our new method to estimate the UV exposure for humans enables, in principle, to calculate the necessary exposure times to gain a healthy vitamin D status for various conditions taking into account the complex geometry of both the human body and the sky radiance. Although it is easy in summer under cloudless skies to obtain a sufficient exposure, the situation is quite different in winter. If the assumptions of the model are correct, the results show that in December in central Europe it is theoretically possible to gain enough UV radiation to produce 1000 IU under clear sky conditions in approximately one hour. This specific situation requires, however, that the whole human body would be fully exposed, which is extremely unlikely or at least inconvenient during winter time. However, for realistic winter time skin exposures it is not possible to get enough exposure for vitamin D production at the beginning of the winter. Under cloudy conditions on December 21 in Hannover even exposing the whole body for the whole day, it would not be possible to gain enough vitamin D. If only hands and face are exposed, the situation becomes even worse. Less than 3% of the daily dose required can be attained. Under these circumstances a person would have to wait more than 35 days before the sufficient daily exposure would be reached – in other words, the winter would have nearly passed by before a sufficient vitamin D status could be reached. These calculations confirm the earlier findings that it is not possible to gain enough vitamin D in winter (20) and the statement in the analysis from McKenzie *et al.* (16) that sufficient vitamin D may be gained in winter are not realistic for the European winter. In this context the role of gaining vitamin D requirements from diet should be reconsidered because the earlier findings that only 10% of vitamin D is gained by food are probably not correct in winter. The mean daily vitamin D intake of German adults ranges between 40 and 120 IU (12). These amounts are not available from solar exposure for a clothed human on a cloudy winter day. We also conclude that for northern midlatitudes the "vitamin D wintertime" does not cover all months between October and March. However, more work is needed to assess the exposure on humans and to determine the exposure times necessary for a healthy vitamin D status as a function of season, time of day, clothing, shading and location.

*Acknowledgements*—These investigations were partly funded by the Austrian climate research program which is supported by the climate and energy fund. We also thank Ben Liley from NIWA, Lauder, New Zealand for his support by making the binary data of the 3D voxel model ready for further analysis as well as Richard McKenzie from NIWA, Lauder for correcting our manuscript.

## REFERENCES

1. Seckmeyer, G., A. Zittermann, R. L. McKenzie and R. Greinert (2012) Solar Radiation: 13. Solar radiation and human Health. In *Encyclopedia of Sustainability Science and Technology*. (Edited by R. A. Meyers), pp. 9649–9672. Springer, New York.
2. Lucas, R. M., A. J. McMichael, B. K. Armstrong and W. T. Smith (2008) Estimating the global disease burden due to ultraviolet radiation exposure. *Int. J. Epidemiol.* **37**, 654–667.
3. WHO (2008) World Health Organization, International Agency for Research on Cancer. Vitamin D and cancer. IARC Working Group Reports. WHO Press, 5, 148 pp.
4. Dobnig, H., S. Pilz, H. Scharnagl, W. Renner, U. Seelhorst, B. Wellnitz, J. Kinkeldei, B. O. Boehm, G. Weihrauch and W. Maerz (2008) Independent association of low serum 25-hydroxyvitamin D and 1,25-dihydroxyvitamin D levels with all-cause and cardiovascular mortality. *Arch. Intern. Med.* **168**, 1340–1349.
5. Ginde, A. A., R. Scragg, R. Schwartz and C. A. Camargo (2009) Prospective study of serum 25-hydroxyvitamin D level, cardiovascular disease mortality, and all-cause mortality in older U.S. *Adults. J. Am. Geriatr. Soc.* **57**, 1595–1603.
6. Giovannucci, E., Y. Liu, B. W. Hollis and E. B. Rimm (2008) 25-hydroxyvitamin D and risk of myocardial infarction in men: A prospective study. *Arch. Intern. Med.* **168**, 1174–1180.
7. Pilz, S., H. Dobnig, G. Nijpels, R. J. Heine, C. D. Stehouwer, M. B. Snijder, R. M. van Dam and J. M. Dekker (2009) Vitamin D and mortality in older men and women. *Clin. Endocrinol.* **71**, 666–672.
8. Wang, T. J., M. J. Pencina, S. L. Booth, P. F. Jacques, E. Ingelsson, K. Lanier, E. J. Benjamin, R. B. D'Agostino, M. Wolf and R. S. Vasan (2008) Vitamin D deficiency and risk of cardiovascular disease. *Circulation* **117**, 503–511.
9. Biesalski, H. K., J. Köhrle and K. Schürmann (2002) *Vitamine, Spurenelemente und Mineralstoffe -Prävention und Therapie mit Mikronährstoffen*. Georg Thieme Verlag, Stuttgart, 774 p.
10. Seckmeyer, G., D. Pissulla, M. Glandorf, D. Henriques, B. Johnsen, A. Webb, A. M. Siani, A. Bais, B. Kjeldstad, C. Brogniez, J. Lenoble, B. Gardiner, P. Kirsch, T. Koskela, J. Kaurola, B. Uhlmann, H. Slaper, P. den Outer, M. Janouch, P. Werle, J. Grobner, B. Mayer, A. de la Casiniere, S. Simic and F. Carvalho (2008) Variability of UV irradiance in Europe. *Photochem. Photobiol.* **84**, 172–9.
11. Webb, A. R., R. Kift, M. T. Durkin, S. J. O'Brien, A. Vail, J. L. Berry and L. E. Rhodes (2010) The role of sunlight exposure in determining the vitamin D status of the U.K. white adult population. *Br. J. Dermatol.* **163**, 1050–1055.
12. Zittermann, A. (2010) The estimated benefits of vitamin D for Germany. *Mol. Nutr. Food Res.* **54**, 1164–1171.
13. Seckmeyer, G., M. Glandorf, C. Wichers, R. L. McKenzie, D. Henriques, F. Carvalho, A. R. Webb, A. M. Siani, A. F. Bais, B. Kjeldstad, C. Brogniez, P. Werle, T. Koskela, K. Lakkala, J. Lenoble, J. Groebner, H. Slaper, P. N. Den Outer and U. Feister (2008) Europe's darker atmosphere in the UV-B. *Photochem. Photobiol. Sci.* **7**, 925–930.
14. Diffey, B. L. (2010) Is casual exposure to summer sunlight effective at maintaining adequate vitamin D status? *Photodematol. Photo* **26**, 172–176.
15. Holick, M. F. (2007) Vitamin D deficiency. *N. Engl. J. Med.* **357**, 266–281.
16. McKenzie, R. L., J. B. Liley and L. O. Björn (2009) UV radiation: Balancing risks and benefits. *Photochem. Photobiol.* **85**, 88–98.
17. Rhodes, L. E., A. R. Webb, H. I. Fraser, R. Kift, M. T. Durkin, D. Allan, S. J. O'Brien, A. Vail and J. L. Berry (2010) Recommended summer sunlight exposure levels can produce sufficient (20 ngml-1) but not the proposed optimal (32ngml-1) 25(OH)D levels at UK latitudes. *J. Invest. Dermatol.* **130**, 1411–1418.
18. Webb, A. R. and O. Engelsen (2006) Calculated ultraviolet exposure levels for a healthy vitamin D status. *Photochem. Photobiol.* **82**, 1697–1703.

19. Webb, A. R., R. Kift, J. L. Berry and L. E. Rhodes (2011) The vitamin D debate:Translating controlled experiments into reality for human sun exposure times. *Photochem. Photobiol.* **87**, 741–745.
20. Webb, A. R., L. Kline and M. F. Holick (1988) Influence of season and latitude on the cutaneous synthesis of vitamin D3: Exposure to winter sunlight in Boston and Edmonton will not promote vitamin D3 synthesis in human skin. *J. Clin. Endocrinol. Metab.* **67**, 373–378.
21. Wolpowitz, D. and B. A. Gilchrest (2006) The vitamin D questions: How much do you need and how should you get it? *J. Am. Acad. Dermatol.* **54**, 301–317.
22. Zeeb, H. and R. Greinert (2010) Bedeutung von Vitamin D in der Krebsprävention - Konflikt zwischen UV-Schutz und Anhebung niedriger Vitamin-D-Spiegel. *Dtsch Arztebl* **107**, 638–647.
23. Bischoff-Ferrari, H. A., E. Giovannucci, W. C. Willett, T. Dietrich and B. Dawson-Hughes (2006) Estimation of optimal serum concentrations of 25-hydroxyvitamin D for multiple health outcomes. *Am. J. Clin. Nutr.* **84**, 18–28.
24. Chel, V. G. M., M. E. Ooms, C. Popp-Snijders, S. Pavel, A. A. Schothorst, C. C. E. Meulemans and P. Lips (1998) Ultraviolet irradiation corrects vitamin D deficiency and suppresses secondary hyperparathyroidism in the elderly. *J. Bone Miner. Res.* **13**, 1238–1242.
25. Vieth, R., H. Bischoff-Ferrari, B. J. Boucher, B. Dawson-Hughes, C. F. Garland, R. P. Heaney, M. F. Holick, B. W. Hollis, C. Lamberg-Allardt, J. J. McGrath, A. W. Norman, S. Scragg, S. J. Whiting, W. C. Willett and A. Zittermann (2007) The urgent need to recommend an intake of vitamin D that is effective. *Am. J. Clin. Nutr.* **85**, 649–650.
26. Wolpowitz, D. and B. A. Gilchrest (2006) Clarifying the vitamin D controversy: the health benefits of supplementation by diet versus sunshine. In *Skin Aging*, Vol. 1. (Edited by B. A. Gilchrist and J. Krutmann), pp. 81–102. Springer, Berlin Heidelberg.
27. Godar, D. E., S. J. Pope, W. B. Grant and M. F. Holick (2012) Solar UV doses of young americans and vitamin D3 production. *Environ. Health Perspect.* **120**, 139–143.
28. Godar, D. E., S. J. Pope, W. B. Grant and M. F. Holick (2011) Solar UV doses of adult Americans and vitamin D3 production. *Dermatoendocrinology* **3**, 243–250.
29. Pope, S. J. and D. E. Godar (2010) Solar UV geometric conversion factors: Horizontal plane to cylinder model. *Photochem. Photobiol.* **86**, 457–466.
30. Oppenrieder, A., P. Höppe, P. Koepke and J. Reuder (2005) Long term measurements of the UV irradiance of inclined surfaces and visualization of UV exposure of the human body. *Meteorol. Z.* **14**, 285–290.
31. Höppe, P., A. Oppenrieder, C. Erianto, P. Koepke, J. Reuder, M. Seefeldner and D. Nowak (2004) Visualization of UV exposure of the human body based on data from a scanning UV-measuring system. *Int. J. Biometeorol.* **49**, 18–25.
32. Vernez, D., A. Milon, L. Francioli, J.-L. Bulliard, L. Vuilleumier and L. Moccozet (2011) A numeric model to simulate solar individual ultraviolet exposure. *J. Photochem. Photobiol., B* **87**, 721–728.
33. Vernez, D., A. Milon, L. Vuilleumier and J.-L. Bulliard (2012) Anatomical exposure patterns of skin to sunlight: Relative contributions of direct, diffuse and reflected ultraviolet radiation. *Br. J. Dermatol.* **167**, 383–390.
34. WMO (2008) Part I. Measurement of Meteorological Variables, Chapter 7 Measurement of Radiation, Annex 7.A Nomenclature of Radiometric and Photometric Quantities. In *Guide to Meteorological Instruments and Methods of Observation*, Vol. 8, No. 7. (Edited by WMO), pp. I7–31, World Meteorological Organization (WMO), Geneva.
35. Bouillon, R., J. Eisman, M. Garabedian, M. F. Holick, J. Kleinschmidt, T. Suda, I. Terenetskaya and A. R. Webb (2006) *Action Spectrum for the Production of Previtamin D3 in Human Skin*, Vol. 174, 12 pp. CIE, Vienna.
36. ICRP (2002) Basic anatomical and physiological data for use in radiological protection: Reference values. *ICRP Publication 89. Ann. ICRP* **32**, 3–4.
37. Petoussi-Henss, N., M. Zankl, U. Fill and D. Regulla (2002) The GSF family of voxel phantoms. *Phys. Med. Biol.* **47**, 89–106.
38. Petoussi-Henss, N., M. Zankl, C. Hoeschen and D. Nosske (2007) Voxel or MIRD-type model: A sensitivity study relevant to nuclear medicine. *IFMBE Proceedings* **14**, 2061–2064.
39. Zankl, M. and A. Wittmann (2001) The adult male voxel model "Golem" segmented from whole-body CT patient data. *Radiat. Environ. Biophys.* **40**, 153–162.
40. Klemp, J. B., M. J. McIrvin and W. S. Boyd (1990) PolyPaint - A Three-Dimensional Rendering Package, pp. 286–293. In Sixth International Conference on Interactive Information and Processing Systems, American Meteorological Society, Boston, MA, 5 February–9 February 1990.
41. Holick, M. F. (2002) Vitamin D: The underappreciated D-lightful hormone that is important for skeletal and cellular health. *Curr. Opin. Endocrinol. Diab.* **9**, 87–98.
42. Fitzpatrick, T. B. (1988) The validity and practicality of Sun-reactive skin types I through VI. *Arch. Dermatol.* **124**, 869–871.
43. Adams, J. A., T. L. Clemens, J. A. Parrish and M. F. Holick (1982) Vitamin-D synthesis and metabolism after ultraviolet radiation of normal and vitamin-D-deficient subjects. *N. Engl. J. Med.* **306**, 722–5.
44. Mayer, B. and A. Kylling (2005) Technical note: The libRadtran software package for radiative transfer calculations - descriptions and examples of use. *Atmos. Chem. Phys*. **5**, 1319–1381.
45. Feister, U. and R. Grewe (1995) Spectral albedo measurements in the UV and visible region over different types of surfaces. *Photochem. Photobiol.* **62**, 736–744.
46. Koepke, P. and M. Mech (2005) UV irradiance on arbitrarily oriented surfaces: variation with atmospheric and ground properties. *Theor. Appl. Climatol.* **81**, 25–32.
47. Mech, M. and P. Koepke (2004) Model for UV irradiance on arbitrarily oriented surfaces. *Theor. Appl. Climatol.* **77**, 151–158.
48. Reuder, J. (1998) Characterisation of Cloud Types for UV Radiation Modelling. In ECUV, European Conference on Atmospheric UV Radiation, Helsinki, Finland, 28 June–2 July 1998.
49. Wuttke, S., G. Seckmeyer, G. Bernhard, J. Ehramjian, R. L. McKenzie, P. Johnston and M. O'Neill (2006) New spectroradiometers complying with the NDSC standards. *J. Atmos. Oceanic. Tech.* **23**, 241–251.
50. Webb, A. R., B. R. DeCosta and M. F. Holick (1989) Sunlight regulates the cutaneous production of vitamin D3 by causing its photodegradation. *J. Clin. Endocrinol. Metab.* **68**, 882–887.
51. Meinhardt-Wollweber, M. and R. Krebs (2012) A computational model for previtamin D3 production in skin. *Photochem. Photobiol. Sci.* **11**, 731–737.
52. Norval, M., L. O. Björn and F. R. de Gruijl (2010) Is the action spectrum for the UV-induced production of previtamin D3 in human skin correct? *Photochem. Photobiol. Sci.* **9**, 11–17.

## 3.2 Research Article B: Is Multidirectional UV Exposure Responsible for Increasing Melanoma Prevalence with Altitude? A Hypothesis Based on Calculations with a 3D-Human Exposure Model

### 3.2.1 Declaration of my contribution

Gunther Seckmeyer conceived the idea to use radiance and exposure as a possible explanation for the strong increase of skin cancer with increasing altitude. I performed the calculations used in this study. Together with Kathrin Graw I analyzed the data. Daniela Haluza, Stana Simic and Stefan Riechelmann contributed materials and analysis tools. I drafted the paper and created all visualizations. All authors contributed substantially with comments and revised the manuscript. The quality of the article was further increased by the valuable remarks of the three anonymous reviewers of the article.

### 3.2.2 Published article

This article has been published with open access in International Journal of Environmental Research and Public Health.
Submitted: 5 August 2016. Accepted: 22 September 2016. Published online: 28 September 2016.

**Schrempf, M., Haluza, D., Simic, S., Riechelmann, S., Graw, K., and Seckmeyer, G.:** Is Multidirectional UV Exposure Responsible for Increasing Melanoma Prevalence with Altitude? A Hypothesis Based on Calculations with a 3D-Human Exposure Model, *Int. J. Environ. Res. Public Health*, 13(10), 961, DOI: 10.3390/ijerph13100961., 2016.

International Journal of
*Environmental Research and Public Health*

MDPI

*Article*

# Is Multidirectional UV Exposure Responsible for Increasing Melanoma Prevalence with Altitude? A Hypothesis Based on Calculations with a 3D-Human Exposure Model

**Michael Schrempf [1,*], Daniela Haluza [2], Stana Simic [3], Stefan Riechelmann [4], Kathrin Graw [5] and Gunther Seckmeyer [1]**

1 Institute of Meteorology and Climatology, Leibniz Universität Hannover, Hannover 30419, Germany; Seckmeyer@muk.uni-hannover.de
2 Institute of Environmental Health, Center for Public Health, Medical University of Vienna, Vienna 1090, Austria; daniela.haluza@meduniwien.ac.at
3 Institute of Meteorology, University of Natural Resources and Applied Life Sciences, Vienna 1190, Austria; stana.simic@boku.ac.at
4 Physikalisch-Technische Bundesanstalt (PTB), Braunschweig 38116, Germany; stefan.riechelmann@ptb.de
5 Deutscher Wetterdienst, Offenbach 63067, Germany; Kathrin.Graw@dwd.de
* Correspondence: schrempf@muk.uni-hannover.de; Tel.: +49-511-762-3165

Academic Editor: Paul B. Tchounwou
Received: 5 August 2016; Accepted: 22 September 2016; Published: 28 September 2016

**Abstract:** In a recent study, melanoma incidence rates for Austrian inhabitants living at higher altitudes were found to increase by as much as 30% per 100 m altitude. This strong increase cannot simply be explained by the known increase of erythemally-weighted irradiance with altitude, which ranges between 0.5% and 4% per 100 m. We assume that the discrepancy is partially explainable by upwelling UV radiation; e.g., reflected by snow-covered surfaces. Therefore, we present an approach where the human UV exposure is derived by integrating incident radiation over the 3D geometry of a human body, which enables us to take upwelling radiation into account. Calculating upwelling and downwelling radiance with a radiative transfer model for a snow-free valley and for snow-covered mountain terrain (with albedo of 0.6) yields an increase in UV exposure by 10% per 100 m altitude. The results imply that upwelling radiation plays a significant role in the increase of melanoma incidence with altitude.

**Keywords:** UV radiation; human exposure; erythema; malignant melanoma; altitude effects; albedo; snow cover; alpine region

## 1. Introduction

Cumulative life-time exposure to natural and artificial UV radiation is associated with chronic skin damage, including skin cancer. Many epidemiological studies prove the fundamental role of UV radiation in the genesis of skin cancer [1–5], of which the most hazardous form is malignant melanoma. Appearing in 1300 cases in 2009 in Austria, it accounted for 3.5% of all malignant tumors [6]. In studies of the increase of melanoma incidence (e.g., by Krishnamurthy [7] in India and by Gerbaud et al. [8] in France) the authors investigated local cancer registries and state that altitude may have an impact on melanoma incidence. Madera et al. [9] conducted a study in the province of Granada, Spain to assess the relationship between altitude, daily erythemal dose, and the prevalence of melanoma, and found a tendency toward increased prevalence of melanoma at higher altitude. A few recent studies focused on skin health and environmental factors in Austria. Haluza et al. [10] published a

comprehensive study on Austrian melanoma incidence and mortality data, investigating its relation to the most important biological and environmental indices, such as gender, age, home district, and altitude. The authors found a significant increase of melanoma incidence with altitude in the Austrian districts with about 50% higher rates in urban compared to rural districts. Moehrle and Garbe [11] showed that the Swiss cancer registries and the Austrian Tyrol registry have much higher incidence rates for cutaneous melanoma than other Central European cancer registries. The authors hypothesize that mountaineering activities in higher altitude may increase the risk for cutaneous melanoma.

As has been shown from numerous radiative transfer studies, UV irradiances change with the observing altitude due to changes in scattering and absorption [12]. The increase of UV irradiance with altitude cannot be simply described by one number, as it is a complex function of altitude, cloudiness, aerosol content, tropospheric ozone absorption, and snow cover [13]. Nevertheless, the percentage increase with altitude is often used as a proxy. Blumthaler et al. [14] measured an increase of the erythemal effective irradiance with altitude of 1.8% per 100 m. Similar values were given by other studies (e.g., Herman et al. [12], McKenzie et al. [15], Cordero et al. [16]), which led to the assumption that there is an upper limit of the increase with altitude, since no values above 4% per 100 m were reported.

Aside from existing studies for Austrian conditions (e.g., Schauberger et al. [17], Schmalwieser et al. [18,19]), a variety of exposure measurements on different subgroups can be found in the literature. Due to different methodological approaches, findings reported in these studies are not directly comparable. To address this issue, Seckmeyer et al. [20] presented a novel method to calculate vitamin-D-weighted exposure by integrating the incident solar spectral radiance over all relevant parts of the human body. It should be noted that individual UV exposure strongly depends on behavioral patterns, and is defined by the duration of the exposure, geometry of the receiving surface, by protection of clothing, the use of sunscreen, hair cover, and shadowing (e.g., Seckmeyer et al. [20], Weihs et al. [21], Haluza et al. [22]). Behavioral patterns are influenced by occupational activities, spare time activities, and the choice of holiday destinations [23]. In regard to recreational activities at higher altitudes, surface reflectance is important, especially in seasonally snow-covered and mountainous regions. The albedo of snow-covered surfaces may vary between 0.02 and 1 [24]. However, it is known that the albedo is influenced by a large surface area of more than 50 km from the observation point [25,26], where rocks, trees, streets and buildings with a lower reflectivity within that range may exist. Therefore, the effective albedo is usually much lower than unity [27–29]. Effective albedo values for the UV range have previously been determined through a combination of radiative transfer modeling and a 3D albedo model [27,29,30], averaging to 0.41 (aged snow) and 0.77 (fresh snow) for a 1000 m snowline. An effective albedo of 0.63 to 0.78 determined for the snowline at 800 m by Simic et al. [31] is comparable to the model calculations presented by Weihs et al. [29]. In Austria, Rengarajan et al. [30] measured the albedo at the Sonnblick observatory in winter. Their experimentally-determined values in the range of 0.73 to 0.78 are quite similar to the albedo values for UVA wavelengths determined in Simic et al. [31] at a low snow line of 800 m.

## 2. Materials and Methods

Haluza et al. [10] analyzed Austrian melanoma incidence data (1990–2010) by district and year, and found that melanoma incidence rates increase with altitude by as much as 30% per 100 m of the main capital of the respective district in which people are living, with about 50% higher rates in urban compared to rural districts. Investigations have shown that the increase in irradiance on a horizontal surface as a function of altitude is much smaller, and can account for only 2% of the effect [14]. This large discrepancy can therefore hardly be explained by the increase in irradiance alone, and requires an alternative explanation. It should be noted that irradiance on a horizontally-oriented surface is not a good indicator to determine the exposure of a human [20]. Instead, the multidirectional downwelling and upwelling UV radiation and a 3D-human model should be considered. Therefore, in the current study, we used the radiance (describing the radiant energy per unit solid angle and

per unit area, thus taking into account the complex radiation field) to investigate if multidirectional UV exposure is partially responsible for increasing melanoma prevalence with altitude.

Earlier investigations (e.g., by Diffey [32] and McKenzie et al. [33]) were based on the irradiance incident on surfaces, whereas the calculated exposure of a voxel model of a human takes into account the complex geometry of the radiation field as well as the geometry of a human body. We refer to a method to calculate biologically-weighted exposure by integrating the incident solar spectral radiance over all relevant parts of the human body [20].

In addition to the downwelling radiance and the direct beam of the sun already used in Seckmeyer et al. [20], we calculated the reflected upwelling radiance from the lower hemisphere for this investigation (see Figure 1). With the assumption that the snow-covered ground is a Lambertian surface, we can calculate the reflected upwelling radiance assuming a constant L (Lambertian surface). The radiance can be derived by the following Equation (1):

$$\begin{aligned} E_{upwelling}(\lambda) &= \int_{\Omega} L_{upwelling}(\lambda)\, cos\,\theta\, d\Omega\,,\ with\ d\Omega = sin\,\theta\, d\theta d\varphi \\ &= \int_{\varphi=0}^{2\pi}\int_{\theta=0}^{\frac{\pi}{2}} L_{upwelling}(\lambda)\, cos\,\theta\, sin\,\theta\, d\theta\, d\varphi \\ &= L_{upwelling}(\lambda)\ \times\ \pi\ \times\ sr \end{aligned} \tag{1}$$

where $E_{upwelling}(\lambda)$ is the spectral reflected irradiance, $L_{upwelling}(\lambda)$ is the spectral upwelling radiance, $d\Omega$ the solid angle, $\theta$ represents the zenith angle, and $\varphi$ the azimuth angle. With the definition, $albedo = \frac{M_G}{E_G}$, where $E_G$ is the short-wave global irradiance and $M_G$ is the radiant exitance of the Earth's surface in $Wm^{-2}$ [34], $E_{upwelling}(\lambda)$ can be related to the global spectral downwelling irradiance ($Eglo_{downwelling}(\lambda)$) as in Equation (2):

$$E_{upwelling}(\lambda) = Eglo_{downwelling}(\lambda)\ \times\ albedo \tag{2}$$

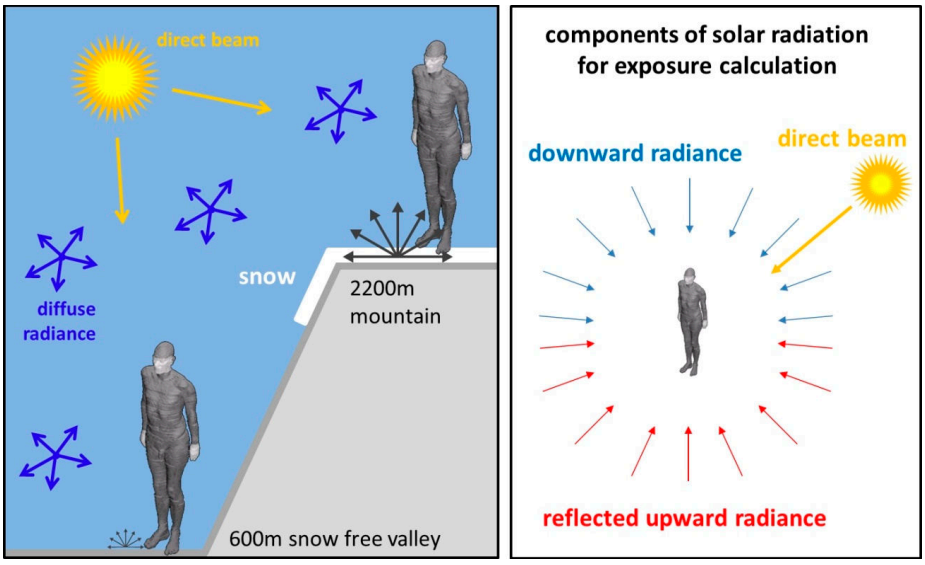


**Figure 1.** Illustration of the simulated locations. The exposure model takes into account the direct, diffuse, and reflected radiations, the complex geometry of a human body, and clothing. The albedo values of the location at 2200 m have been varied from 0.02 to 0.6. For a lower-altitude location at 600 m, an albedo of 0.02 was used.

*Int. J. Environ. Res. Public Health* **2016**, *13*, 961 

The spectral reflected upwelling radiance $L_{upwelling}(\lambda)$ is then given by Equation (3):

$$L_{upwelling}(\lambda) = \frac{E_{upwelling}(\lambda)}{\pi \times sr} = \frac{Eglo_{downwelling}(\lambda) \times albedo}{\pi \times sr} \quad (3)$$

to calculate the human exposure, Seckmeyer et al. [20] combined the downwelling radiance with the geometry of the 3D-model seen from the upper hemisphere. Analogously, the reflected upwelling radiance is combined with the geometry of the 3D-model seen from the lower hemisphere (Figure 1).

## 3. Results

*Hypothesis*

In this investigation, the UV exposure of a human as defined in Seckmeyer et al. [20] is calculated for the wavelength range of 250–400 nm. Two hypothetical locations on 31 March 2016 with a latitude of 47° N are considered, one located in a snow-free valley at 600 m and one with varying albedo located on a mountain at 2200 m altitude (see Figure 1). Additionally, the irradiance is calculated for both locations. For the snow-free ground location, an albedo of 0.02 is used, which is typical for many surfaces in the UV wavelength region (e.g., grass) [35]. Since the albedo is influenced by a large surface area and there are objects with a lower reflectivity (e.g., rocks and trees) within that area, the assumption is made that the albedo extends to infinity, and that an effective albedo is used. For the mountain location, the effective albedo values of 0.02, 0.2, 0.4, and 0.6 were considered. The calculated spectra were weighted with the erythemal action spectrum. The exposure calculations presumed a human with winter clothing, where only hands and face are exposed (see Figure 1).

Figure 2 depicts simulated values of the irradiance and the exposure for the valley location at 600 m, as well as for the mountain top location at 2200 m for 31 March 2016 with a solar zenith angle (SZA) of 45°. All mountain values are greater than the valley values. However, the albedo has a greater influence on the exposure than on the irradiance.

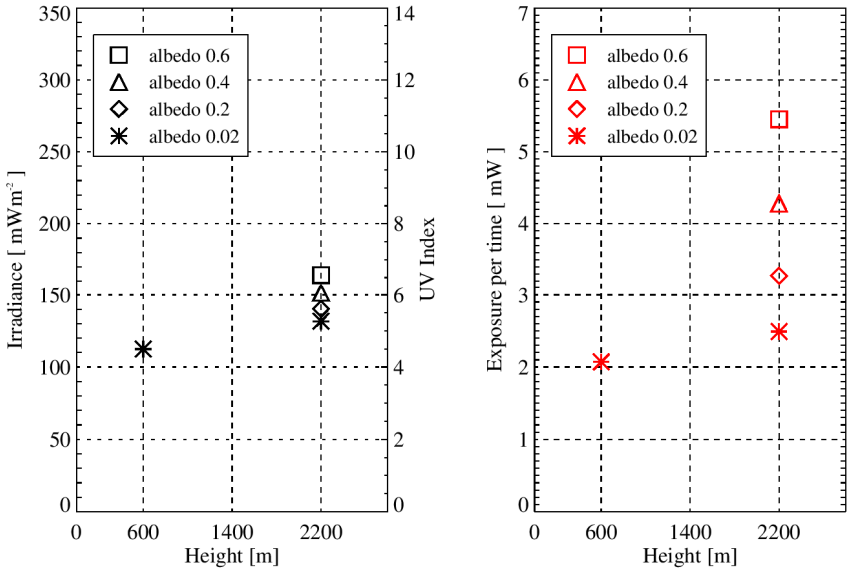


**Figure 2.** Simulated values of the irradiance (**left plot**) and the exposure of a human with winter clothing (**right plot**) for the valley and mountain locations are shown. The simulations were performed for a hypothetical location at 47° N for 31 March 2016 with a solar zenith angle (SZA) of 45°. The influence of the albedo is larger for the exposure (integrated radiance on a human) than for the irradiance.

Gradients in % per 100 m have been calculated to compare the increase in exposure values with altitude to the increase in irradiance with altitude, and the melanoma incidence rates increase with altitude. The UV exposure and irradiance values are displayed in Figure 2, and the calculated gradients of the increase with altitude of these values are listed in Table 1. The gradients are calculated with Equation (4):

$$gradient = \frac{\left(\frac{mountain\ value}{valley\ value}\right) - 1}{\frac{\Delta\ altitude}{100\ m}} \quad (4)$$

**Table 1.** Simulated values of the irradiance and the human exposure for the valley and mountain location are shown. Additionally, the gradients of the increase with altitude of the simulated values were calculated with Equation (4), where $\Delta altitude$ = 1600 m was used. The influence of the albedo is larger for the exposure of a human than for the irradiance.

| Location | Irradiance | | Exposure of a Human | |
|---|---|---|---|---|
| | Value [$\frac{mW}{m^2}$] | Gradient [%] | Value [$mW$] | Gradient [%] |
| Valley (Albedo 0.02) | 112.46 | - | 2.07 | - |
| Mountain (Albedo 0.02) | 131.63 | 1.07 | 2.49 | 1.27 |
| Mountain (Albedo 0.2) | 140.25 | 1.54 | 3.28 | 3.64 |
| Mountain (Albedo 0.4) | 151.28 | 2.16 | 4.28 | 6.66 |
| Mountain (Albedo 0.6) | 164.19 | 2.88 | 5.45 | 10.21 |

It is evident that the gradients are increasing with higher albedo values on the mountain. Although the gradients of human exposure are always larger than those of irradiance, with a small albedo (e.g., 0.02), the ground reflection is minimal and the gradient of human exposure is therefore only about 1.2 times as large as the gradient in irradiance. However, for higher albedo values (e.g., 0.4 and 0.6), the gradient of the exposure is about 3 and 3.5 times as large, demonstrating that the ground reflection has an enormous impact on the total exposure. In addition, simulations have been performed for an urban valley location (with urban aerosol conditions instead of rural), where the total aerosol amount is higher than with rural settings. Consequently, there is an increased absorption of radiation by aerosols and thus lower exposure values at the valley location. The calculation of the gradient with an urban valley location and a rural mountain location resulted in a 15% per 100 m increase of human exposure in the case of a mountain top albedo of 0.6. This is about 50% higher than the gradient for a rural valley location (see Table 2). Larger gradients due to urban valley conditions equally occur for the irradiance. However, these gradients are still small.

**Table 2.** Comparison between gradients of rural and urban valley location values to mountain location values as increase in % per 100 m for human exposure. The gradients were calculated with Equation (4), where $\Delta altitude$ = 1600 m was used. Due to the urban aerosol conditions, the urban valley exposure value is lower compared to the rural valley value, resulting in larger gradients in the increase of the human exposure with altitude.

| Location | Exposure of a Human (Rural Valley Location) | | Exposure of a Human (Urban Valley Location) | |
|---|---|---|---|---|
| | Value [$mW$] | Gradient [%] | Value [$mW$] | Gradient [%] |
| Valley (Albedo 0.02) | 2.07 | - | 1.59 | - |
| Mountain (Albedo 0.02) | 2.49 | 1.27 | 2.49 | 3.52 |
| Mountain (Albedo 0.2) | 3.28 | 3.64 | 3.28 | 6.60 |
| Mountain (Albedo 0.4) | 4.28 | 6.66 | 4.28 | 10.52 |
| Mountain (Albedo 0.6) | 5.45 | 10.21 | 5.45 | 15.12 |

Since there are no routine measurements of surface albedo at Sonnblick observatory, Simic et al. [31] deployed an algorithm that uses routine observations of snow condition (snow height, time since last snowfall, and snow line) to estimate effective spectrally-invariant surface albedo in the UV range on a daily basis. Albedo values determined in this study ranged from 0.08 to 0.30 with snowline at 2500 m, and up to 0.55 to 0.75 with snowline at 1000 m. Based on these simulations and measurements, we use 0.6 as a constant albedo value for the mountain location at 2200 m altitude for an investigation of the solar zenith angle dependence on the radiation quantities (Figure 3). The calculations show that the diurnal variations of the gradients of the exposure and of the irradiance are small. The gradient of the exposure ranges between 9.7% and 11.1% per 100 m for SZA ranging between 45° and 89°.

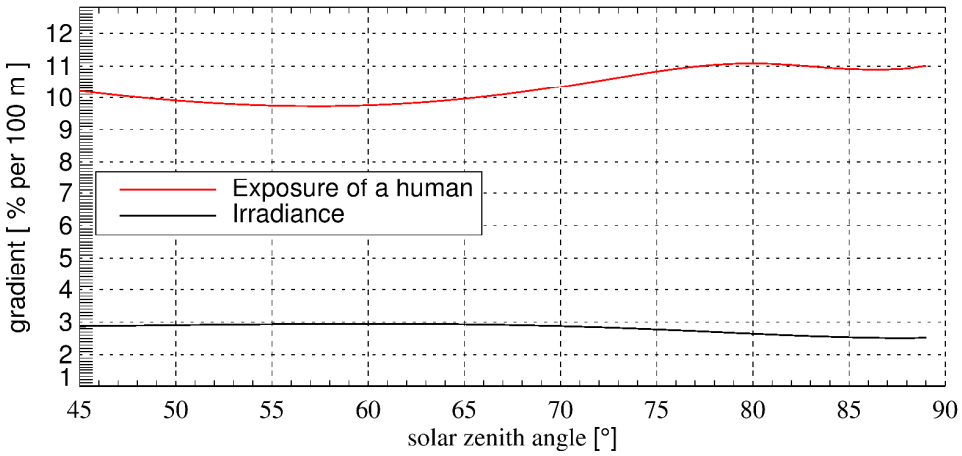


**Figure 3.** Gradients of valley (albedo = 0.02) to mountain (albedo = 0.6) values as increase with altitude in % per 100 m in dependence of the SZA. The gradients were calculated with Equation (4).

## 4. Discussion

For this study, the simulations were calculated by the DISORT code of the UVSPEC model in the LibRadTran package [36]. Since two hypothetical locations were investigated, only basic parameters with conservative settings were used to create simple situations. These results show that under basic conditions, the gradients of the increase with altitude for human exposure are much greater than for literature values of the irradiance. In reality, the differences between the valley and mountain top atmospheric parameters could be larger, which would result in even greater gradients. The parameters with different values depending on location used in this study are listed in Table 3. The total ozone-column value for the mountain top is smaller than the valley value, due to the decrease of tropospheric ozone by 3.5 DU per 1000 m altitude [37]. For the investigation of a rural and urban valley location, the LibRadTran parameter Boundary layer aerosol was used [36].

**Table 3.** Parameter values used in this study.

| Parameter | Valley Location | Mountain Top Location |
|---|---|---|
| Total Ozone Column | 300 | 294.4 |
| Horizontal Visibility | 20 km | 30 km |
| Boundary Layer Aerosol | Rural/Urban | Rural |

As shown in this study, the irradiance on a horizontal surface should not be used to connect radiation changes with the increase in melanoma incidences with altitude. Instead, exposure may be

used as it takes into account the complex geometry of a human body and radiation from multiple directions, including reflected radiation from the ground.

We suggest further investigation using newly-developed techniques to measure the spectral radiance of more than 100 directions simultaneously [38]. With such a system, the downwelling and the ground-reflected upwelling radiation could be measured at different locations (e.g., valley and mountain locations) and used as input in the exposure model. Since such systems are not very mobile, additional data at numerous locations could be acquired using personal dosimeters. Personal dosimeters cannot replace spectroradiometer measurements, as the former often show large deviations from spectroradiometer measurements [39]. However, if dosimeters are carefully characterized and preselected, the use of dosimeters could extend the amount of data to estimate the exposure of a human in mountainous snow-free and snow-covered areas. In fact, dosimeter campaigns have already been performed, but rarely in mountainous regions. Siani et al. [40] conducted measurements with personal dosimeters in alpine sites by mounting dosimeters on the forehead of skiers. However, they measured with only one dosimeter and compared the measurements with irradiance measurements. Instead, to realistically estimate the human exposure, it would be necessary to use multiple dosimeters placed at different places on the human body to take the radiation from multiple directions into account simultaneously, including reflections from the ground.

## 5. Conclusions

In the current study, we demonstrated that upwelling radiation is a relevant factor that needs to be considered when investigating human exposure and its impact on skin cancer incidence. This is particularly important when the surface is covered with snow, thus causing a significant increase in the upwelling UV radiation. The increase in UV exposure with altitude shown here may help explain the increase in melanoma incidence with altitude, whereas the increase in irradiance with altitude leads to the incorrect conclusion that UV radiation plays a minor role for the altitude-related melanoma incidences. Additionally, human behavior is also a prominent factor that may determine the actual UV dose received (exposure integrated over time). A comparison of different valley locations showed lower exposure values with urban aerosol conditions due to higher total aerosol amounts. In contrast to two locations with rural aerosol settings, the calculated gradient for an urban valley location and a rural mountain location resulted in a 50% higher increase in exposure with altitude. This result, and high doses of intermittent UV exposure through recreational activities at snow-covered locations (e.g., skiing, swimming, sunbathing) may also help to explain higher incidence rates in urban districts compared to those in rural ones. Despite the complexity of assessing the real exposure of humans, differences in irradiance cannot explain the evidence in skin-cancer incidence with altitude. Instead, the exposure or radiance should be considered in further studies.

**Acknowledgments:** This study was partly supported by the interdisciplinary project "UVSkinRisk—Health at risk through UVR-induced Skin Cancer in the Context of a Changing Climate" supported by the Austrian Climate Research Program (ACRP). We also thank Hanns Moshammer from the Medical University of Vienna, Austria and Ben Liley from NIWA, Lauder, New Zealand for their comments.

**Author Contributions:** Gunther Seckmeyer conceived the idea to use radiance and exposure in context of this study of the altitude dependence on radiation quantities. Michael Schrempf and Gunther Seckmeyer designed this investigation. Michael Schrempf performed the simulations. Michael Schrempf and Kathrin Graw analyzed the data. Daniela Haluza, Stana Simic and Stefan Riechelmann contributed materials and analysis tools. Michael Schrempf wrote the paper. All authors contributed substantially with comments and revised the manuscript.

**Conflicts of Interest:** The authors declare no conflicts of interest.

## References

1. Radiation/IARC Working Group on the Evaluation of Carcinogenic Risks to Humans. Available online: http://monographs.iarc.fr/ENG/Monographs/vol100D/mono100D.pdf (accessed on 5 August 2016).

2. Haluza, D.; Simic, S.; Höltge, J.; Cervinka, R.; Moshammer, H. Connectedness to nature and public (skin) health perspectives: Results of a representative, population-based survey among austrian residents. *Int. J. Environ. Res. Public Health* **2014**, *11*, 1176–1191. [CrossRef] [PubMed]
3. De Gruijl, F.R.; van Kranen, H.J.; Mullenders, L.H. UV-induced DNA damage, repair, mutations and oncogenic pathways in skin cancer. *Photochem. Photobiol. B* **2001**, *63*, 19–27. [CrossRef]
4. Cleaver, J.E.; Crowley, E. UV damage, DNA repair and skin carcinogenesis. *Front. Biosci.* **2002**, *7*, 1024–1043. [CrossRef]
5. Armstrong, B.K.; Kricker, A. The epidemiology of UV induced skin cancer. *Photochem. Photobiol. B* **2001**, *63*, 8–18. [CrossRef]
6. Zielonke, N. *Krebsinzidenz und Krebsmortalität in Österreich*; Statistik Austria: Wien, Austria, 2012.
7. Krishnamurthy, S. The geography of non-ocular malignant melanoma in India: Its association with latitude, ozone levels and UV light exposure. *Int. J. Cancer* **1992**, *51*, 169–172. [CrossRef] [PubMed]
8. Gerbaud, L.; Lejeune, M.; Abou-Samra, T.; Doz, M.; Mathey, M.; D'Incan, M.; Dechelotte, P.; Souteyrand, P.; Glanddier, P. Epidemiological survey of melanoma in the Auvergne Region (France): Is there an increased incidence in auvergne? *Eur. J. Epidemiol.* **2003**, *18*, 331–335. [CrossRef] [PubMed]
9. Aceituno-Madera, P.; Buendía-Eisman, A.; Olmo, F.; Jiménez-Moleón, J.; Serrano-Ortega, S. Melanoma, altitude and UV-B radiation. *Actas Dermosifiliogr.* **2011**, *102*, 199–205. [CrossRef] [PubMed]
10. Haluza, D.; Simic, S.; Moshammer, H. Temporal and spatial melanoma trends in austria: An ecological study. *Int. J. Environ. Res. Public Health* **2014**, *11*, 734–748. [CrossRef] [PubMed]
11. Moehrle, M.; Garbe, C. Does mountaineering increase the incidence of cutaneous melanoma? *Dermatology* **1999**, *199*, 201–203. [CrossRef] [PubMed]
12. World Meteorological Organization (WMO). *Scientific Assessment of Ozone Depletion: 1998*; WMO: Geneva, Switzerland, 1999.
13. Seckmeyer, G.; Mayer, B.; Bernhard, G.; Erb, R.; Albold, A.; Jäger, H.; Stockwell, W.R. New maximum UV irradiance levels observed in central europe. *Atmos. Environ.* **1997**, *31*, 2971–2976. [CrossRef]
14. Blumthaler, M.; Ambach, W.; Ellinger, R. Increase in solar UV radiation with altitude. *Photochem. Photobiol. B* **1997**, *39*, 130–134. [CrossRef]
15. McKenzie, R.L.; Johnston, P.V.; Smale, D.; Bodhaine, B.; Madronich, S. Altitude effects on UV spectral irradiance deduced from measurements at lauder, new zealand and at mauna loa observatory, Hawaii. *J. Geophys. Res.* **2001**, *106*, 22845–22860. [CrossRef]
16. Cordero, R.; Damiani, A.; Seckmeyer, G.; Jorquera, J.; Caballero, M.; Rowe, P.; Ferrer, J.; Mubarak, R.; Carrasco, J.; Rondanelli, R. The solar spectrum in the atacama desert. *Sci. Rep.* **2016**, *6*, 22457. [CrossRef] [PubMed]
17. Schauberger, G. Anisotropic model for the diffuse biologically-effective irradiance of solar UV-radiation on inclined surfaces. *Theor. Appl. Climatol.* **1992**, *46*, 45–51. [CrossRef]
18. Schmalwieser, A.W.; Enzi, C.; Wallisch, S.; Holawe, F.; Maier, B.; Weihs, P. UV exposition during typical lifestyle behavior in an urban environment. *Photochem. Photobiol.* **2010**, *86*, 711–715. [CrossRef] [PubMed]
19. Schmalwieser, A.W.; Cabaj, A.; Schauberger, G.; Rohn, H.; Maier, B.; Maier, H. Facial solar UV exposure of austrian farmers during occupation. *Photochem. Photobiol.* **2010**, *86*, 1404–1413. [CrossRef] [PubMed]
20. Seckmeyer, G.; Schrempf, M.; Wieczorek, A.; Riechelmann, S.; Graw, K.; Seckmeyer, S.; Zankl, M. A novel method to calculate solar UV exposure relevant to vitamin d production in humans. *Photochem. Photobiol.* **2013**, *89*, 974–983. [CrossRef] [PubMed]
21. Weihs, P.; Schmalwieser, A.; Reinisch, C.; Meraner, E.; Walisch, S.; Harald, M. Measurements of personal UV exposure on different parts of the body during various activities. *Photochem. Photobiol.* **2013**, *89*, 1004–1007. [CrossRef] [PubMed]
22. Haluza, D.; Simic, S.; Höltge, J.; Cervinka, R.; Moshammer, H. Gender aspects of recreational sun-protective behavior: Results of a representative, population-based survey among austrian residents. *Photodermatol. Photoimmunol. Photomed.* **2016**, *32*, 11–21. [CrossRef] [PubMed]
23. Thieden, E.; Philipsen, P.A.; Heydenreich, J.; Wulf, H.C. UV radiation exposure related to age, sex, occupation, and sun behavior based on time-stamped personal dosimeter readings. *Arch. Dermatol.* **2004**, *140*, 197–203. [CrossRef] [PubMed]
24. Wuttke, S.; Seckmeyer, G.; Konig-Langlo, G. Measurements of spectral snow albedo at Neumayer, Antarctica. *Ann. Geophys.* **2006**, *24*, 7–21. [CrossRef]

25. Degünther, M.; Meerkötter, R.; Albold, A.; Seckmeyer, G. Case study of the influence of inhomogeneous surface albedo on UV irradiance. *Geophys. Res. Lett.* **1998**, *25*, 3587–3590. [CrossRef]
26. Smolskaia, I.; Wuttke, S.; Seckmeyer, G.; Micheal, K. Influence of Surface Reflectivity on Radiation in the Antarctic Environment. Available online: https://spie.org/Publications/Proceedings/Paper/10.1117/12.689693?origin_id=x4325&start_volume_number=6300 (accessed on 5 August 2016).
27. Schwander, H.; Mayer, B.; Ruggaber, A.; Albold, A.; Seckmeyer, G.; Koepke, P. Method to determine snow albedo values in the ultraviolet for radiative transfer modeling. *Appl. Opt.* **1999**, *38*, 3869–3875. [CrossRef] [PubMed]
28. Weihs, P.; Lenoble, J.; Blumthaler, M.; Martin, T.; Seckmeyer, G.; Philipona, R.; de la Casiniere, A.; Sergent, C.; Gröbner, J.; Cabot, T.; et al. Modeling the effect of an inhomogeneous surface albedo on incident UV radiation in mountainous terrain: Determination of an effective surface albedo. *Geophys. Res. Lett.* **2001**, *28*, 3111–3114. [CrossRef]
29. Weihs, P.; Scheifinger, H.; Rengarajan, G.; Simic, S. Effect of topography on average surface albedo in the ultraviolet wavelength range. *Appl. Opt.* **2000**, *39*, 3592–3603. [CrossRef] [PubMed]
30. Rengarajan, G.; Weihs, P.; Simic, S.; Mikielewicz, W.; Laube, W. Albedo measurement system for UVA and the visible wavelength. *Radiat. Prot. Dosimetr.* **2000**, *91*, 197–199. [CrossRef]
31. Simic, S.; Weihs, P.; Vacek, A.; Kromp-Kolb, H.; Fitzka, M. Spectral UV measurements in austria from 1994 to 2006: Investigations of short- and long-term changes. *Atmos. Chem. Phys.* **2008**, *8*, 7033–7043. [CrossRef]
32. Diffey, B.L. Is casual exposure to summer sunlight effective at maintaining adequate vitamin D status? *Photodermatol. Photoimmunol. Photomed.* **2010**, *26*, 172–176. [CrossRef] [PubMed]
33. McKenzie, R.L.; Liley, J.B.; Björn, L.O. UV radiation: Balancing risks and benefits. *Photochem. Photobiol.* **2009**, *85*, 88–98. [CrossRef] [PubMed]
34. Seckmeyer, G.; Bais, A.; Bernhard, G.; Blumthaler, M.; Booth, C.R.; Disterhoft, P.; Eriksen, P.; McKenzie, R.L.; Miyauchi, M.; Roy, C. *Instruments to Measure Solar Ultraviolet Irradiance. Part 1: Spectral Instruments*; World Meteorological Organisation: Geneva, Switzerland, 2001; p. 30.
35. Feister, U.; Grewe, R. Spectral albedo measurements in the UV and visible regions over different types of surfaces. *Photochem. Photobiol.* **1995**, *62*, 736–744. [CrossRef]
36. Shettle, E.P. In Models of Aerosols, Clouds, and Precipitation for Atmospheric Propagation Studies. Available online: http://adsabs.harvard.edu/abs/1990apuv.agar.....S (accessed on 5 August 2016).
37. Pfeifer, M.T.; Koepke, P.; Reuder, J. Effects of Altitude and Aerosol on UV Radiation. Available online: http://onlinelibrary.wiley.com/doi/10.1029/2005JD006444/full (accessed on 5 August 2016).
38. Riechelmann, S.; Schrempf, M.; Seckmeyer, G. Simultaneous measurement of spectral sky radiance by a non-scanning multidirectional spectroradiometer (MUDIS). *Meas. Sci. Technol.* **2013**, *24*, 125501. [CrossRef]
39. Seckmeyer, G.; Klingebiel, M.; Riechelmann, S.; Lohse, I.; McKenzie, R.L.; Ben Liley, J.; Allen, M.W.; Siani, A.M.; Casale, G.R. A critical assessment of two types of personal UV dosimeters. *Photochem. Photobiol.* **2012**, *88*, 215–222. [CrossRef] [PubMed]
40. Siani, A.; Casale, G.R.; Diémoz, H.; Agnesod, G.; Kimlin, M.G.; Lang, C.A.; Colosimo, A. Personal UV exposure in high albedo alpine sites. *Atmos. Chem. Phys.* **2008**, *8*, 3749–3760. [CrossRef]


## 3.3 Research Article C: Einfluss der Verschattung auf die Vitamin-D-gewichtete UV-Exposition eines Menschen

### 3.3.1 Declaration of my contribution

I and Gunther Seckmeyer conceived the idea to derive obstructions from hemispherical sky images to study urban UV exposure. Gunther Seckmeyer had the idea to simplify the complexity of the exposure calculation by neglecting the contributions from the obstructed sky areas and I extended the algorithms. Kezia Lange provided the data of the radiance simulations. Together with Nadine Thuns I performed the field measurements and analyzed the data. I drafted the article and created all visualizations. All authors contributed substantially with comments and revised the manuscript.

### 3.3.2 Published article

This article has been published in Aktuelle Dermatologie. According to the approved license from Georg Thieme Verlag KG, only the abstracts of the article are allowed to be printed. The Full-Text article can be accessed online.
Submitted: 11 February 2017. Published online e-First: 29 August 2017.

**Schrempf, M., Thuns, N., Lange, K., and Seckmeyer, G.:** Einfluss der Verschattung auf die Vitamin-D-gewichtete UV-Exposition eines Menschen, *Aktuelle Derm*, DOI: 10.1055/s-0043-105258., URL: `https://doi.org/10.1055/s-0043-105258`, 2017.

# Einfluss der Verschattung auf die Vitamin-D-gewichtete UV-Exposition eines Menschen

M. Schrempf, N. Thuns, K. Lange, G. Seckmeyer

# Impact of Shadowing on the Vitamin D Weighted Exposure of a Human

M. Schrempf, N. Thuns, K. Lange, G. Seckmeyer

Institut für Meteorologie und Klimatologie, Leibniz Universität Hannover, Hannover D-30419;
Korrespondenz: Michael Schrempf, schrempf@muk.uni-hannover.de; Tel.: +49-511-762-3165

**Zusammenfassung:**

Die Vitamin-$D_3$-gewichtete UV-Exposition eines aufrecht stehenden Menschen wurde für ausgewählte urbane Umgebungen bestimmt, um den Einfluss der Verschattung durch Gebäude oder Bewuchs auf die Exposition zu untersuchen. Die Exposition wird berechnet unter Berücksichtigung der Strahldichte, also der Strahlungsenergie von direkter Sonnenstrahlung und diffuser Himmelsstrahlung aus verschiedenen Einfalls- und Azimutwinkeln und der 3D Geometrie eines Modellmenschen. Die Verschattung wird durch Hemisphären-Bilder bestimmt, die mithilfe einer Fotokamera mit Fischaugenobjektiv aufgenommen wurden, wobei angenommen wird, dass die Strahlung verschatteter Himmelssegmente vernachlässigbar klein ist. Dadurch werden den Himmel verdeckende Hindernisse räumlich hochaufgelöst erfasst und als Input in das Expositionsmodell eingegeben. Die Vitamin-$D_3$-gewichtete Exposition betrug an einer bebauten Straße am 21. Dezember zu Sonnenhöchststand ungefähr 50% und am 21. März 70% von der Exposition einer hindernisfreien Umgebung.

**Abstract:**

The vitamin $D_3$ weighted UV exposure of a human with vertical posture was calculated for specific urban locations to investigate the impact of shadowing by buildings or vegetation on the exposure. The exposure is calculated by taking into account the radiance, i.e. the radiant energy from direct solar radiation and diffuse sky radiation from different incident and azimuth angles and the 3D geometry of a human model. Obstructions shading the sky radiance are derived in high spatial resolution from hemispherical-Images, taken by a digital camera with a fisheye lens. The radiance from shaded sky regions is neglected in the UV. The derived shadowing information is used as input in the exposure model. The vitamin $D_3$ weighted UV exposure on a street within a city on December 21 at noon is approximately 50% and on March 21 at noon 70%, of the exposure compared to an unobstructed location.

## 3.4 Research Article D: Impact of Orientation on the Vitamin D Weighted Exposure of a Human in an Urban Environment

### 3.4.1 Declaration of my contribution

I and Gunther Seckmeyer conceived the idea to derive obstructions from hemispherical sky images to study urban UV exposure. Gunther Seckmeyer had the idea to simplify the complexity of the exposure calculation by neglecting the contributions from the obstructed sky areas and I extended the algorithms. Kezia Lange provided the data of the radiance simulations. Together with Nadine Thuns I performed the field measurements and analyzed the data. I drafted the article and created all visualizations. All authors contributed substantially with comments and revised the manuscript. The quality of the article was further increased by the valuable remarks of the three anonymous reviewers of the article.

### 3.4.2 Published article

This article has been published with open access in International Journal of Environmental Research and Public Health.
Submitted: 19 June 2017. Accepted: 10 August 2017. Published online: 16 August 2017.

**Schrempf, M., Thuns, N., Lange, K., and Seckmeyer, G.:** Impact of Orientation on the Vitamin D Weighted Exposure of a Human in an Urban Environment, *Int. J. Environ. Res. Public Health*, 14(8), 920, DOI: 10.3390/ijerph14080920., 2017.

International Journal of
*Environmental Research and Public Health*

MDPI

*Article*

# Impact of Orientation on the Vitamin D Weighted Exposure of a Human in an Urban Environment

**Michael Schrempf *, Nadine Thuns, Kezia Lange and Gunther Seckmeyer**

Institute of Meteorology and Climatology, Leibniz Universität Hannover, 30419 Hannover, Germany; thuns@muk.uni-hannover.de (N.T.); lange@muk.uni-hannover.de (K.L.); seckmeyer@muk.uni-hannover.de (G.S.)

* Correspondence: schrempf@muk.uni-hannover.de; Tel.: +49-511-762-3165

Academic Editor: Hanns Moshammer
Received: 19 June 2017; Accepted: 10 August 2017; Published: 16 August 2017

**Abstract:** The vitamin $D_3$-weighted UV exposure of a human with vertical posture was calculated for urban locations to investigate the impact of orientation and obstructions on the exposure. Human exposure was calculated by using the 3D geometry of a human and integrating the radiance, i.e., the radiant energy from the direct solar beam and the diffuse sky radiation from different incident and azimuth angles. Obstructions of the sky are derived from hemispherical images, which are recorded by a digital camera with a fisheye lens. Due to the low reflectivity of most surfaces in the UV range, the radiance from obstructed sky regions was neglected. For spring equinox (21 March), the exposure of a human model with winter clothing in an environment where obstructions cover 40% of the sky varies by up to 25%, depending on the orientation of the human model to the sun. The calculation of the accumulated vitamin $D_3$-weighted exposure of a human with winter clothing walking during lunch break shows that human exposure is reduced by the obstruction of buildings and vegetation by 40%.

**Keywords:** UV radiation; human exposure; vitamin D; urban environment; hemispherical sky images; radiance

## 1. Introduction

Ultraviolet radiation from the sun causes a considerable global disease burden, including acute and chronic health effects on the skin, the eyes and the immune system [1]. Negative effects of an increased UV exposure include, for example, erythema, sunburn and keratitis [2,3]. In addition, UV radiation is a fundamental parameter in the genesis of skin cancer [4,5]. On the other hand, UV is essential for the vitamin $D_3$ production of humans [1,6]. In the following, vitamin D is used as a general term, whereas we use the expression vitamin $D_3$ to describe UV-related issues. There is evidence that suggests vitamin D levels could be seen as an indicator of health risk relating to some sorts of cancers, infectious diseases (e.g., dental caries, pneumonia), and autoimmune diseases (e.g., diabetes mellitus type 1, multiple sclerosis) among others. Furthermore, there are established links with musculoskeletal health, Parkinson's disease and rickets [7,8]. Evidence is abundant that UVB exposure, vitamin D intake, and vitamin D concentrations are inversely correlated with many cancers (e.g., breast, lung, ovarian and colorectal cancer) [9–11]. The main source of vitamin D for humans is the vitamin D synthesis in the human skin due to solar UVB radiation (280–315 nm), although radiation between 280 and 290 nm is almost completely absorbed by ozone in the atmosphere. Dietary intake contributes only a small percentage (10%) to the necessary supply [12]. There are large seasonal differences in the production of vitamin D [13,14], which are mainly caused by the varying solar zenith angle and the different areas of skin that are exposed to solar radiation. Although vitamin $D_3$ can be stored

*Int. J. Environ. Res. Public Health* **2017**, *14*, 920 

in body fat and mobilized during winter months when little, if any, vitamin $D_3$ is produced in the skin [15], more than 50% of the German population have an insufficient vitamin D supply [16]. In this context, several studies refer to the so-called "vitamin D winter", which is the period of time where an adequate vitamin D status cannot be gained by solar UV exposure. The vitamin D winter for mid-northern latitudes is often stated to range from October to March [13,17–19]. Insufficient vitamin D levels can not only occur in winter time because of low UV exposure values, but also due to environmental obstructions (e.g., vegetation or buildings). The calculation of the vitamin $D_3$-weighted human exposure in an urban environment is necessary in order to estimate if sufficient vitamin $D_3$ could be synthesized in everyday situations.

## 2. Materials and Methods

### *2.1. State of the Art*

Earlier exposure investigations (e.g., by Diffey [17] and McKenzie et al. [20]) were based on the irradiance incident on horizontal or vertical surfaces. To better represent the UV dose of a human outdoors, Godar and Pope [21–23] converted the weighted irradiance of a horizontal plane into that of a cylinder by using geometric conversion factors. However, these theoretical estimations were performed for an unobstructed location only. Kawanishi [24] used hemispherical images to estimate the shadowing of the sky by sunscreens, although the subject of his study was the protection against erythemally-weighted radiation on a horizontal plane. Parisi et al. [25] included the shadowing of the sky by trees in their study of UV exposure. For their investigations, they used UV dosimeters on rotating mannequins that matched the stature of an average human. The instruments were distributed over the entire mannequin surface to measure the radiation on as much of the body surface area as possible. In a recent study, Parisi et al. [26] attached dosimeters at the vertex and forehead of a mannequin head and compared measurements conducted under different shade structures and in direct sun. However, rather than vitamin $D_3$-weighted human exposure, erythemally weighted doses were being investigated in these studies. Additionally, one single location may not be representative for an urban environment, because obstructions at different locations differ in shape and size, and therefore cover different parts of the sky. The irradiance on a horizontal surface should not be used for exposure calculations because the radiation field of the sky would have to be described by a single number only, which does not reflect the complex reality. Instead, the quantity "radiance" should be used (describing the radiant energy per unit solid angle and per unit area), thus taking into account the complex radiation field. Seckmeyer et al. [27] developed an exposure model based on radiance in combination with a 3D-voxel model of a human. Most surfaces show a very low reflectivity in the UV range, therefore the radiance from obstructed directions can be neglected, which enables the determination of the exposure of a human by calculating the multidirectional downwelling radiance originating from unobstructed directions. The obstructions of a location in an urban environment can, for example, be seen in Figure 1.

We refer to the method of Seckmeyer et al. [27] to calculate biologically-weighted human exposure by integrating the incident solar spectral radiance over all relevant parts of the human body. The area elements of the human model are defined as projection area $A_{\mathrm{proj}}$, which takes into account the geometrical properties as well as the clothing of the human.

We define the human exposure as the total biologically-weighted radiant energy received by the exposed body surfaces of a human. The equation for the calculation of the human exposure is given by:

$$Human\ exposure_{\mathrm{VitD}} = \int_{t_1}^{t_2} \int_{0}^{\pi/2} \int_{0}^{2\pi} L_{\mathrm{VitD}}(\varepsilon, \varphi, t) \cdot A_{\mathrm{proj}}(\varepsilon, \varphi)\, \mathrm{d}\varphi\, \mathrm{d}\varepsilon\, \mathrm{d}t. \quad (1)$$

where $L_{\mathrm{VitD}}$ is defined as the vitamin $D_3$-weighted radiance and the different directions in the sky are defined by the incident angle ($\varepsilon$) and the azimuth angle ($\varphi$). It should be noted that the quantity "human exposure", defined in Equation (1), must not be confused with the quantity "radiant exposure",

*Int. J. Environ. Res. Public Health* **2017**, *14*, 920 

which is defined by the CIE as the time integral of the irradiance [28]. In the following, the expression exposure always relates to the human exposure defined in this study.

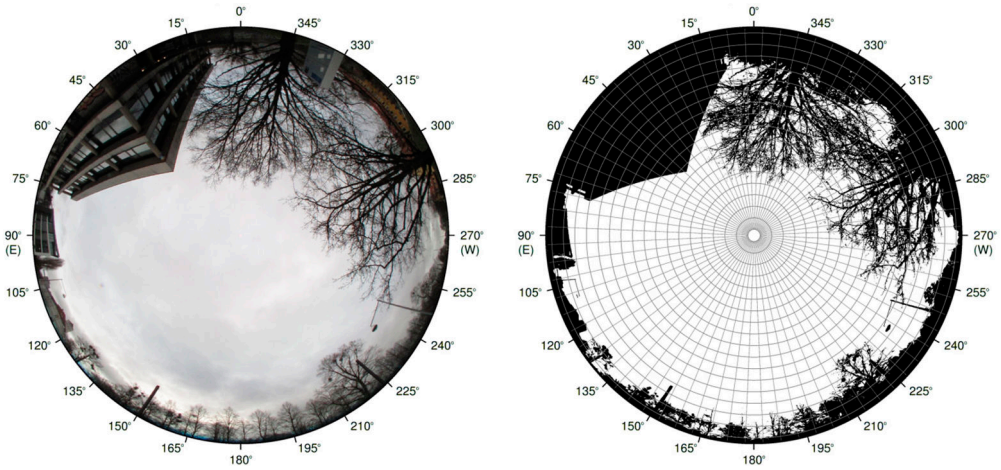


**Figure 1.** Hemispherical image taken in front of the Institute of Meteorology and Climatology of the Leibniz Universität Hannover (**left**) and the image with the derived obstruction information (**right**), where the derived obstructions shadowing the sky are shown in black and sky in white. The image is segmented by the grid shown, which illustrates the different directions (sky segments). The ratio of the amount of pixels characterized as obstructions and the total pixel count results in 39% obstructed sky.

The human model used in this study is based on a computed tomography scan of a patient, who is 38 years old, 176 cm of height, has a weight of 68.9 kg and skin type 2, and thus approximately represents an average male adult [27,29]. The model can wear winter clothing, where only face and hands are exposed (1455 $cm^2$ exposed skin area, 93% covered skin area to the total skin area) and also summer clothing, where face, neck, arms and hands are exposed (4160 $cm^2$ exposed skin area, 80% covered skin area to the total skin area). In Figure 2, the visualized voxel models wear winter and summer clothing, and are shown as front perspective from the direction $\varphi = 150$ and $\varepsilon = 30$.

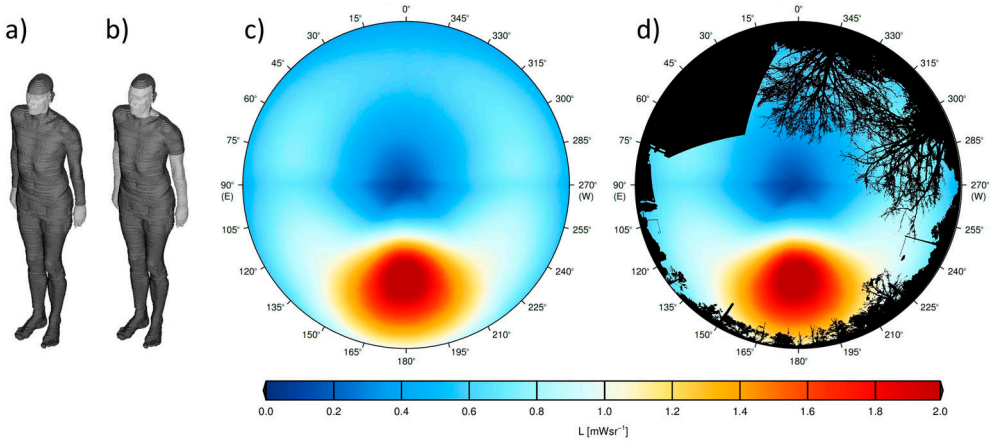


**Figure 2.** Visualization of the front of the model human with winter clothing (**a**) and summer clothing (**b**); The vitamin $D_3$-weighted radiance on 21 March at noon, weighted with the geometry of a human with winter clothing oriented south (180°) is shown in (**c**); The combination of the weighted radiance distribution from (**c**) and the obstruction information from Figure 1 is shown in (**d**).

### *2.2. Advanced Model*

The obstruction of the sky is calculated using hemispherical images taken by a digital camera with a fisheye lens (see, for example, Figure 1). The projection function of the fisheye lens is equidistant, which provides proper segmentation in equal solid angles [30]. For the derivation of the obstruction, a threshold with values between 0 and 255 is introduced, which is calculated as the mean of the count values of the red, green and blue color of each pixel, and can be expressed as:

$$threshold_{i,j} = \frac{red_{i,j} + green_{i,j} + blue_{i,j}}{3} \quad (2)$$

Pixels with a calculated threshold lower than 125 are defined as obstructions, the others are identified as unobstructed sky. Obstructions can best be detected in hemispherical images taken under overcast conditions, since the obstructions are relatively dark compared to the sky. The albedo of typical surfaces (e.g., street, concrete, vegetation) in the UVB wavelength region is small, with values between 0.02 and 0.1 [31,32]. Seckmeyer et al. [27] stated that for an albedo of 0.02, the extra exposure from an isotropic surface reflection is lower than 3% and can therefore be neglected for low albedo values. For this investigation, we assume that the reflectivity of the surface materials of the detected obstructions is low and can be neglected. It should be noted that this assumption may not be appropriate for some surfaces like snow or glass windows. However, snow wasn't present in our investigations and windows usually do not cover a large fraction of the sky.

Since the spatial resolution of the hemispherical images with about 3 million pixels is much larger than the spatial resolution of the different sky directions used in the exposure model (sky segments, see Figure 1), mean values of the high resolution obstruction information for each sky segment are calculated.

The obstructions derived from selected locations are implemented in the exposure model by extending the method of Seckmeyer et al. [27] by multiplying the obstruction information with the vitamin $D_3$-weighted radiance and the geometric factor of each direction. The formula for the calculation of the human exposure weighted with the obstruction information can be expressed as:

$$Human\ exposure_{\mathrm{VitD}} = \int_{t_1}^{t_2} \int_{0}^{\pi/2} \int_{0}^{2\pi} L_{\mathrm{VitD}}(\varepsilon, \varphi, t) \cdot obstruction(\varepsilon, \varphi) \cdot A_{\mathrm{proj}}(\varepsilon, \varphi)\, \mathrm{d}\varphi\, \mathrm{d}\varepsilon\, \mathrm{d}t. \quad (3)$$

For this study, the simulations were calculated by the DISORT code of the UVSPEC model in the LibRadTran package [33]. As input parameters, a total ozone column of 300 DU, a horizontal visibility of 50 km and an UV albedo of 0.02 were used. In Figure 2, the major contribution to the human exposure originating from areas around the solar disk can be recognized. It should be noted that these areas are still diffuse sky radiation; the solar disk that is the cause for direct irradiance has a much smaller area.

## 3. Results

In Seckmeyer et al. [27], it was shown that the impact of the orientation of an unclothed human on an obstruction free plane on 21 June at noon is less then ±4% and is primarily caused by the direct part of the solar radiation. In this study, we investigated the dependency of the orientation of a human with winter clothing in an urban environment. The human exposure on 21 March at noon (solar zenith angle of 52°) in front of the Institute of Meteorology and Climatology and in front of the university cafeteria strongly depends on the orientation, and is shown in Figure 3.

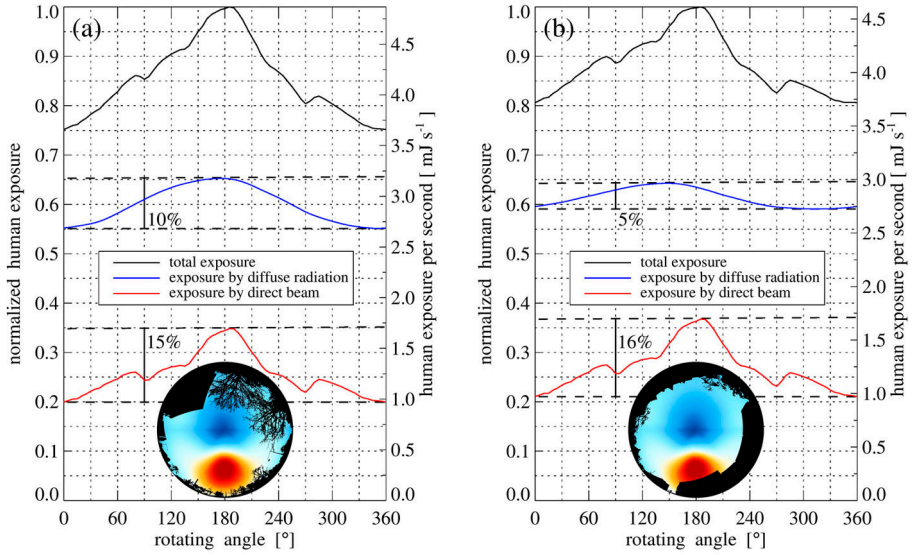


**Figure 3.** The vitamin $D_3$-weighted exposure of a human with winter clothing on 21 March at noon in front of the Institute of Meteorology and Climatology (**a**) and the university cafeteria (**b**) in normalized and absolute units. The human exposure depends on the orientation of the human model towards the sun. The total exposure (black line) is 25% (**a**) and 20% (**b**) smaller if the human is orientated with the face opposite to the sun (0°). The variation of the exposure by the diffuse part of the solar radiation of (**a**) is greater than of (**b**) due to a different distribution of the obstructions. The weighted radiance and the obstruction information of the locations are shown at the bottom of the plots (see also Equation (3) and Figure 2).

To mimic an everyday situation for students, the vitamin $D_3$-weighted exposure of a moving human was calculated for a winter and a summer scenario (see Table 1). The human is walking on 21 March and 21 June around noon on two different routes from the Institute of Meteorology and Climatology to the university cafeteria. The first route follows the streets "Nienburger Straße" and "Callinstraße" through built-up areas to the cafeteria and takes 10 min by foot. The second route follows a path through the "Georgengarten" and the street "Schneiderberg", takes 18 min and leads mainly through a recreational park (see also Figure 4). On both routes the human walked on the sunny side of the street to maximize the exposure to solar radiation. The obstruction information was derived in high spatial resolution by moving along the selected footpaths with a GPS-receiver with a sampling rate of 1 s and simultaneously taking hemispherical images with a sampling rate of 4 s. For each image the obstruction was calculated and the related geographic coordinates were assigned. The obstruction information were derived for winter conditions (without foliage) and summer conditions (with foliage).

To calculate the exposure of a moving human the obstruction information nearest to each coordinate of the GPS-receiver was selected and the actual vitamin $D_3$-weighted exposure was calculated according to Equation (3). The orientation of the human is necessary for the calculation, and is assumed to be the same as the direction of movement derived from the GPS-receiver data. The calculated exposure of a human with winter clothing walking to the university cafeteria on the two selected footpaths on 21 March is shown as a function of the time in Figure 5. The vitamin $D_3$-weighted human exposure on the first route ("Nienburger Straße") results in 2.1 J, and the human exposure on this route without obstructions would be 3.48 J. Therefore, the exposure is reduced to 2.1 J (60% of the unobstructed case) by buildings and vegetation. The 18 min walk on the second path through the recreational park results in a vitamin $D_3$-weighted exposure of 6.26 J for the unobstructed case or 3.94 J with obstructions (63% of the unobstructed case). The accumulated exposure after 10 min for the

two routes is very similar and results in a nearly equal vitamin $D_3$-weighted human exposure (see Figure 5).

**Table 1.** Calculated vitamin $D_3$-weighted exposure of a human walking to the university cafeteria on the two selected routes on 21 March and 21 June with winter and summer clothing, respectively. The values of the accumulated human exposure are given in joules (J) and international units (IU). The conversion to IU can be performed by multiplying the human exposure in J by the conversion factor of 70.97 (IU $J^{-1}$), as stated in [27].

| Route | Exposure of a Human 21 March (Winter Clothing) | | Exposure of a Human 21 June (Summer Clothing) | |
|---|---|---|---|---|
| | (J) | (IU) | (J) | (IU) |
| Built-up area (unobstructed) | 3.48 | 247 | 19.26 | 1367 |
| Built-up area (obstructed) | 2.10 | 149 | 10.14 | 720 |
| Recreational park (unobstructed) | 6.26 | 444 | 35.44 | 2515 |
| Recreational park (obstructed) | 3.94 | 280 | 16.28 | 1155 |

The calculated exposure of a human with summer clothing walking to the university cafeteria on the two selected footpaths on 21 June is shown as a function of the time in Figure 6. The vitamin $D_3$-weighted human exposure on the first route ("Nienburger Straße") results in 10.14 J and the exposure on this way without obstructions would be 19.26 J (53% of the unobstructed case). The 18 min walk on the second path through the recreational park results in a vitamin $D_3$-weighted human exposure of 35.44 J for the unobstructed case or 16.28 J with obstructions (46% of the unobstructed case).

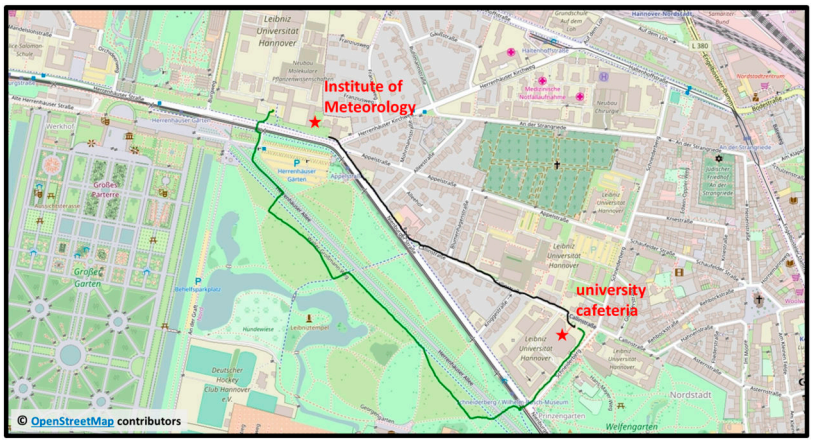


**Figure 4.** Visualized GPS-data of the two different routes used for the exposure calculation of a moving human in an urban environment. The routes start at the Institute of Meteorology and Climatology and end at the university cafeteria and follow paths through built-up areas (black line) and a recreational park (green line). Map data © OpenStreetMap contributors, CC BY-SA [34].

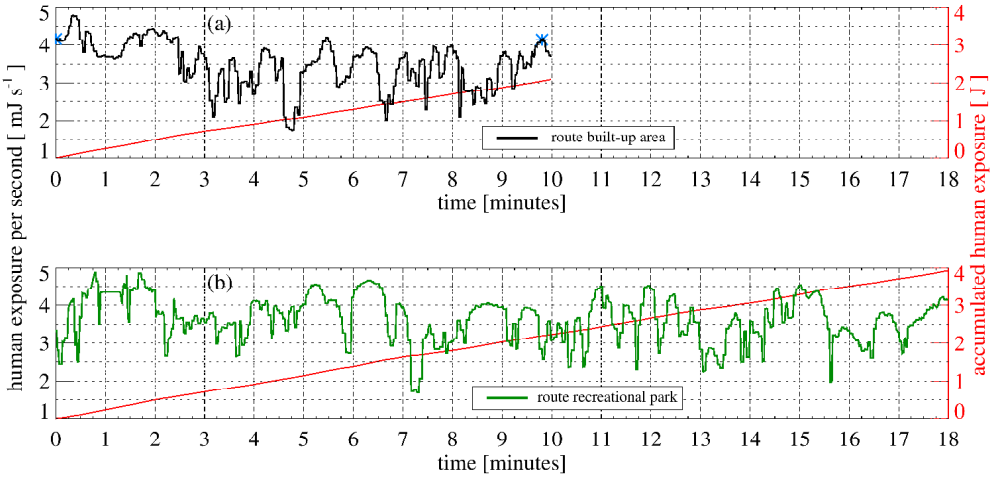


**Figure 5.** The calculated vitamin $D_3$-weighted exposure of a human with winter clothing walking to the university cafeteria on the two selected routes, through a built-up area (**a**) and through a recreational park (**b**), on 21 March is shown as a function of the time. Additionally, the accumulated exposure is displayed in red. The blue stars mark the locations shown in Figure 3.

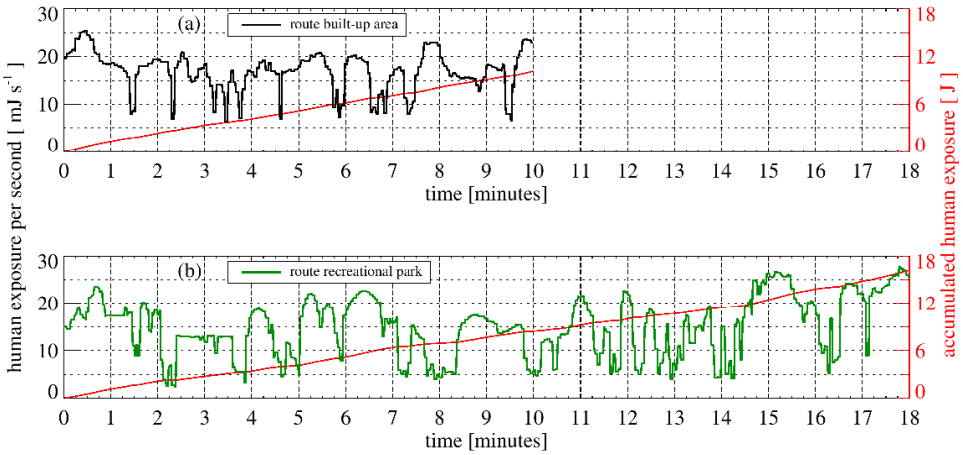


**Figure 6.** The calculated vitamin $D_3$-weighted exposure of a human with summer clothing walking to the university cafeteria on the two selected routes, through a built-up area (**a**) and through a recreational park (**b**), on 21 June is shown as a function of the time. Additionally, the accumulated exposure is displayed in red.

## 4. Discussion

When in front of the university cafeteria, and the human face is orientated directly away from the sun, the exposure is about 20% lower (see Figure 3b). This is caused both by direct sun and diffuse sky radiation around the sun. Although the contribution of the direct beam to the exposure is small compared to the contribution of diffuse sky radiation, the direct beam contributes significantly to the variation of the exposure due to different orientations. In comparison to the environment of Figure 3b, the variation of the exposure by diffuse sky radiation can increase when the diffuse sky radiation around the sun is unobstructed, and parts of the sky opposite the sun are covered by obstructions

(see Figure 3a). For a lower solar zenith angle than 52° used in Figure 3 (e.g., noon on 21 June), the absolute values are greater, but the relative shape of the functions remain nearly the same.

For the location in front of the institute on 21 March and a solar zenith angle of 75°, the direct component is only 8% of the total exposure when the human face is orientated towards the sun. The ratio of direct to diffuse exposure decreases with increasing solar zenith angle, and the diffuse component becomes the dominant factor in the variation of the exposure due to different orientations. However, the absolute exposure values for situations with greater solar zenith angles are small. Therefore, the dependence of the orientation on the exposure is of little importance in these situations.

The result of the accumulated exposure for the two investigated routes, with nearly equal values after 10 min, leads to the conclusion that vegetation in winter and spring (e.g., trees and bushes without foliage) may have a comparable impact on human exposure to buildings. However, the result of the accumulated exposure after 10 min with the obstruction information from summer showed that vegetation (e.g., trees and bushes with foliage) from the route through the recreational park has a greater impact on human exposure than buildings.

The results of this study show that, under clear sky situations, the exposure values for 21 March are still low, if only a few minutes of the lunch break are used for sun exposure. For 21 June, however, enough vitamin $D_3$ can be produced with a 20 min walk during lunch break in an urban environment, if 1000 IU are assumed to lead to an adequate vitamin D status [20,27,35,36]. To directly compare our values with the results of Webb and Engelsen [37] and Engelsen [38], we performed calculations for Boston with the same clothing and similar atmospheric conditions as used in these studies. The results of these calculations agree well with the values of [37,38] for the spring and summer scenarios. However, for 21 December, the exposure time from our exposure model is lower than the exposure time from Webb and Engelsen [37]. This is probably a result of the different exposure models (plane surface model [37] and 3-dimensional human exposure model [27]), and comparisons should therefore be treated with caution.

All results are calculated for clear sky conditions. In most cases, however, there are clouds. For these conditions, the exposure is further reduced by cloudiness. The effects of clouds are complex, and usually lead to a higher spatial and temporal variation of sky radiance compared to cloudless skies [39]. An investigation of the effects of clouds would therefore be desirable, but is beyond the scope of this paper. Additionally, a varying total ozone column also results in a varying exposure. Further, it should be noted that for the calculation of the vitamin $D_3$-weighted exposure, several simplifying assumptions were made, which are listed in Seckmeyer et al. [27].

Since the presented results are based on model calculations only, a validation of these calculations with measurements of the spectral radiance would be desirable. For this, a newly-developed technique may be used that measures the spectral radiance of more than 100 directions simultaneously [39]. Using this instrument, the complex and rapidly changing radiation field can be captured with a temporal resolution of seconds. However, such measurements are not yet operational, and could therefore not be used for this study. Additionally, it would be desirable to perform dosimeter measurements in an urban environment, and compare those with calculations from our exposure model. Personal dosimeters cannot replace spectroradiometer measurements, as the former often show large deviations from spectroradiometer measurements [40]. However, if dosimeters are carefully characterized and preselected, the use of dosimeters could extend the amount of data to estimate the exposure of a human in an urban environment.

## 5. Conclusions

There are large seasonal differences in the production of vitamin D that result in an insufficient vitamin D supply in humans living at middle or high latitudes. However, low UV exposure levels do not only occur in winter time; obstructions in urban environments have an impact on human exposure as well. In the current study, we demonstrated the exposure of a human in an urban environment to be dependent on the orientation of the human towards the sun. To maximize the UV exposure in an

urban environment, an orientation towards the sun should be chosen when possible. Additionally, human behavior—e.g., the location and time spent outside—is the prominent factor that determines the actual UV dose received (exposure integrated over time). For humans with the goal of spending time outside to produce vitamin $D_3$, a park may be more attractive and enjoyable than an urban environment. However, it was further shown that the accumulated exposure values of a moving human through a recreational park and a built-up area are about the same in winter time. This means that the impact of vegetation in winter and early spring (without foliage) on exposure is comparable to the impact of buildings. Thus, locations with as little obstructions as possible should be chosen to maximize the UV exposure and, consequently, vitamin $D_3$-production. To further improve the exposure calculation of everyday situations in an urban environment, instead of simulations of clear sky conditions, actual measurements of the sky radiation for different atmospheric conditions should be considered.

**Acknowledgments:** The publication of this article was funded by the Open Access fund of Leibniz Universität Hannover. We also thank Stefan Riechelmann from the Physikalisch-Technische Bundesanstalt, Braunschweig, Germany for his comments.

**Author Contributions:** Michael Schrempf and Gunther Seckmeyer conceived the idea to derive obstructions from hemispherical sky images in context of this study of urban exposure calculation. Gunther Seckmeyer had the idea to simplify the complexity of the exposure calculation by neglecting the contributions from the obstructed sky areas. Michael Schrempf designed this investigation and developed the extending algorithms. Kezia Lange provided the data of the radiance simulations. Nadine Thuns and Michael Schrempf performed the field measurements and analyzed the data. Michael Schrempf wrote the paper. All authors contributed substantially with comments and revised the manuscript.

**Conflicts of Interest:** The authors declare no conflicts of interest.

## References

1. Seckmeyer, G.; Zittermann, A.; McKenzie, R.; Greinert, R. Solar radiation: 13. Solar radiation and human health. In *Encyclopedia of Sustainability Science and Technology*; Geuymard, C., Ed.; Springer: New York, NY, USA, 2012; pp. 9649–9672.
2. Lucas, R.M.; McMichael, A.J.; Armstrong, B.K.; Smith, W.T. Estimating the global disease burden due to ultraviolet radiation exposure. *Int. J. Epidemiol.* **2008**, *37*, 654–667. [CrossRef] [PubMed]
3. Juzeniene, A.; Brekke, P.; Dahlback, A.; Andersson-Engels, S.; Reichrath, J.; Moan, K.; Holick, M.F.; Grant, W.B.; Moan, J. Solar radiation and human health. *Rep. Prog. Phys.* **2011**, *74*, 56. [CrossRef]
4. Lucas, R.; McMichael, T.; Smith, W.; Armstrong, B. Solar ultraviolet radiation: Global burden of disease from solar ultraviolet radiation. In *Environmental Burden of Disease Series, No. 13*; World Health Organization: Geneva, Switzerland, 2006.
5. Haluza, D.; Simic, S.; Höltge, J.; Cervinka, R.; Moshammer, H. Connectedness to nature and public (skin) health perspectives: Results of a representative, population-based survey among Austrian residents. *Int. J. Environ. Res. Public Health* **2014**, *11*, 1176–1191. [CrossRef] [PubMed]
6. World Health Organization, International Agency for Research on Cancer. *Vitamin D and Cancer*; Iarc Working Group Reports; WHO Press: Geneva, Switzerland, 2008; p. 148.
7. IARC, Working Group on Vitamin D. *Vitamin D and Cancer/A Report of the Iarc Working Group on Vitamin D*; IARC Working Group Report; World Health Organisation, International Agency for Research on Cancer: Lyon, France, 2008; p. 449.
8. Grant, W.B. The role of geographical ecological studies in identifying diseases linked to UVB exposure and/or vitamin D. *Dermato-Endocrinology* **2016**, *8*, e1137400. [CrossRef] [PubMed]
9. Moukayed, M.; Grant, W.B. Molecular link between vitamin D and cancer prevention. *Nutrients* **2013**, *5*, 3993–4021. [CrossRef] [PubMed]
10. Grant, W.B. Roles of solar uvb and vitamin D in reducing cancer risk and increasing survival. *Anticancer Res.* **2016**, *36*, 1357–1370. [PubMed]
11. Moukayed, M.; Grant, W.B. The roles of UVB and vitamin D in reducing risk of cancer incidence and mortality: A review of the epidemiology, clinical trials, and mechanisms. *Rev. Endocr. Metab. Disord.* **2017**, *18*, 167–182. [CrossRef] [PubMed]

12. Biesalski, H.K.; Köhrle, J.; Schürmann, K. *Vitamine, Spurenelemente Und Mineralstoffe*; Georg Thieme Verlag: Stuttgart, Germany, 2002; p. 820. ISBN 978-3-13-129371-8.
13. Webb, A.R.; Kift, R.; Durkin, M.T.; O'Brien, S.J.; Vail, A.; Berry, J.L.; Rhodes, L.E. The role of sunlight exposure in determining the vitamin D status of the U.K. White adult population. *Br. J. Dermatol.* **2010**, 1050–1055. [CrossRef] [PubMed]
14. Wabitsch, M.; Koletzko, B.; Moß, A. Vitamin-D-versorgung im säuglings-, kindes- und jugendalter. *Monatsschrift Kinderheilkd.* **2011**, *159*, 766–774. [CrossRef]
15. Holick, M.F. Vitamin D: Importance in the prevention of cancers, type 1 diabetes, heart disease, and osteoporosis. *Am. J. Clin. Nutr.* **2004**, *79*, 362–371. [PubMed]
16. Zittermann, A. The estimated benefits of vitamin D for Germany. *Mol. Nutr. Food Res.* **2010**, 1164–1171. [CrossRef] [PubMed]
17. Diffey, B.L. Is casual exposure to summer sunlight effective at maintaining adequate vitamin D status? *Photodermatol. Photoimmunol. Photomed.* **2010**, *26*, 172–176. [CrossRef] [PubMed]
18. Webb, A.R.; Kline, L.; Holick, M.F. Influence of season and latitude on the cutaneous synthesis of vitamin D3: Exposure to winter sunlight in boston and edmonton will not promote vitamin D3 synthesis in human skin. *J. Clin. Endocrinol. Metab.* **1988**, *67*, 373–378. [CrossRef] [PubMed]
19. Zeeb, H.; Greinert, R. Übersichtsarbeit: Bedeutung von vitamin D in der krebsprävention: Konflikt zwischen UV-schutz und anhebung niedriger vitamin-D-spiegel? *Dtsch. Arzteblatt-Arztliche Mitt.-Ausg. B* **2010**, *107*, 638–647.
20. McKenzie, R.L.; Liley, J.B.; Björn, L.O. UV radiation: Balancing risks and benefits. *Photochem. Photobiol.* **2009**, *85*, 88–98. [CrossRef] [PubMed]
21. Godar, D.E.; Pope, S.J.; Grant, W.B.; Holick, M.F. Solar UV doses of adult Americans and vitamin D3 production. *Dermato-Endocrinology* **2011**, *3*, 243–250. [CrossRef] [PubMed]
22. Godar, D.E.; Pope, S.J.; Grant, W.B.; Holick, M.F. Solar UV doses of young Americans and vitamin D3 production. *Environ. Health Perspect.* **2012**, *120*, 139–143. [CrossRef] [PubMed]
23. Pope, S.J.; Godar, D.E. Solar UV geometric conversion factors: Horizontal plane to cylinder model. *Photochem. Photobiol.* **2010**, *86*, 457–466. [CrossRef] [PubMed]
24. Kawanishi, T. Evaluation of ultraviolet radiation protection of a membrane structure using a uc shade chart. In Proceedings of the ANZAScA2010, Auckland, New Zealand, 24–26 November 2010.
25. Parisi, A.V.; Kimlin, M.G.; Wong, J.; Wilson, M. Personal exposure distribution of solar erythemal ultraviolet radiation in tree shade over summer. *Phys. Med. Biol.* **2000**, *45*, 349. [CrossRef] [PubMed]
26. Parisi, A.V.; Eley, R.; Downs, N. Determination of the usage of shade structures via a dosimetry technique. *Photochem. Photobiol.* **2012**, *88*, 1012–1015. [CrossRef] [PubMed]
27. Seckmeyer, G.; Schrempf, M.; Wieczorek, A.; Riechelmann, S.; Graw, K.; Seckmeyer, S.; Zankl, M. A novel method to calculate solar UV exposure relevant to vitamin D production in humans. *Photochem. Photobiol.* **2013**, *89*, 974–983. [CrossRef] [PubMed]
28. CIE. *S 017: ILV: International Lighting Vocabulary*; CIE: Vienna, Austria, 2011.
29. Valentin, J. Basic anatomical and physiological data for use in radiological protection: Reference values: Icrp publication 89. *Ann. ICRP* **2002**, *32*, 1–277. [CrossRef]
30. Tohsing, K.; Schrempf, M.; Riechelmann, S.; Schilke, H.; Seckmeyer, G. Measuring high-resolution sky luminance distributions with a ccd camera. *Appl. Opt.* **2013**, *52*, 1564–1573. [CrossRef] [PubMed]
31. Feister, U.; Grewe, R. Spectral albedo measurements in the UV and visible regions over different types of surfaces. *Photochem. Photobiol.* **1995**, *62*, 736–744. [CrossRef]
32. McKenzie, R.; Kotkamp, M.; Ireland, W. Upwelling UV spectral irradiances and surface albedo measurements at Lauder, New Zealand. *Geophys. Res. Lett.* **1996**, *23*, 1757–1760. [CrossRef]
33. Shettle, E.P. Models of Aerosols, Clouds, and Precipitation for Atmospheric Propagation Studies. In *Atmospheric Propagation in the UV, Visible, IR and mm-Region and Related System Aspects, Proceedings of the AGARD no. 454, Copenhagen, Denmark, 9–13 October 1989*; AGARD: Neuilly sur Seine, France, 1989.
34. Openstreetmap Copyright and License. Available online: http://www.openstreetmap.org/copyright (accessed on 14 August 2017).
35. Holick, M.F. Vitamin D deficiency. *N. Engl. J. Med.* **2007**, *357*, 266–281. [CrossRef] [PubMed]
36. Holick, M.F. Vitamin D: The underappreciated d-lightful hormone that is important for skeletal and cellular health. *Curr. Opin. Endocrinol. Diabetes Obes.* **2002**, *9*, 87–98. [CrossRef]

37. Webb, A.R.; Engelsen, O. Calculated ultraviolet exposure levels for a healthy vitamin D status. *Photochem. Photobiol.* **2006**, *82*, 1697–1703. [CrossRef] [PubMed]
38. Engelsen, O. The relationship between ultraviolet radiation exposure and vitamin D status. *Nutrients* **2010**, *2*, 482–495. [CrossRef] [PubMed]
39. Riechelmann, S.; Schrempf, M.; Seckmeyer, G. Simultaneous measurement of spectral sky radiance by a non-scanning multidirectional spectroradiometer (mudis). *Meas. Sci. Technol.* **2013**, *24*, 125501. [CrossRef]
40. Seckmeyer, G.; Klingebiel, M.; Riechelmann, S.; Lohse, I.; McKenzie, R.L.; Ben Liley, J.; Allen, M.W.; Siani, A.M.; Casale, G.R. A critical assessment of two types of personal UV dosimeters. *Photochem. Photobiol.* **2012**, *88*, 215–222. [CrossRef] [PubMed]

# 4 Human exposure based on radiance measurements, improved by simulations

Radiance is a multidimensional quantity (e.g. azimuth angle, zenith angle, time, wavelength), thus measurements of sky radiance are complex and extensive. Therefore, all investigations presented in this thesis so far are based on simulated radiances. Instead of using sky radiance simulations, measurements of sky radiance performed at a specific location are necessary in order to derive a more realistic exposure of a human. Commonly used instruments for radiance measurements are scanning instruments with an acquisition time of minutes. A system that can measure the radiance distribution of the sky in seconds, was recently developed at the Institute of Meteorology and Climatology (IMuK). With the development of this system, the idea evolved to integrate this instrument in realistic human exposure investigations. For this purpose, an extensive almost six month long campaign was organized and conducted. Due to the high complexity of the campaign and the enormous amount of data produced during this campaign (more than 3 terabyte and 4 million files), the work presented in this thesis primarily focuses on the development and validation of the methods to include radiance measurements in the exposure model. To demonstrate the applicability, a few results of actual human exposure calculations based on measurements are shown. The used instruments as well as the campaign setup are described in Section 4.1. In Section 4.2 a method is introduced to enhance the quality of the measured spectra in the UV wavelength region. These improved data are used to calculate the human exposure. In Section 4.3 the results of these calculations are shown.

## 4.1 Measurement campaign

A continuous winter measurement campaign was conducted from November 2014 to April 2015 on the measurement platform of the IMuK. The main objective of this campaign was to carry out long term simultaneous UV *radiance* measurements in high temporal resolution. In addition, the quantities *global irradiance* and *direct irradiance* were measured for the purpose of validation and the calculation of human exposure, respectively. Therefore, several different instruments were used in this campaign, which are described in Section 4.1.1. In Section 4.1.2 the campaign setup and the instrument settings are described.

### 4.1.1 Instruments

During the measurement campaign several different instruments were in operation. The main instrument of this campaign was the recently developed multidirectional spectroradiometer MUDIS. The other instruments were used for the calibration process of MUDIS, the validation and to derive additional radiometric quantities. In the following, the different instruments are described. A comparison of some of the instrument characteristics is shown in Table 4.1

- **Multidirectional Spectroradiometer (MUDIS)**
  MUDIS is a recently developed spectroradiometer, capable of simultaneously measuring the spectral radiance in 113 different directions in high temporal resolution. In contrast to scanning systems, the measurement duration of MUDIS is in the range of seconds. The instrument is based on a hyperspectral imager consisting of a UV-sensitive CCD

camera to which a bundle of optical fibers is attached. The other ends of the fibers are embedded in a hemispherical shaped dome in which the 113 fibers are evenly distributed in zenith and azimuth directions. MUDIS has been calibrated relative to the calibrated scanning CCD spectroradiometer (intercalibration), because the process as well as the equipment for a direct calibration was not fully developed at that time. MUDIS was used without the shading unit which prevents direct sunlight from reaching the entrance optics, because it was not operational at that time. Comparable to other array spectroradiometers, stray light is also a concern for MUDIS. The reasons are basically the same as for the scanning CCD spectroradiometer (see also the section below). Details of MUDIS, including the applied method for stray light correction, are described in Riechelmann (2014).
**Main purpose:** radiance measurements in high temporal resolution
**In operation:** November 2014 - April 2015

- **Scanning CCD Spectroradiometer (SCCD)**
  The SCCD system consists of a *BlackComet* CCD array spectroradiometer (StellarNet Inc., Tampa, Florida, USA), which is sensitive in the UV and visible wavelength range. Inside the CCD array spectroradiometer the signal is dispersed into a spectrum by a grating and detected by a CCD array detector. The major advantage of array spectroradiometers is their fast detection of the spectrum, the main disadvantage of array spectroradiometers is their inability to reduce stray light to an acceptable level (Seckmeyer et al., 2010). Stray light can be caused by imperfections of the diffraction grating, overlap of diffraction orders, but also by mirrors, screw heads and other surfaces (Riechelmann, 2014). As a result, the design of the CCD array spectroradiometer as a single monochromator leads to an inefficient rejection of stray light. This is a serious problem of array spectroradiometers because it limits the detectable radiance and if not corrected is a large contribution to the overall uncertainty (Seckmeyer et al., 2010). Attached to the instrument is a single radiance entrance optics via an optical fiber. The entrance optics is mounted on a positioning device *Skyscanner* (Czibula & Grundmann GmbH, Berlin, Deutschland) that is able to scan a desired pattern of points in the hemisphere. A SCCD sky scan identical to the MUDIS entrance optics dome pattern takes about 12 min (Riechelmann et al., 2013). The SCCD has been calibrated based on a 1000 W tungsten halogen lamp, which is traceable to the Physikalisch-Technische Bundesanstalt. Details on the calibration process are described in Pissulla et al. (2009).
  **Main purpose:** radiance measurements for intercalibration of MUDIS
  **In operation:** November 2014 - April 2015

- **Direct Normal Irradiance CCD Spectroradiometer (DNI-CCD)**
  The DNI-CCD system consists of a *SD2000* CCD array spectroradiometer (Ocean Optics, Dunedin, Florida, USA), which is sensitive in the UV and visible wavelength range. Since this instrument is similar to the *BlackComet* CCD array spectroradiometer, see also the section of the SCCD for more information about stray light. Attached to the instrument is a single direct irradiance entrance optics via an optical fiber. The entrance optics is mounted on a positioning device *VPT-501* (Eneo, Rödermark, Hessen, Deutschland) that is able to track the sun's path in the hemisphere. The DNI-CCD has been calibrated based on a 1000 W tungsten halogen lamp, which is traceable to the Physikalisch-Technische Bundesanstalt.
  **Main purpose:** direct irradiance measurements as input for the exposure model
  **In operation:** mid February 2015 - April 2015, technical problems with the positioning device prevented a prior use of the system

- **Double Monochromator-based Spectroradiometer (NDACC)**
  The spectroradiometer is a highly accurate instrument which complies with the Network for the Detection of Atmospheric Composition Changes (NDACC) standards and consists of a *DTMc300* double monochromator (Bentham Instruments Ltd., Reading, United Kingdom). The double monochromator consists of two identical single Czerny-Turner monochromators where stray light is suppressed by a number of baffles and slits (Wuttke et al., 2006). Because this type of monochromator uses a rotating dispersing element to consecutively focus a specific wavelength of the dispersed spectrum onto an exit slit, the NDACC spectroradiometer is a wavelength scanning instrument. Due to its superior stray light reduction and its wavelength accuracy this instrument is used as reference spectroradiometer (Riechelmann, 2014). A global irradiance entrance optics is attached to the instrument via an optical fiber. The NDACC instrument has been calibrated based on a 1000 W tungsten halogen lamp, which is traceable to the Physikalisch-Technische Bundesanstalt. The Instrument was operated by myself and Christopher Mustert.
  **Main purpose:** global irradiance measurements and reference instrument for validation purposes
  **In operation:** November 2014 - March 2015

- **Hemispherical Sky Imager (HSI)**
  The HSI system was developed at the IMuK and consists of a digital compact camera equipped with fisheye lens, which provides a field of view of 183° (Tohsing et al., 2013). The camera is mounted in a weatherproof housing and takes images of the entire hemisphere with an interval of one minute. The resulting images of the hemisphere have a diameter of about 2121 pixels and a resolution of about 3.5 million pixels. A mobile version of this HSI system was used in Articles C and D for the acquisition of hemispherical images to derive obstructions
  **Main purpose:** hemispherical images in high spatial and temporal resolution, used for visual illustration of the atmospheric conditions
  **In operation:** November 2014 - April 2015

**Table 4.1:** Overview of some characteristics of the measuring devices for a simple comparison between the instruments. * The DNI-CCD does not perform sky scans, however, there is angular dependence due to the tracked position of the sun over the day.

| | MUDIS | SCCD | DNI-CCD | NDACC | HSI |
|---|---|---|---|---|---|
| Quantity | $L$ | $L$ | $E_{direct}$ | $E$ | Images |
| Sensitive in the UV | YES | YES | YES | YES | |
| Spectral measurements | YES | YES | YES | YES | |
| Measurements within seconds | YES | YES | YES | | |
| Angular dependence of sky scan | YES | YES | YES* | | YES |
| Sky scan within seconds | YES | | | | YES |
| Superior stray light suppression | | | | YES | |

For further details of the instruments please also see Riechelmann (2014).

### 4.1.2 Campaign setup

The campaign setup is based on campaigns performed in 2012 and 2013, which are described in more detail in Riechelmann et al. (2013) and Riechelmann (2014). MUDIS, SCCD, NDACC and HSI were set up end of October on the measuring platform at the IMuK. The DNI-CCD for the direct irradiance measurements was set up in February, after technical problems with the positioning device were solved. With exception of the HSI, all instruments were operated in two weatherproof and temperature stabilized boxes, which provided a 20°C ambient temperature. The variation of the temperature in the box of NDACC, SCCD and DNI-CCD was less than ±1°C. The variation of the temperature in the box of MUDIS was less then ±3°C. Although the spectral ranges of all spectroradiometers were different, there was an overlap in the wavelength range 280-680 nm. Because the sampling intervals of the instruments were also different, the measurements were interpolated to a sampling interval of 0.25 nm. In addition, the bandwidths of the instruments were different (e.g. the NDACC instrument has a much smaller bandwidth than the MUDIS). In order to compare measurements of different instruments, the spectra were convoluted with an appropriate slit function. To ensure the comparability of data with a high temporal resolution from different instruments, the computer clocks of all systems were set to be automatically synchronized by an internet time server once a day. Due to the different measurement techniques and measured quantities, the instruments have different spatial and temporal settings, which are listed in the following.

- **MUDIS:** The measurement of the whole pattern is performed simultaneously with an integration time of 100 ms and 50 averages, resulting in a measurement duration of about 5 s for one scan. The measurement of a scan is repeated every 10 seconds.
- **SCCD:** With an integration time of 50 ms and 40 averages, the radiance measurement of a single direction takes about 2 s. Including the movement of the positioning device, this results in a measurement duration of 12 minutes for the scan of the whole sky pattern.
- **DNI-CCD:** The direct irradiance is measured every 5 s with an integration time of 3 ms and 50 averages.
- **NDACC:** The NDACC instrument is a wavelength scanning device which leads, with the settings used in this campaign, to a measurement duration of about 19 minutes for a complete spectrum of the global irradiance. The measurements were repeated every 20 minutes.
- **HSI:** Every minute three images with an exposure time of 1/500 s, 1/1000 s and 1/2000 s and with an aperture of F4 are taken.

Measurements have been carried out starting about 30 minutes before sunrise and ending about 30 minutes after sunset every day. As mentioned in Section 4.1.1, the SCCD, DNI-CCD and NDACC instrument have been calibrated in the laboratory based on a 1000 W tungsten halogen lamp, which has been calibrated by the Physikalisch-Technische Bundesanstalt. The change in sensitivity through the transport of the instruments to the measuring platform was checked and corrected by using a field calibrator and 100 W lamps. With each instrument, measurements of the 100 W lamps were performed in the field calibrator before and after the transport. The ratio between lab and field measurement yields the change to the lab calibration. With the same method, the stability of the instruments during the campaign was analyzed weekly. As mentioned in Section 4.1.1, the MUDIS instrument was intercalibrated with the SCCD. This was done by comparing synchronized data sets from MUDIS and SCCD, which is described in detail in Riechelmann et al. (2013) and Riechelmann (2014).

## 4.2 Improvement of UV-radiance measurements by simulations

Figure 4.1 shows the vitamin $D_3$-weighted spectrum of the global irradiance, measured by the NDACC spectroradiometer on 21 November 2014 at 11:00 UTC at the IMuK at overcast conditions. It illustrates the vitamin $D_3$-weighted spectrum in colored 5 nm regions and the corresponding percentage of these regions to the integral of the weighted irradiance. Figure 4.1 also shows that the wavelength region 305-315 nm makes up almost 80 % of the integrated vitamin $D_3$-weighted irradiance, which expresses the importance of this wavelength region in the UVB. For clear sky conditions, the spectrum would be slightly shifted to smaller wavelengths, however, the overall result would remain almost the same. The amount of

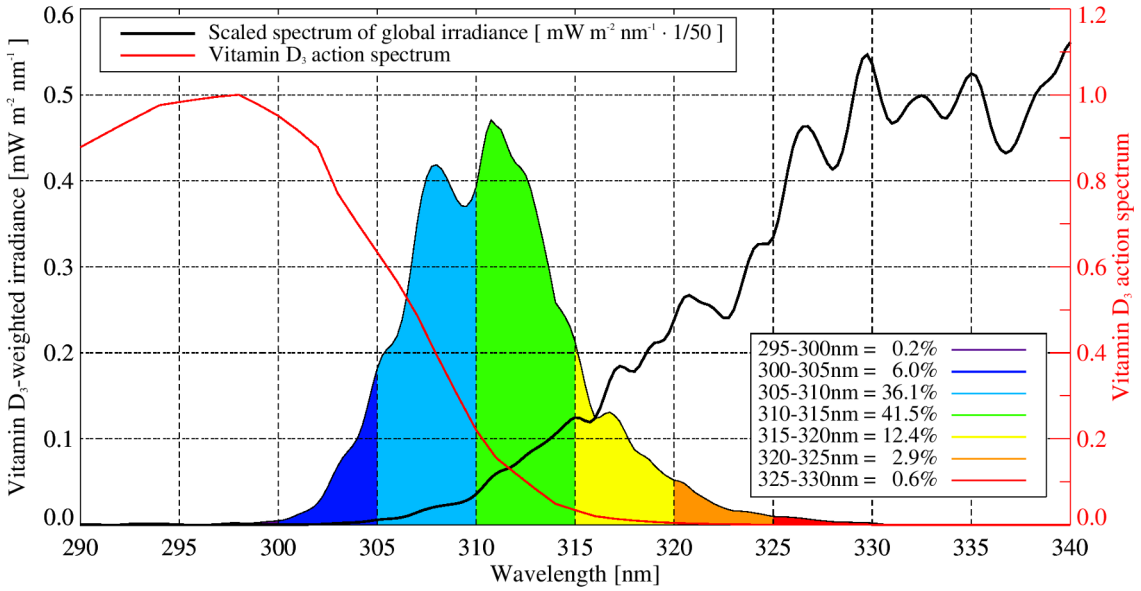


**Figure 4.1:** Vitamin $D_3$-weighted irradiance measured by the NDACC spectroradiometer on 21 November 2014 at 11:00 UTC at the IMuK at overcast conditions. The percentage of 5 nm regions to the total weighted irradiance is calculated and displayed as colored regions (another 0.3 % are provided by 280-295 nm). In addition, the scaled unweighted spectrum of the irradiance (black line) and the vitamin $D_3$ action spectrum (red line) are shown.

radiation in the UVB reaching the Earth's surface is very low and can only accurately be measured with very sensitive instruments with excellent stray light reduction. As mentioned in Section 4.1.1, the NDACC instrument complies with these requirements, however, it is a wavelength scanning device and therefore not suitable for radiance measurements with high temporal resolution. Although the measurement duration of array spectroradiometers (e.g. MUDIS, SCCD) is very short, the UVB radiation can mostly not accurately be measured by these instruments and therefore not directly be used in vitamin $D_3$-related investigations. A comparison of measurements of the campaign performed within this thesis showed that vitamin $D_3$-weighted MUDIS measurements are often about a factor of three higher or lower than the vitamin $D_3$-weighted NDACC measurements (see validation of extension method in Section 4.2.3). This demonstrates the need for a method to enhance the measured spectra in the UVB. In order to nevertheless use MUDIS radiance measurements, an extension method was developed that spectrally substitutes and extends parts of the measured spectra with an adjusted radiative transfer simulation. This extension method is presented in Section 4.2.1.

Because no radiance measurements could be conducted with the NDACC instrument during the winter campaign, radiance measurements performed in the summer by Riechelmann

(2014) have been used for the introduction of the extension method as well as for parts of the validation shown in Section 4.2.2. The validation of the applied extension method on radiance measurements of the winter campaign is shown in Section 4.2.3.

### 4.2.1 Extension method

The extension method is based on the assumption that the considered measured spectrum is correct starting from a defined wavelength, here denoted as $SWE$ (starting wavelength of extension method). Below the $SWE$, the measured spectrum is substituted by a simulation, adjusted based on the measurement above the $SWE$ and the ozone satellite measurement of the corresponding day. This way, the measurement can be improved below the $SWE$ and even extended below the detection threshold of the instrument. The simulated spectra necessary for the extension method are provided by a five-dimensional lookup table. In the following the dimensions of the lookup table are listed:

- **dimension 1:** simulated radiance values of the zenith angles
- **dimension 2:** simulated radiance values of the azimuth angles
- **dimension 3:** spectral information of the simulated radiance values, ranging from 280-400 nm with a wavelength interval of 0.25 nm
- **dimension 4:** solar zenith angles (SZA) ranging from 28°-90°
- **dimension 5:** ozone ranging from 250 DU - 500 DU in 5 DU intervals

The spectra stored in the lookup table are calculated for clear sky conditions with the radiative transfer model UVSPEC from the libRadtran package (Mayer and Kylling, 2005), which was already mentioned in Section 2.1.1. For each measurement, the corresponding simulated radiance spectrum must be selected from the lookup table.

The ozone value of the corresponding day of the measurement is extracted from the NIWA combined total column ozone data base by Bodeker et al. (2001) which was created for Hannover and provided by J. Ben Liley[1]. In this database, the total ozone column is listed for each day. Once the simulation is selected, it is adapted to the corresponding measurement by multiplication with a linear correction function. This function is derived from the ratio of measurement and simulation above the $SWE$. In Figure 4.2, the ratios of a clear sky zenith measurement and a cloudy zenith measurement to the corresponding simulations are shown. Due to their wavelength dependent transmission, clouds affect the ratio between measured and simulated spectra from the lookup table calculated for clear sky conditions. In this case, the ratio shows a wavelength dependent tilt compared to the case of clear sky (see Fig. 4.2). Seckmeyer et al. (1996) showed that the slope of the transmission of clouds in the UV range is almost constant for thin clouds. Despite a cloud type dependent slope of the transmission, a nearly linear function can be assumed for ratios of measurements under cloudy conditions and clear sky model simulations. It should be noted that the ratio of the overcast case of Figure 4.2 shows a particularly steep slope, which does not represent the general ratio of a cloudy condition and clear sky model simulation. However, it demonstrates the overall applicability of the method as shown in Section 4.2.2.

By fitting the ratio in the wavelength range between the $SWE$ and 400 nm with a first degree polynomial equation, a fit function $fit_{ratio}(\lambda)$ can be calculated (see also Eq. (4.1)).

$$fit_{ratio}(\lambda) = \text{fitting-function}\Big(ratio_{\,SWE-400\text{nm}}\Big) \tag{4.1}$$

[1] personal communication, J. Ben Liley, National Institute of Water & Atmospheric Research (NIWA), Lauder, New Zealand

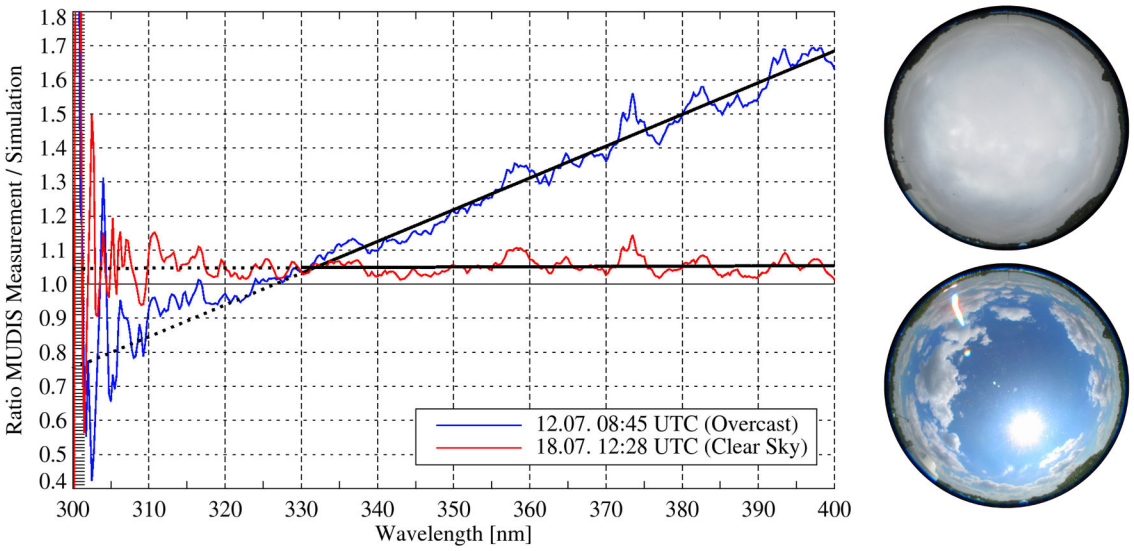


**Figure 4.2:** Ratios of two MUDIS zenith measurements from the campaign by Riechelmann (2014) to simulations are shown. Also displayed are the linear fits calculated for the wavelength range 330 - 400 nm (solid black lines) and the extrapolated parts of the fits (dotted black lines). Hemispherical images for the times of both measurements are placed on the right.

The calculated fit functions of both ratios as well as the extrapolated parts of the fit functions are also displayed in Figure 4.2.
The spectrum of the adjusted simulation is derived by multiplying the fit function with the simulation.

$$adjusted\ simulation(\lambda) = simulation(\lambda) \cdot fit_{ratio}(\lambda) \tag{4.2}$$

To obtain the extended MUDIS spectrum, the wavelength region from 280 nm $-$ $SWE$ of the uncorrected MUDIS spectrum is substituted with the corresponding spectral range of the adjusted simulation. This is shown in equation (4.3).

$$extended\ MUDIS(\lambda) = \begin{cases} adjusted\ simulation(\lambda)\,, & 280\,\text{nm} \leq \lambda \leq SWE \\ MUDIS\ measurement(\lambda)\,, & SWE < \lambda \leq 400\,\text{nm} \end{cases} \tag{4.3}$$

In Figure 4.3, synchronized NDACC, uncorrected MUDIS and extended MUDIS spectra of the same measurement times as presented in Figure 4.2 are shown. In addition, the ratios between the MUDIS and the NDACC spectra are displayed. While the ratios between uncorrected MUDIS and NDACC measurements show high variations below 310 nm, the variations of the ratios between extended MUDIS data and NDACC measurements are within 10 %. This result shows that the extension method works for radiance measurements for clear sky as well as for overcast conditions. In this thesis, the $SWE$ was set to 330 nm, because an investigation showed better agreements between NDACC and extended MUDIS data with this value than with values of shorter wavelengths.

Further results of the applied extension method and the demonstration of the diurnal applicability are presented in the following validation sections.

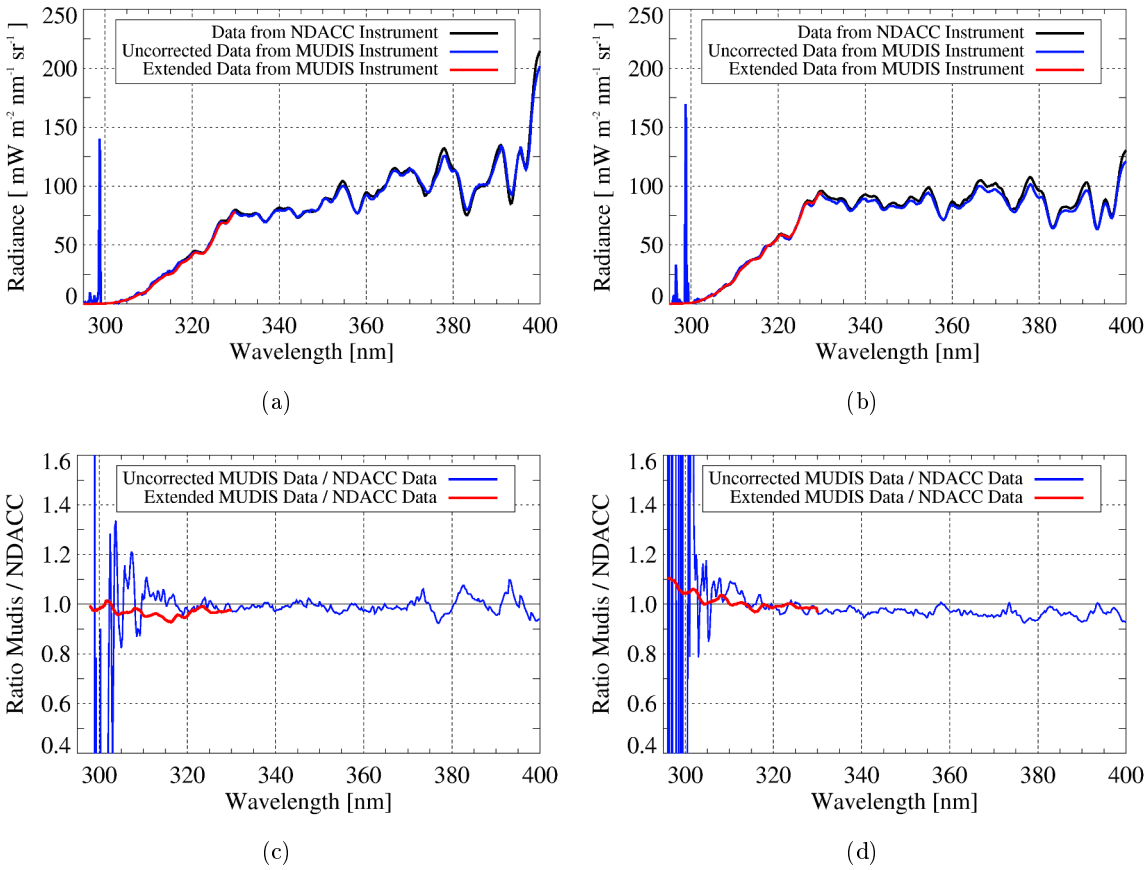


**Figure 4.3:** Synchronized NDACC, uncorrected MUDIS and extended MUDIS spectra of the zenith radiance measurements at IMuK are shown for 12 July 2013 at 8:45 UTC (Overcast; a) and for 18 July 2013 at 12:25 UTC (Clear Sky; b). The times indicate the start times of the NDACC instrument scan. The ratios of the synchronized MUDIS and NDACC spectra of the upper plots are displayed in (c) and (d), respectively. In contrast to the ratios of MUDIS and NDACC measurements, the variations of the ratios between extended MUDIS data and NDACC measurements are within 10 %.

### 4.2.2 Validation of extension method with NDACC zenith radiance measurements

For the validation of the extension method, the NDACC and MUDIS zenith radiance measurements of the 2013 summer campaign by Riechelmann (2014) were used. The campaign took place from 12 July to 19 July 2013 on the measuring platform at the IMuK. During this campaign, different cloud conditions (i.e. cloud cover and cloud type) prevailed, including clear sky, broken cloud and overcast conditions (for more details see Riechelmann (2014)). These days therefore provided a useful database for the validation. However, it should be noted that only zenith measurements were conducted by the NDACC instruments during this campaign.

The extension method was applied on the uncorrected MUDIS spectra and then synchronized with all of the NDACC measurements of the campaign. In Figure 4.4, the diurnal variation of the synchronized vitamin $D_3$-weighted radiances from 12 July are shown. In addition, the ratios of these MUDIS and NDACC radiances are plotted. It can be seen that vitamin $D_3$-weighted uncorrected MUDIS measurements are mostly more than 25 % higher or lower than vitamin $D_3$-weighted NDACC measurements. The vitamin $D_3$-weighted radiances, calculated from the extended MUDIS data are in good agreement with the mea-

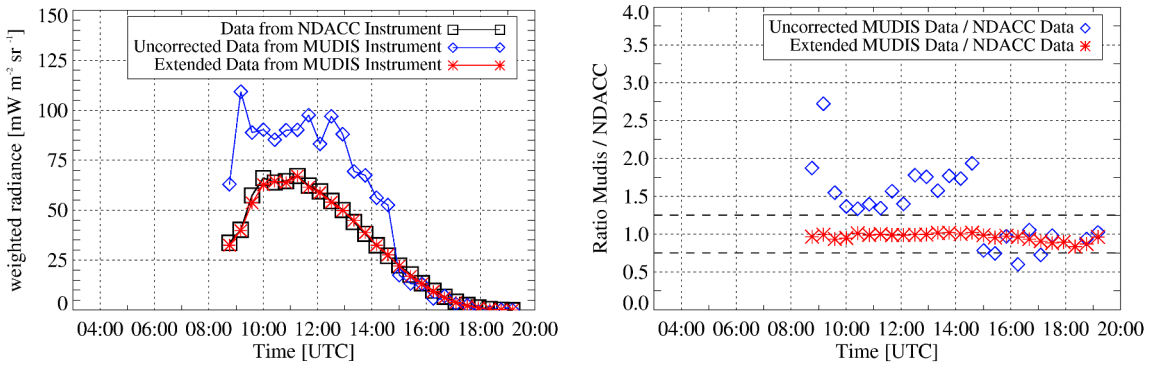


(a) (b)

**Figure 4.4:** Diurnal variation of synchronized vitamin $D_3$-weighted radiances, calculated from NDACC, uncorrected MUDIS and extended MUDIS data of 12 July 2013 (a). In plot (b) the ratios of synchronized MUDIS and NDACC data are shown. The two horizontal black dashed lines mark the region between 0.75 and 1.25.

surements of the NDACC instrument over the entire day. In Figure 4.5, the ratios of all synchronized vitamin $D_3$-weighted MUDIS and NDACC radiances of the 2013 summer campaign are plotted. The vitamin $D_3$-weighted radiances, calculated from the extended MUDIS

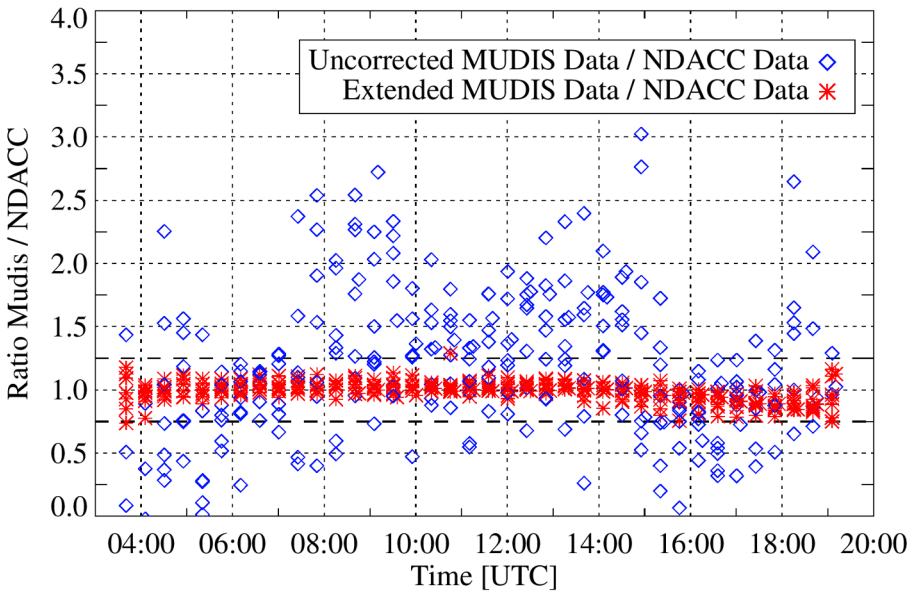


**Figure 4.5:** Ratios of all synchronized vitamin $D_3$-weighted MUDIS and NDACC radiances from the 2013 summer campaign of Riechelmann (2014). The two horizontal black dashed lines mark the region between 0.75 and 1.25.

data, are in good agreement with the NDACC measurements over all days of the campaign, whereas the vitamin $D_3$-weighted uncorrected MUDIS radiance is up to a factor three higher than the NDACC radiance. These results demonstrate the diurnal and general applicability of the extension method.

As mentioned above, only zenith radiance measurements were performed with the NDACC instrument during the 2013 summer campaign. This is due to the long measurement duration of about 20 minutes for one spectrum. Because a complete scan of the MUDIS pattern

with the NDACC instrument would take about 38 hours, it is not feasible to measure the radiance in more than one direction. Therefore, only the zenith direction of the MUDIS radiance measurements was validated. However, the zenith direction has in no aspect any special characteristics compared to the other directions. Furthermore, the radiances from all directions are measured in exactly the same way, due to the simultaneous measuring principle of MUDIS. As a consequence of these facts, it is assumed that all other directions would yield the same result as the presented validation. Beside of this assumption, the radiance measurements from all directions are validated in Section 4.2.3 based on the diffuse irradiance.

### 4.2.3 Validation of extension method with NDACC diffuse irradiance measurements

The extension method was also validated with measurements of the 2014/2015 winter campaign performed within this thesis. Analogous to the validation in the previous section, the extension method was applied to the uncorrected MUDIS radiances. However, because the NDACC instrument measured global irradiance in this campaign, no direct comparison of radiance measurements could be performed. In order to use the NDACC irradiance measurements for the validation, the MUDIS radiance spectra were integrated to diffuse irradiance spectra with Equation (2.18) described in Section 2.2. At last, the uncorrected MUDIS, extended MUDIS and NDACC irradiances were synchronized and weighted with the vitamin $D_3$ action spectrum. In Figure 4.6, the diurnal variation of synchronized vitamin $D_3$-weighted irradiances, calculated from NDACC, uncorrected MUDIS and extended MUDIS data of 21 November 2014 are shown. The vitamin $D_3$-weighted irradiances calculated from the extended MUDIS data are in good agreement with the NDACC measurements over the entire day, whereas the vitamin $D_3$-weighted uncorrected MUDIS irradiance shows large deviations. As can be seen in the ratios plotted in Figure 4.6, the extended MUDIS data lies within 10 % of the NDACC irradiance. In contrast to these values, the vitamin $D_3$-weighted uncorrected MUDIS irradiance is often up to a factor four higher. To validate the applied extension

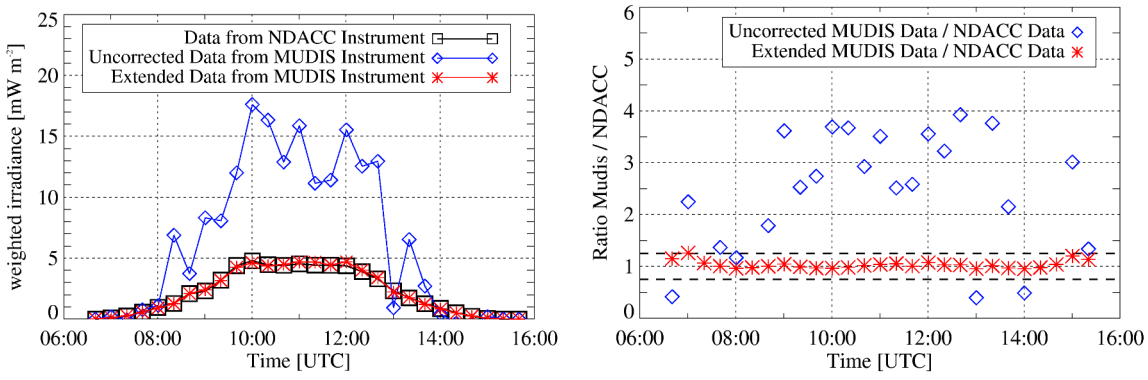


(a) (b)

**Figure 4.6:** Diurnal variation of synchronized vitamin $D_3$-weighted irradiances, calculated from NDACC, uncorrected MUDIS and extended MUDIS data for 21 November 2014 (a). In plot (b) the ratios of synchronized MUDIS and NDACC data are shown. The two horizontal black dashed lines mark the region between 0.75 and 1.25.

method for a longer time span, measurements of the months November and December were analyzed. From these months all days were used where the direct beam of the sun was blocked by clouds. This is important, because MUDIS can only measure diffuse radiance.

The global irradiance entrance optics of the NDACC instrument, however, receives both diffuse and direct radiation from all directions. Therefore, only diffuse irradiances derived by these two instruments can be compared. In Figure 4.7, the ratios of all synchronized vitamin $D_3$-weighted MUDIS and NDACC irradiances of November and December are plotted. The

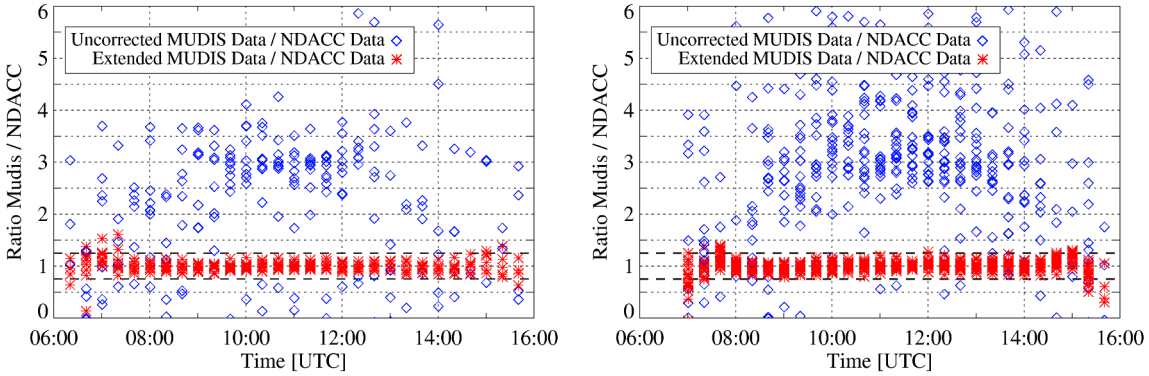


(a) (b)

**Figure 4.7:** Ratios of synchronized vitamin $D_3$-weighted MUDIS and NDACC irradiances of November 2014 (a) and December 2014 (b). Shown are all the diffuse irradiances of days, where the direct beam of the sun was blocked by clouds. The two horizontal black dashed lines mark the region between 0.75 and 1.25.

vitamin $D_3$-weighted irradiances, calculated from the extended MUDIS data, are in good agreement with the NDACC measurements over all days of November and December. In contrast, the ratios of vitamin $D_3$-weighted uncorrected MUDIS and NDACC irradiances show high variations, with values of the uncorrected MUDIS irradiance up to a factor six higher than the NDACC irradiance. In comparison to the ratios of the synchronized MUDIS and NDACC measurements of the 2013 summer campaign (Fig. 4.5), the ratios of the synchronized MUDIS and NDACC measurements of the months November and December 2014 (Fig. 4.7) show overall higher deviations. Nevertheless, the extended MUDIS data derived by the extension method shows an overall good agreement, with deviations less than 25% for almost the entire day. This is illustrated by the horizontal black dashed lines in Figure 4.7, which mark the region between 0.75 and 1.25.

In addition to the validation results presented in Section 4.2.2, these results demonstrate the diurnal and general applicability of the extension method for the MUDIS measurements conducted in the 2014/2015 winter campaign.

### 4.2.4 Discussion

As described in the Sections 4.2.2 and 4.2.3, measurements from two campaigns, from 12-19 July 2013 (summer campaign) and from November-December 2014 (winter campaign), have been used for the validation of the extension method. During both campaigns, various weather conditions prevailed with different cloud conditions concerning cloud cover (including clear sky, broken cloud, overcast conditions) and cloud type (including Cirrus, Cumulus, Stratus, Nimbostratus), which was documented based on hemispherical sky images from the HSI system. The representativeness of the measurement times used in the validation has been analyzed by pyranometers operated by the IMuK. The total diffuse irradiance of the months July, November and December was compared to the corresponding averages over the years 2009-2016. For July 2013, the results showed a deviation of 2 % to the average which is within its standard deviation of 7 %. For the months November and December 2014, the deviation

to the average was 2 % and 12 %. With a standard deviation of 3 % and 9 %, November is representative for other years, whereas the deviation for December is slightly higher than the standard deviation. An extensive representativity study, which was performed for the winter campaign measurements within another thesis, came to the same conclusions (see Section 3; Seckmeyer et al., submitted ). It was shown that the mean irradiance of December 2014 was lower than most other years, which can be attributed to a higher cloud impact. However, the good agreement between NDACC and extended MUDIS measurements for December 2014 demonstrates the functionality of the extension model even for months with higher cloud impact (see Figure 4.7).

For the validation, synchronized spectra of NDACC, uncorrected MUDIS and extended MUDIS measurements have been used. Since the measurement duration for a NDACC spectrum (280 - 330 nm) is about 240 s and radiance measurements were acquired every 12 s (summer campaign) and 10 s (winter campaign), a synchronized spectrum consists of 20 and 24 MUDIS measurements, respectively. For the 8 days of the 2013 summer campaign 292 synchronized spectra are available, thus resulting in about 5 800 MUDIS measurements which were involved in the validation. For the validation based on the months November and December, 256 and 553 synchronized spectra have been used. This results in more than 19 000 MUDIS measurements in total that have been applied for the validation.

Since UV radiation below 340 nm is absorbed by ozone and the absorption increases with decreasing wavelength, it should be noted that the total ozone column is the most important input parameter concerning the application of the extension model. Therefore, the selection of the radiance simulation with the correct total ozone column is particularly important. Because of this reason the ozone values of the corresponding days were taken from the NIWA combined total column ozone data base by Bodeker et al. (2001) which was created for Hannover and provided by J. Ben Liley. Although the validation showed good agreements between reference data and extended data, selected ozone values from this database may not be completely correct. Investigations have shown that, if a spectrum was selected that was simulated for a 30 DU higher ozone value, the resulting ratio between NDACC spectrum and the synchronized extended MUDIS spectrum was shifted up to 20 %. For a more accurate error estimate, an extensive investigation of the impact of the ozone input parameter on the extension method for different atmospheric conditions must be conducted in the future.

Due to the high uncertainties in the wavelength range below 330 nm of the measured radiance spectra of the winter campaign, a $SWE$ of 330 nm was used. As mentioned before, this value was chosen, because an investigation showed better agreements between NDACC and extended MUDIS data with this value than with shorter wavelengths values. An investigation showed that the vitamin $D_3$-weighted extended MUDIS measurements based on a $SWE$ of 320 nm can be up to about 20 % higher or lower than vitamin $D_3$-weighted extended MUDIS measurements based on a $SWE$ of 330 nm. However, exemplary calculations also have shown that for some measurements of the 2013 summer campaign a $SWE$ down to 315 nm could be used with similar results as with a $SWE$ of 330 nm. This is due to the fact that most of the uncertainties in these spectra are below 310 nm, which can also be seen in Figure 4.3. In comparison to the 2013 summer campaign, the higher uncertainties above 310 nm in the spectra of the 2014/2015 winter campaign are attributed to slightly wrong offset settings in the stray light correction of the MUDIS measurements. The MUDIS post-processing routines were restructured and converted from a text-file-based to a NetCDF-file-based version by a third party before the application in this thesis. As a result, it seems that in the new post-processing routines new offset settings are required, which may not have been perfectly set. However, in Riechelmann et al. (2013) and Riechelmann (2014) several additional parameters are stated which can cause the differences in the uncertainties of the measurements from the summer and the winter campaign. Beside the different seasons, the wider field of

view of MUDIS compared to the SCCD and uncertainties of the SCCD positioning unit and the tilt of the field of view of the individual MUDIS fibers could be given as examples.

It can be stated that a lower $SWE$ could be used, if the uncertainties in the measured spectra are reduced. Although the cases presented in this chapter can be seen as examples and the validation was not performed for the months January - April, based on the facts discussed above and the results of the validation of the extension method presented in Section 4.2.2 and Section 4.2.3, the extension method is found to be generally applicable for vitamin $D_3$-related investigations.

## 4.3 Vitamin $D_3$-weighted human exposure calculations based on measurements

To calculate the actual vitamin $D_3$-weighted human exposure for the months November - April, the radiance measurements performed with MUDIS and the direct irradiance measurements performed with the DNI-CCD were used. Both measurements are described in Section 4.1. For the calculations of the human exposure, the exposure model described in Section 2.1 was used. For the calculation only days were considered, where measurements are available from sunrise to sunset (scenario 1) and from 11:00-12:00 UTC (scenario 2). The number of days that met these requirements are listed in Table 4.2. As mentioned in Section

**Table 4.2:** Number of days, where MUDIS measurements are available from sunrise to sunset and from 11:00-12:00 UTC. In addition, the number of days with direct irradiance measurements from 11:00-12:00 UTC are listed. The measurements started on 8 November (radiance) and 7 February (direct irradiance) and ended on 24 April.

| Month | **MUDIS radiance** days with measurements from sunrise to sunset | **MUDIS radiance** days with measurements between 11 - 12 UTC | **direct irradiance** days with measurements from sunrise to sunset |
|---|---|---|---|
| November | 17 / 23 | 21 / 23 | - |
| December | 26 / 31 | 29 / 31 | - |
| January | 26 / 31 | 28 / 31 | - |
| February | 26 / 28 | 27 / 28 | 19 / 22 |
| March | 29 / 31 | 31 / 31 | 30 / 31 |
| April | 18 / 24 | 21 / 24 | 23 / 24 |

4.1.1, direct irradiances are only available from beginning February - April due to technical problems with the positioning device. In the investigation of Article D, an algorithm was applied that calculated the percentage of the direct beam and the diffuse radiance to the total human exposure (see Article D in Section 3.4). With this algorithm and clear sky simulations, it was analyzed, if the direct beam can be neglected in months with low sun elevation. Based on the exposure of a human with winter clothing in an unobstructed environment for a full day, the portion of the direct irradiance between 8 November and 1 February is less than 10 %. On 19 February, the proportion of the direct irradiance is about 16 % (full day exposure) and about 20 % (11:00-12:00 UTC exposure). Based on these results for clear sky simulations, it was assumed that the direct beam can be neglected for exposure calculations in the months November - February, where no direct irradiance measurements are available. Between 20 February and 24 April, direct irradiance measurements are almost continuously available (see Table 4.2).

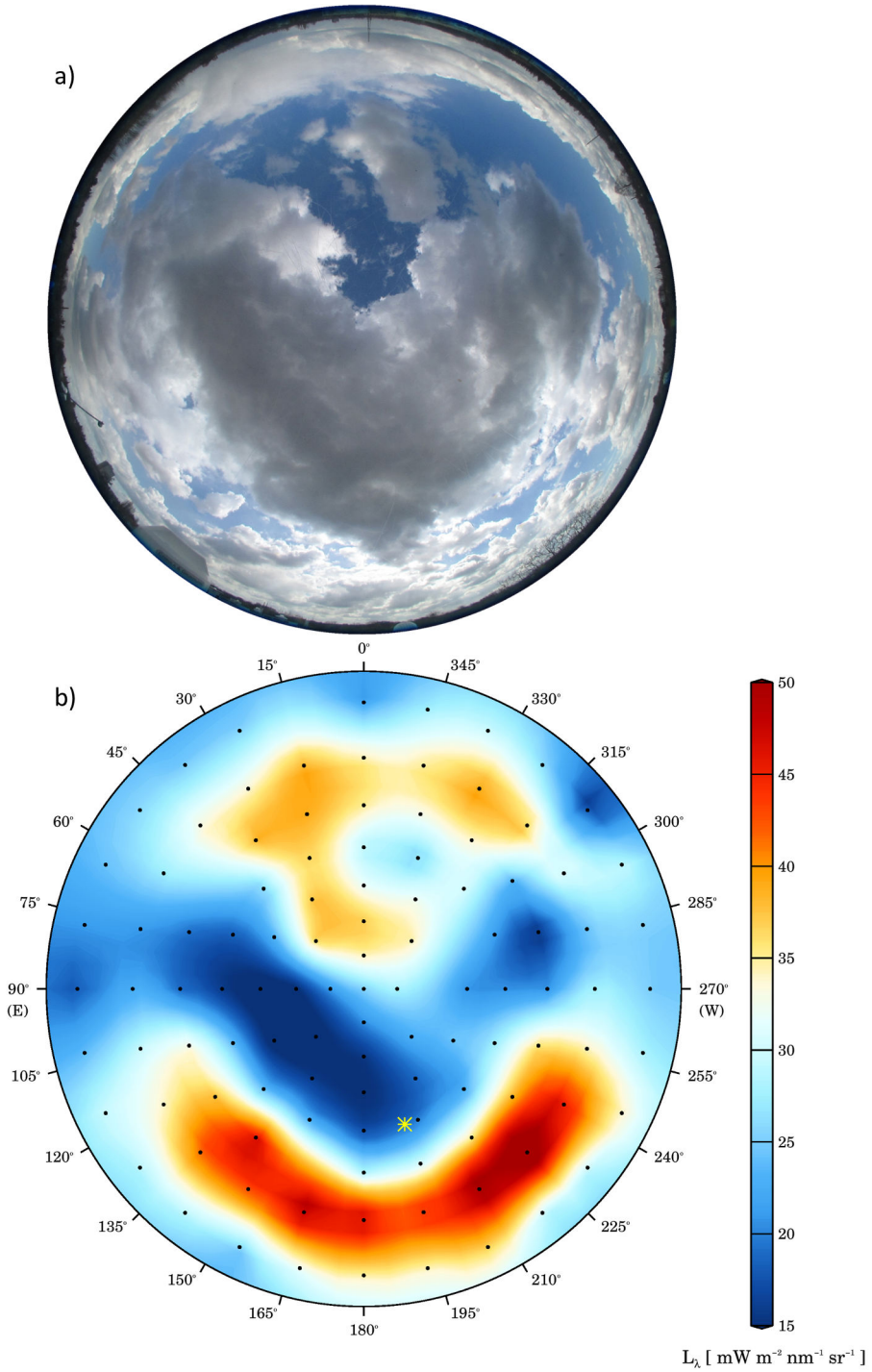


**Figure 4.8:** Hemispherical image of the sky on 4 April 2015 at 12:14 UTC (a). Spatial distribution of extended radiance at 320 nm measured with MUDIS (b). The yellow asterisk marks the position of the sun and the black dots display the measured directions.

For the calculation of vitamin $D_3$-weighted human exposure, the radiance spectra of the time periods in Table 4.2 were extended as described in Section 4.2. The direct irradiance was compared to simulations and agrees reasonably well in the visible and UVA wavelength range, however, it shows larger deviations in the UVB. Therefore, the direct irradiance measurements were also improved with the extension method described in Section 4.2, only that a direct irradiance lookup table was used. Figure 4.8 shows the measured radiance at 320 nm and the corresponding hemispherical image from 4 April 2015 at 12:14 UTC as a function of zenith and azimuth angle. At this time the sun, indicated by the yellow asterisk in the plot, is blocked by a cloud. As a result, high radiance values can be seen around the heart-shaped dark gray cloud. For the radiance measurements to be used in the exposure model, the spatial resolution of the extended radiance dataset must be interpolated to an equidistant grid with a resolution of 5° in azimuth and zenith direction. The interpolated grid is shown in Figure 4.9.

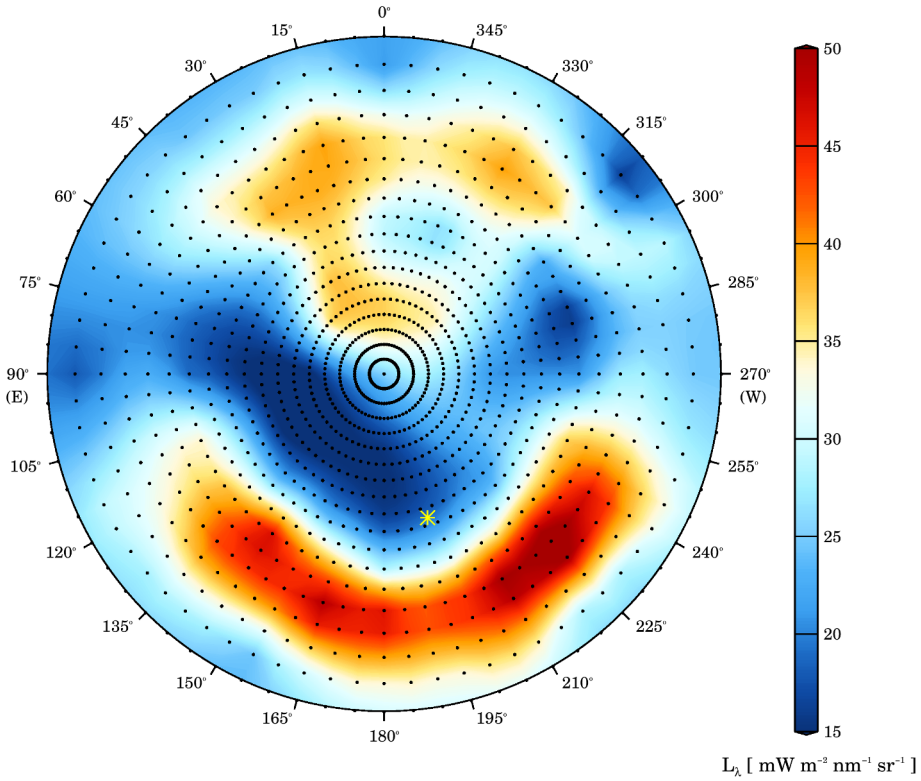


**Figure 4.9:** Spatial distribution of extended radiance at 320 nm measured with MUDIS on 4 April 2015 at 12:14 UTC. The black dots mark the interpolated equidistant grid with a 5° resolution in azimuth and zenith direction.

For the following calculations, a threshold of 1000 IU is used which is stated in Section 1.3.1 to be sufficient for a healthy vitamin D status. Two scenarios of vitamin $D_3$-weighted exposure of a human in winter clothing in an unobstructed environment were investigated: (1) calculations with an exposure time over the entire day (i.e. from sunrise to sunset) for the months November - April; and (2) calculations with an exposure time from 11:00 - 12:00 UTC for the months February - April. Although the first scenario with its long exposure time would be an unrealistic behavior, it shows the maximum of exposure that theoretically would have been possible with winter clothing during these months. The second scenario with an exposure time from 11:00 - 12:00 UTC represents the exposure during lunch break, if it would have been spent outside.

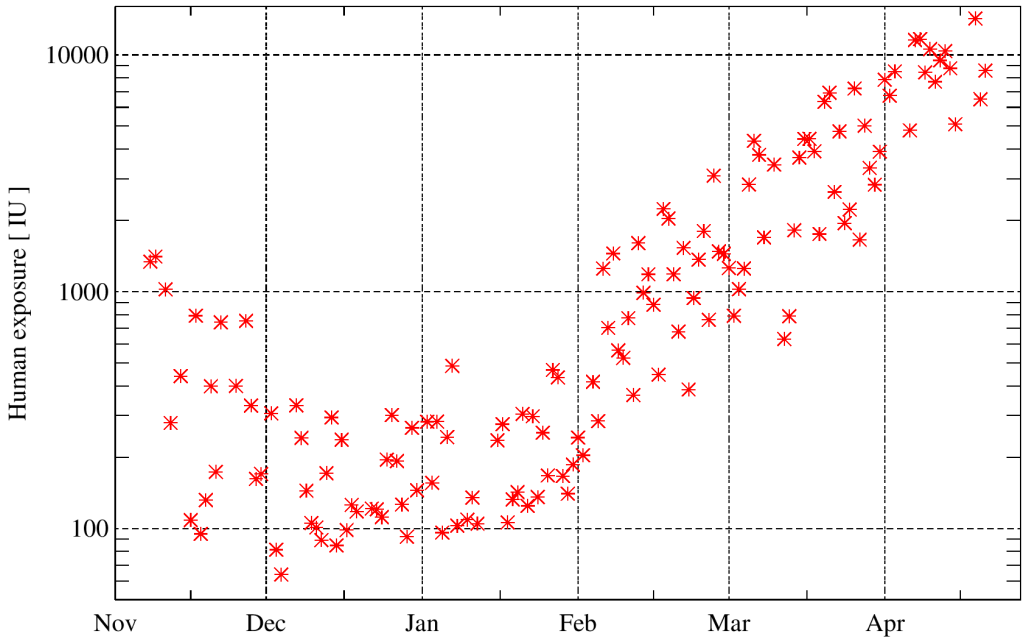


**Figure 4.10:** Exposure calculated for a human with winter clothing in an unobstructed environment for an exposure time from sunrise to sunset. The exposure was calculated for all complete measurement days from November 2014 to April 2015 and is given in international units. It should be noted that the y-axis is shown in a logarithmic scale.

In Article A, an exposure calculation for a homogeneous cloud case for a human with winter clothing on 21 December was presented. This resulted in an exposure time of 35 days to theoretically obtain 1000 IU. The calculated human exposure for an exposure time from sunrise to sunset for all days from November to April is shown in Figure 4.10. The monthly mean human exposure of December 2014 was 163 IU which would result in an exposure time of about 6 days to obtain 1000 IU. This indicates that the homogeneous cloud, presented in Article A for 21 December for Hannover, is very thick and presents an extreme case. Nevertheless, the actual human exposure calculated for all days of the 2014/2015 winter campaign confirms the statement from Section 1.3.1 that an adequate vitamin D status cannot realistically be gained by solar UV exposure in wintertime.

In Figure 4.11, the results of the human exposure calculations for the lunch break scenario are illustrated as a histogram plot. As mentioned above, they are based on measurements of the months February - April 2015 are illustrated as a histogram plot. The number of days is shown for which a certain range of calculated exposure values occurred. To further differentiate between February - April, the months are colored differently. It can be seen that for not a single day in February 2015, sufficient vitamin $D_3$ (1000 IU) could be obtained during 11:00 - 12:00 UTC if spent outside. In March and April it became possible to reach optimal vitamin $D_3$ status during lunch break, although it must be kept in mind that this investigation was done for an unobstructed environment.

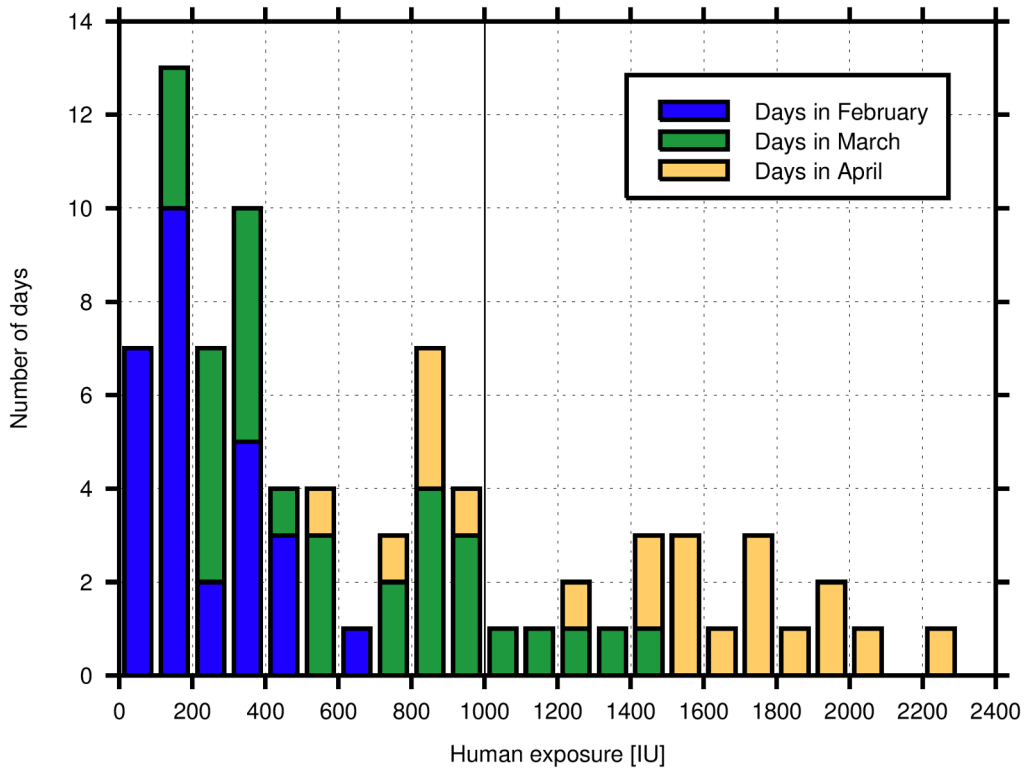


**Figure 4.11:** Histogram of human exposure calculated for a human with winter clothing in an unobstructed environment for an exposure time from 11:00-12:00 UTC. The exposure was calculated based on measurements of the months February - April 2015 and is given in IU. The number of days for which a calculated exposure value in IU is reached is plotted on the y-axis. For example, an exposure between 300 - 400 IU could have been reached on 10 days, 5 in February and 5 in March illustrated by the different colors. The vertical black line, marks the threshold of 1000 IU. It is shown that for not a single day in February 2015, a human could have obtained 1000 IU vitamin $D_3$.

# 5 Summary and conclusions

The scope of the present thesis was to further develop novel methods to calculate biologically-weighted UV exposure of humans in different environments. In contrast to earlier investigations that are based on the irradiance on surfaces, the calculations of the novel exposure model take into account the geometry of a human and the angular distribution of the radiation field. As human model a three-dimensional voxel model is used, which was segmented from data of a whole-body computed tomography scan of a patient and therefore approximately represents the geometry of an average male adult. This human model can be clothed differently, which enables for example the calculation of required exposure times to gain a healthy vitamin D status for various scenarios and seasons. Since the interaction of radiation with the human skin is highly complex and calculations are extensive, several assumptions and simplifications have been made. For example it was assumed that all skin surfaces are equal in sensitivity and can be treated as lambertian surfaces that follow the cosine of the incident angle. All assumptions made, lead to a relatively simple model that allows fast though detailed calculations.

By applying the new model on radiative transfer simulations of radiances, it could be demonstrated that it is easy in summer under cloudless skies to obtain a sufficient exposure. However, for a human with realistic winter clothing (only hands and face exposed), the statement by Webb et al. (1988) is confirmed that it is not possible to obtain sufficient exposure for vitamin $D_3$ production under a cloudless sky in most of the winter months, even if the body is exposed for the whole day. It can also be concluded that for Hannover the "vitamin D wintertime" does not cover all months between October and March. However, to assess the actual exposure of humans and to determine the exposure times necessary for a healthy vitamin D status as a function of season, time of day, location, clothing and obstructions of the environment, further parameters must be included.

Therefore, another goal of this thesis, beside the further development of the exposure model, was to extend this model to consider different environments. The advanced model was used to investigate the human exposure in specific research questions. For example it was demonstrated that upwelling radiation is a relevant factor that needs to be considered when the human exposure is investigated for surfaces with high albedo values. This is particularly important for snow-covered surfaces, which cause a significant increase in the upwelling UV radiation. The advanced model was used in an idealized investigation about skin cancer incidence in the mountainous region of the Austrian Alps. The result showed that the increase of UV exposure with altitude may help to explain the increase of melanoma incidence with altitude. In contrast, taking the irradiance as a measure for exposure would lead to the incorrect conclusions that UV radiation plays a minor role for the altitude-related melanoma incidences.

Furthermore, the model was expanded to conduct realistic exposure calculations in environments where parts of the sky are covered for example by buildings or vegetation. These obstructions reduce the incident radiation from specific directions and are therefore derived as a function of azimuth and zenith angle from hemispherical images, taken by a mobile camera system. The angular dependence of obstructions is shown by exposure calculations of two different locations with almost the same proportion of sky covered by obstructions which resulted in exposure values that are different by a factor of two. Further investigations demonstrated that the human exposure in an obstructed environment depends on the orien-

tation of the human towards the sun. In addition, it was shown by a moving human that the impact by vegetation of a recreational park is comparable to the impact by buildings. For humans with the goal of spending time outside to produce vitamin $D_3$, a recreational park may seem more attractive than an urban environment. As a consequence of the above mentioned results, not only an orientation towards the sun but also locations with as little obstructions as possible should be chosen to maximize the UV exposure and, consequently, the vitamin $D_3$-production.

So far all exposure calculations were based on radiances, simulated with a radiative transfer model for specific atmospheric conditions of different scenarios. To calculate the actual human exposure based on real atmospheric conditions, radiance measurements have been conducted with the multidirectional spectroradiometer MUDIS at a high temporal resolution in winter 2014/2015. The advantage of this instrument is that rapid spectral and spatial changes of the radiance distribution of the sky can be captured. To be used in vitamin $D_3$-weighted exposure calculations, the measured spectra need to be enhanced in the wavelength range relevant for vitamin $D_3$-production. Therefore, an extension method was developed which was successfully validated and applied on all performed radiance measurements. From the results of the validation, it can be concluded that the extension method is generally applicable for MUDIS radiance measurements. As a consequence, the improved spectra allow the determination of actual vitamin $D_3$-weighted human exposure at high temporal resolution. This is especially important when short exposure periods are investigated, which is for example the case for accumulated exposure investigations during lunch break or of a moving human. In contrast, scanning instruments would have provided, due to their longer measurement durations, only a few measurements of an averaged sky distribution. As mentioned above, the statement that it is not possible to realistically gain enough vitamin D in winter, was already confirmed by simulations. This statement was also confirmed by actual vitamin $D_3$-weighted human exposure calculations which have been derived based on the 2014/2015 winter measurements. However, exposure calculations based on measurements from February - April 2015 revealed that March is the first month with days, where a sufficient vitamin $D_3$ status could be obtained by a human who exposes face and hands between 11:00 - 12:00 UTC in an unobstructed environment. Thus it would be reasonable starting to spend more time outside around end of winter (e.g. walk to the cafeteria) in order to noticeably increase one's own vitamin $D_3$ status.

Despite some assumptions and simplifications made, the developed exposure model enabled detailed investigations of biologically-weighted UV exposure of a human in different environments. Its findings contribute to an improved understanding of vitamin D and erythemally-weighted UV exposure and provide new research possibilities for specific and everyday human exposure situations.

# 6 Outlook

Although the developed exposure model already enables the calculation of biologically-weighted human UV exposure for any location and realistic atmospheric conditions at a high level of detail, several further developments of the exposure model are feasible in order to increase the accuracy and the area of application. The following advancements of the model and research topics should be addressed in the future:

- **Weighting of single area elements:** To calculate for example the time for a sunburn on a specific body part, the erythemally-weighted incident radiation on a specific area element must be calculated. Therefore, the projection areas currently applied in the exposure model cannot be used, since they represent crossections of the entire human. Instead, the erythemally-weighted incident radiation on small polygon-surfaces of the human model, which represent small skin elements, could be calculated. These polygon-surfaces already exist in the exposure model and are calculated in the derivation process of the projection areas. Therefore, the model must be extended to enable calculations between the incident radiances and the polygon-surfaces.
- **Skin type:** All investigations in this thesis were conducted for a human with skin type II. To consider different pigmentations of the skin, additional conversion factors for other skin types should be derived.
- **Inhomogeneous ground:** The model presented in this thesis is able to consider upwelling radiation in the exposure calculation of a human. However, the ground is assumed to be a homogeneous Lambertian surface. To consider an inhomogeneous ground with different surface albedo values (e.g. at the beach with water and sand surfaces around the human), the derivation of the upwelling radiance must be modified.
- **Exposure maps:** It has been shown in this thesis that for specific locations the actual human exposure can be calculated. However, for city planning purposes these selective calculations may not be able to represent certain areas of interest. Therefore, with the necessary surface data (e.g. buildings, vegetation) available, it would be feasible to calculate the exposure for specific areas in a high spatial resolution. Illustrated as exposure maps, these could identify locations with health risk or benefits.
- **Actual summer exposure:** Due to the fact, that the indoor working population may be prevented from exposing themselves to midday sun, the production of vitamin $D_3$ by outdoor exposure might be lower than often stated in literature. Therefore, realistic human exposure calculations in an urban environment with authentic working clothes and the exposure behavior of exemplary humans should be conducted. The diurnal variation of the calculated exposure may help to asses potential health risks.
- **Dosimeter:** It would be desirable to perform dosimeter measurements in an urban environment, and compare those to calculations from the exposure model. Carefully characterized and preselected dosimeters could extend the amount of data to estimate the exposure of a human in an urban environment. Such dosimeters could provide measurements of the diurnal variations of the human exposure of a number of test persons.

# Bibliography


Biesalski, H. K., Köhrle, J., and Schürmann, K.: Vitamine, Spurenelemente und Mineralstoffe, p. 820, Georg Thieme Verlag, Stuttgart, New York, doi:10.1055/b-002-13397, URL https://www.thieme-connect.de/products/ebooks/book/10.1055/b-002-13397, 2002.

Bischoff-Ferrari, H. A., Giovannucci, E., Willett, W., Dietrich, T., and Dawson-Hughes, B.: Estimation of optimal serum concentrations of 25-hydroxyvitamin D for multiple health outcomes, Am. J. Clin. Nutr., 84, 18–28, 2006.

Bodeker, G. E., Scott, J. C., Kreher, K., and McKenzie, R. L.: Global ozone trends in potential vorticity coordinates using TOMS and GOME intercompared against the Dobson network: 1978-1998, Journal of Geophysical Research: Atmospheres, 106, 23 029–23 042, doi:10.1029/2001jd900220, 2001.

Chel, V. G. M., Ooms, M. E., Popp-Snijders, C., Pavel, S., Schothorst, A. A., Meulemans, C. C. E., and Lips, P.: Ultraviolet irradiation corrects vitamin D deficiency and suppresses secondary hyperparathyroidism in the elderly., J Bone Miner Res., 13, 1238–1242, doi:10.1359/jbmr.1998.13.8.1238, 1998.

CIE: Erythema Reference Action Spectrum and Standard Erythema Dose. Technical Report CIE S007E, Report, International Commission on Illumination, 1998.

CIE: Action spectrum for the production of previtamin $D_3$ in human skin. Technical Report 174., Report, International Commission on Illumination, 2006.

CIE: S 017, ILV: International Lighting Vocabulary, 2011.

DGE: DGE (German Nutrition Society), Österreichische Gesellschaft für Ernährung, Schweizerische Gesellschaft für Ernährungsforschung, Schweizerische Vereinigung für Ernährung D-A-CH-Referenzwerte für die Nährstoffzufuhr, vol. 1. Aufl., 5. korr. Nachdruck 2013, Neuer Umschau, Neustadt an der Weinstraße, 2012.

Diffey, B. L.: Is casual exposure to summer sunlight effective at maintaining adequate vitamin D status?, Photodermatol. Photoimmunol. Photomed., 26, 172–176, 2010.

Godar, D. E., Pope, S. J., Grant, W. B., and Holick, M. F.: Solar UV doses of adult Americans and vitamin D3 production, Dermatoendocrinol., 3, 243–250, doi:10.4161/derm.3.4.15292, 2011.

Godar, D. E., Pope, S. J., Grant, W. B., and Holick, M. F.: Solar UV doses of young Americans and vitamin D3 production, Environ. Health Perspect., 120, 139, 2012.

Grant, W. B.: The role of geographical ecological studies in identifying diseases linked to UVB exposure and/or vitamin D, Dermatoendocrinol., 8, e1137400, doi:10.1080/19381980.2015.1137400, 2016a.

Grant, W. B.: Roles of Solar UVB and Vitamin D in Reducing Cancer Risk and Increasing Survival, Anticancer Res., 36, 1357–1370, URL http://ar.iiarjournals.org/content/36/3/1357.abstract, 2016b.

Häckel, H.: Meteorologie, vol. 6, UTB GmbH, 2008.

Haluza, D., Simic, S., Höltge, J., Cervinka, R., and Moshammer, H.: Connectedness to nature and public (skin) health perspectives: Results of a representative, population-based survey among Austrian residents, Int. J. Environ. Res. Public Health, 11, 1176–1191, 2014.

Holick, M. F.: Vitamin D: importance in the prevention of cancers, type 1 diabetes, heart disease, and osteoporosis, Am. J. Clin. Nutr., 79, 362–371, 2004.

Holick, M. F.: Vitamin D Deficiency, N. Engl. J. Med., 357, 266–281, doi:10.1056/NEJMra070553, 2007.

Höppe, P., Oppenrieder, A., Erianto, C., Koepke, P., Reuder, J., Seefeldner, M., and Nowak, D.: Visualization of UV exposure of the human body based on data from a scanning UV-measuring system, Int. J. Biometeorol., 49, 18–25, doi:10.1007/s00484-004-0211-9, 2004.

Juzeniene, A., Brekke, P., Dahlback, A., Andersson-Engels, S., Reichrath, J., Moan, K., Holick, M. F., Grant, W. B., and Moan, J.: Solar radiation and human health, Rep. Prog. Phys., 74, 56, 2011.

Kawanishi, T.: Evaluation of Ultraviolet Radiation Protection of a Membrane Structure Using a UC Shade Chart, Proceedings of ANZASCA2010, 2010.

Lucas, R., McMichael, T., Smith, W., and Armstrong, B.: Solar Ultraviolet Radiation: Global Burden of Disease from Solar Ultraviolet Radiation., Environmental Burden of Disease Series, No. 13, World Health Organization, Geneva, 2006.

Lucas, R. M., McMichael, A. J., Armstrong, B. K., and Smith, W. T.: Estimating the global disease burden due to ultraviolet radiation exposure, Int. J. Epidemiol., 37, 654–667, doi:10.1093/ije/dyn017, URL `http://ije.oxfordjournals.org/content/37/3/654.abstract`, 2008.

MacLaughlin, J., Anderson, R., and Holick, M.: Spectral character of sunlight modulates photosynthesis of previtamin D3 and its photoisomers in human skin, Science, 216, 1001–1003, 1982.

Mayer, B. and Kylling, A.: Technical note: The libRadtran software package for radiative transfer calculations - description and examples of use, Atmos. Chem. Phys., 5, 1855–1877, 2005.

McKenzie, R. L., Liley, J. B., and Björn, L. O.: UV Radiation: Balancing Risks and Benefits, Photochem. Photobiol., 85, 88–98, doi:10.1111/j.1751-1097.2008.00400.x, 2009.

Moukayed, M. and Grant, W. B.: Molecular Link between Vitamin D and Cancer Prevention, Nutrients, 5, 3993, doi:10.3390/nu5103993, URL `http://www.mdpi.com/2072-6643/5/10/3993`, 2013.

Moukayed, M. and Grant, W. B.: The roles of UVB and vitamin D in reducing risk of cancer incidence and mortality: A review of the epidemiology, clinical trials, and mechanisms, Rev. Endocr. Metab. Disord., 18, 167–182, doi:10.1007/s11154-017-9415-2, URL `http://dx.doi.org/10.1007/s11154-017-9415-2`, 2017.

Oppenrieder, A., Höppe, P., Koepke, P., and Reuder, J.: Long term measurements of the UV irradiance of inclined surfaces and visualization of UV exposure of the human body, Meteorol. Z., 14, 285–290, doi:10.1127/0941-2948/2005/0032, 2005.

Parisi, A. V., Kimlin, M. G., Wong, J., and Wilson, M.: Personal exposure distribution of solar erythemal ultraviolet radiation in tree shade over summer, Phys. Med. Biol., 45, 349, 2000.

Parisi, A. V., Eley, R., and Downs, N.: Determination of the usage of shade structures via a dosimetry technique, Photochem. Photobiol., 88, 1012–1015, doi:10.1111/j.1751-1097.2012.01111.x, 2012.

Petty, G.: A first course in atmospheric radiation, vol. 2, Sundog Pub., 2006.

Pissulla, D., Seckmeyer, G., Cordero, R. R., Blumthaler, M., Schallhart, B., Webb, A., Kift, R., Smedley, A., Bais, A. F., Kouremeti, N., Cede, A., Herman, J., and Kowalewskig, M.: Comparison of atmospheric spectral radiance measurements from five independently calibrated systems, Photochem Photobiol Sci, 8, 516–527, 2009.

Pope, S. J. and Godar, D. E.: Solar UV geometric conversion factors: horizontal plane to cylinder model, Photochem. Photobiol., 86, 457–466, doi:10.1111/j.1751-1097.2009.00679.x, 2010.

Rhodes, L. E., Webb, A. R., Fraser, H. I., Kift, R., Durkin, M. T., Allan, D., O'brien, S. J., Vail, A., and Berry, J. L.: Recommended Summer Sunlight Exposure Levels Can Produce Sufficient ($\geq 20ng\ ml^{-1}$) but Not the Proposed Optimal ($\geq 32ng\ ml^{-1}$) 25 (OH) D Levels at UK Latitudes, J. Invest. Dermatol., 130, 1411–1418, doi:10.1038/jid.2009.417, 2010.

Riechelmann, S.: Simultaneous measurement of spectral sky radiance: Development, characterization and validation of a non-scanning multidirectional spectroradiometer (MUDIS), PhD thesis, Leibniz Universität Hannover, Institut für Meteorologie und Klimatologie, Herrenhäuser Straße 2, 30419 Hannover, 2014.

Riechelmann, S., Schrempf, M., and Seckmeyer, G.: Simultaneous measurement of spectral sky radiance by a non-scanning multidirectional spectroradiometer (MUDIS), Meas. Sci. Technol., 24, 125 501, 2013.

Schrempf, M., Haluza, D., Simic, S., Riechelmann, S., Graw, K., and Seckmeyer, G.: Is multidirectional UV exposure responsible for increasing melanoma prevalence with altitude? A hypothesis based on calculations with a 3D-human exposure model, Int J Environ Res Public Health, 13, 961, 2016.

Schrempf, M., Thuns, N., Lange, K., and Seckmeyer, G.: Impact of Orientation on the Vitamin D Weighted Exposure of a Human in an Urban Environment, Int J Environ Res Public Health, 14, 920, URL `http://www.mdpi.com/1660-4601/14/8/920`, 2017a.

Schrempf, M., Thuns, N., Lange, K., and Seckmeyer, G.: Einfluss der Verschattung auf die Vitamin-D-gewichtete UV-Exposition eines Menschen, Akt. Dermatol., doi:10.1055/s-0043-105258, 2017b.

Seckmeyer, G., Erb, R., and Albold, A.: Transmittance of a cloud is wavelength-dependent in the UV-range, Geophys. Res. Lett., 23, 2753–2755, 1996.

Seckmeyer, G., Glandorf, M., Wichers, C., McKenzie, R., Henriques, D., Carvalho, F., Webb, A. R., Siani, A. M., Bais, A., Kjeldstad, B., Brogniez, C., Werle, P., Koskela, T., Lakkala, K., Lenoble, J., Groebner, J., Slaper, H., denOuter, P., and Feister, U.: Europe's darker atmosphere in the UV-B, Photochem. Photobiol. Sci., 7, 925–30, doi:10.1039/b804109a, URL `http://www.ncbi.nlm.nih.gov/pubmed/18688499`, 2008.

Seckmeyer, G., Bais, A., Bernhard, G., Blumthaler, M., Drüke, S., Kiedron, P., Lantz, K., McKenzie, R. L., and Riechelmann, S.: Instruments to Measure Solar Ultraviolet Radiation, Part 4: Array Spectroradiometers, Report, World Meteorological Organization, 2010.

Seckmeyer, G., A.Zittermann, McKenzie, R., and Greinert, R.: Solar Radiation: 13. Solar radiation and human Health, pp. 9649–9672, Springer, 2012.

Seckmeyer, G., Schrempf, M., Wieczorek, A., Riechelmann, S., Graw, K., Seckmeyer, S., and Zankl, M.: A Novel Method to Calculate Solar UV Exposure Relevant to Vitamin D Production in Humans, Photochem. Photobiol., 89, 974–983, 2013.

Tohsing, K., Schrempf, M., Riechelmann, S., Schilke, H., and Seckmeyer, G.: Measuring high-resolution sky luminance distributions with a CCD camera, Appl. Opt., 52, 1564–1573, 2013.

Tohsing, K., Schrempf, M., Riechelmann, S., and Seckmeyer, G.: Validation of spectral sky radiance derived from all-sky camera images - a case study, Atmos Meas Tech, 7, 2137–2146, doi:10.5194/amt-7-2137-2014, 2014.

Valentin, J.: Basic anatomical and physiological data for use in radiological protection: reference values: ICRP Publication 89, Annals of the ICRP, 32, 1–277, doi:10.1016/S0146-6453(03)00002-2, 2002.

Vernez, D., Milon, A., Francioli, L., Bulliard, J., Vuilleumier, L., and Moccozet, L.: A numeric model to simulate solar individual ultraviolet exposure, Photochem. Photobiol., 87, 721–728, doi:10.1111/j.1751-1097.2011.00895.x, 2011.

Vernez, D., Milon, A., Vuilleumier, L., and Bulliard, J.: Anatomical exposure patterns of skin to sunlight: relative contributions of direct, diffuse and reflected ultraviolet radiation, Br. J. Dermatol., 167, 383–390, doi:10.1111/j.1365-2133.2012.10898.x, 2012.

Vieth, R., Bischoff-Ferrari, H., Boucher, B. J., Dawson-Hughes, B., Garland, C. F., Heaney, R. P., Holick, M. F., Hollis, B. W., Lamberg-Allardt, C., McGrath, J. J., Norman, A. W., Scragg, R., Whiting, S. J., Willett, W. C., and Zittermann, A.: The urgent need to recommend an intake of vitamin D that is effective, Am. J. Clin. Nutr., 85, 649–650, 2007.

Wabitsch, M., Koletzko, B., and Moß, A.: Vitamin-D-Versorgung im Säuglings-, Kindes- und Jugendalter, Monatsschr. Kinderheilkd., 159, 766–774, 2011.

Webb, A. R. and Engelsen, O.: Calculated ultraviolet exposure levels for a healthy vitamin D status, Photochem. Photobiol., 82, 1697–1703, doi:10.1562/2006-09-01-RA-670, 2006.

Webb, A. R., Kline, L., and Holick, M. F.: Influence of season and latitude on the cutaneous synthesis of vitamin D3: Exposure to winter sunlight in Boston and Edmonton will not promote vitamin D3 synthesis in human skin, J. Clin. Endocrinol. Metab., 67, 373–378, doi:10.1210/jcem-67-2-373, 1988.

Webb, A. R., Kift, R., Durkin, M. T., O'Brien, S. J., Vail, A., Berry, J. L., and Rhodes, L. E.: The role of sunlight exposure in determining the vitamin D status of the U.K. white adult population, Br. J. Dermatol., pp. 1050–1055, 2010.

Webb, A. R., Kift, R., Berry, J. L., and Rhodes, L. E.: The vitamin D debate: translating controlled experiments into reality for human sun exposure times, Photochem. Photobiol., 87, 741–745, doi:10.1111/j.1751-1097.2011.00898.x, 2011.

Weltner, K., Wiesner, H., Heinrich, P., Engelhardt, P., and Schmidt, H.: Mathematik für Physiker 2: Basiswissen für das Grundstudium der Experimentalphysik, vol. 15, Springer Berlin Heidelberg, 2008.

WHO: World Health Organization, International Agency for Research on Cancer. Vitamin D and cancer. IARC Working Group Reports, WHO Press, 5, 148, 2008.

WMO: Part I. Measurement of Meteorological Variables, Guide to Meteorological Instruments and Methods of Observation, Geneva, 7 edn., 2008.

Wolpowitz, D. and Gilchrest, B. A.: The vitamin D questions: how much do you need and how should you get it?, J. Am. Acad. Dermatol., 54, 301–317, 2006a.

Wolpowitz, D. and Gilchrest, B. A.: Clarifying the vitamin D controversy: the health benefits of supplementation by diet versus sunshine, vol. 1, pp. 81–102, Springer, Berlin Heidelberg, doi:10.1007/3-540-32953-6, 2006b.

Wuttke, S., Seckmeyer, G., Bernhard, G., Ehramjian, J., McKenzie, R., Johnston, P., and O'Neill, M.: New Spectroradiometers Complying with the NDSC Standards, J Atmos Ocean Technol, 23, 241–251, doi:10.1175/JTECH1826.1, URL http://journals.ametsoc.org/doi/abs/10.1175/JTECH1826.1, 2006.

Zeeb, H. and Greinert, R.: Übersichtsarbeit: Bedeutung von Vitamin D in der Krebsprävention: Konflikt zwischen UV-Schutz und Anhebung niedriger Vitamin-D-Spiegel?, Deutsches Ärzteblatt-Ärztliche Mitteilungen-Ausgabe B, 107, 638–647, 2010.

Zittermann, A.: The estimated benefits of vitamin D for Germany, Mol. Nutr. Food Res., pp. 1164 – 1171, 2010.

# Acknowledgments

I would like to thank all persons who contributed to the success of this work and who supported me during the last years. Particularly, I would like to acknowledge:

- My advisor Prof. Dr. Gunther Seckmeyer for his guidance through the progress of this thesis, for many fruitful discussions about scientific and other questions and continuous support and advice in manifold ways. I further received the chance to travel abroad, participating in an exciting campaign in the Chilean Andes and getting into contact with scientists all over the world.
- Prof. Dr. Günter Groß and Prof. Dr. Armin Zitterman who acted as the co-reviewers of this PhD thesis.
- My former and current colleagues I've worked with at the IMuK, especially Angelika Niedzwiedz, Nadine Thuns, Kezia Lange and Holger Schilke.
- legen...wait for it...dary Dr. Stefan Riechelmann for being a great friend, former colleague and short time roommate :-), helping me out on countless occasions in the labs, on the roof and in the field. Thanks for all the fruitful discussions.
- Uli Meyer and Dr. Notker Fechner who have been essential for so many special projects and tasks. Berit Parbel, Petra Kraege, Christiane Brünig for all their great support in bureaucratic matters. The many enjoyable chats with all of you will certainly be remembered.
- Special thanks to Dr. Linda Voß, Dr. Stefan Riechelmann, Dr. Farah Kanani-Sühring, Angelika Niedzwiedz, Nadine Thuns and Kezia Lange for proofreading (parts) of this thesis.
- My friends Dr. Farah Kanani-Sühring, Dr. Matthias Sühring, Jens Fricke and Viola Weniger, and my friends from all over the place for an awesome time.
- My family supporting me in all aspects of my life.
- The biggest Thank You to Linda who gave continuous motivation and support, especially in the last weeks before printing. Even the times when I was down, you always managed to cheer me up!

This PhD project was partly funded by the climate and energy fund within the Austrian climate research program under grant K10AC0K00056, by the German Federal Ministry of Education and Research (BMBF) research project IREPS under grant 01DN13059 and by the BMBF research project MOSAIK under grant 01LP1601A within the framework of Research for Sustainable Development.

# Curriculum Vitae

| | | |
|---|---|---|
| **Personal Details** | Family Name | Schrempf |
| | First Name | Michael |
| | Date of birth | 04 May 1983 |
| | Place of birth | Nürtingen, Germany |
| | Nationality | German |
| **Academic Career** | Since 09/2011 | **Research associate** at the Institute of Meteorology and Climatology, Leibniz Universität Hannover, Germany |
| | 10/2008 - 06/2011 | **Research assistant** at the Max Planck Institute for Gravitational Physics (Albert Einstein Institute), Hannover, Germany and<br>**Research assistant** at diverse institutes of the Leibniz Universität Hannover, Germany:<br>- Institute of Meteorology and Climatology<br>- Institute of Quantum Optics<br>- Institute for Solid State Physics |
| **Scientific Campaigns** | 07/2015 | Participation at the **Black Carbon Campaign 2015** in the Chilean Andes, within the framework of the IREPS project |
| | 07/2014 | Organization of and participation at an international **NDACC intercomparison** campaign at the Institute of Meteorology and Climatology, Leibniz Universität Hannover, Germany, within the framework of the IREPS project |

| | | |
|---|---|---|
| **University Education** | 08/2011 | **German "Diplom" in meteorology**. Final grade: magna cum laude (1.4). Diploma thesis on "Entwicklung eines Algorithmus zur Wolkenerkennung in Digitalbildern des Himmels". |
| | 04/2009 - 03/2010 | **Student representative**, at the Institute of Meteorology and Climatology, Leibniz Universität Hannover, Germany. |
| | 10/2005 - 08/2011 | **Studies in meteorology**, Leibniz Universität Hannover, Germany. |
| | 10/2003 - 09/2005 | **Studies in mechanical engineering**, Technische Universität Braunschweig, Germany. |

**Publications**

**Riechelmann, S., Schrempf, M., and Seckmeyer, G.:** Simultaneous measurement of spectral sky radiance by a non-scanning multidirectional spectroradiometer (MUDIS), Meas. Sci. Technol., 24, 125501, 2013.

**Schrempf, M., Haluza, D., Simic, S., Riechelmann, S., Graw, K., and Seckmeyer, G.:** Is multidirectional UV exposure responsible for increasing melanoma prevalence with altitude? A hypothesis based on calculations with a 3D-human exposure model, Int J Environ Res Public Health, 13, 961, 2016.

**Schrempf, M., Thuns, N., Lange, K., and Seckmeyer, G.:** Impact of Orientation on the Vitamin D Weighted Exposure of a Human in an Urban Environment, Int J Environ Res Public Health, 14, 920, 2017a.

**Schrempf, M., Thuns, N., Lange, K., and Seckmeyer, G.:** Einfluss der Verschattung auf die Vitamin-D-gewichtete UV-Exposition eines Menschen, Akt Dermatol, 10.1055/s-0043-105258, 2017b.

**Seckmeyer, G., Schrempf, M., Wieczorek, A., Riechelmann, S., Graw, K., Seckmeyer, S., and Zankl, M.:** A Novel Method to Calculate Solar UV Exposure Relevant to Vitamin D Production in Humans, Photochem. Photobiol., 89, 974-983, DOI: 10.1111/php.12074, 2013.

**Seckmeyer, G., Schrempf, M., Stührmann, A., and Niedzwiedz, A.:** Solar Simulators for Healthy Vitamin D Synthesis, Anticancer Res., 36, 1423-1428, 2016.

**Seckmeyer, G., Mustert, C., Schrempf, M., Richard L. McKenzie, R. L., Liley, J. B., Kotkamp, M., Bais, A. F., Gillotay, D., Slaper, H., Siani, A.M., Smedley, A. R.D., Webb, A.:** Why is it so hard to gain enough Vitamin D by solar exposure in the European winter?, submitted to Meteorol. Z., in review.

**Tohsing, K., Schrempf, M., Riechelmann, S., Schilke, H., and Seckmeyer, G.:** Measuring high-resolution sky luminance distributions with a CCD camera, Appl. Opt., 52, 1564-1573, 2013.

**Tohsing, K., Schrempf, M., Riechelmann, S., and Seckmeyer, G.:** Validation of spectral sky radiance derived from all-sky camera images-a case study, Atmos Meas Tech, 7, 2137-2146, 10.5194/amt-7-2137-2014, 2014.

**Werkmeister, A., Lockhoff, M., Schrempf, M., Tohsing, K., Liley, B., and Seckmeyer, G.:** Comparing satellite-to ground-based automated and manual cloud coverage observations-a case study, Atmos Meas Tech, 8, 2001-2015, 10.5194/amt-8-2001-2015, 2015.

**Conference Contributions**

**Seckmeyer, G., Schrempf, M., Lange, K., Thuns, N.:** Shading and Vitamin D-Weighted Exposure, Joint International Symposium Vitamin D in Prevention and Therapy and Biologic Effects of Light, Homburg, Germany, 2017.

**Seckmeyer, G., Schrempf, M.:** Is the UV index suitable for determining the vitamin D weigthed exposure? Third International Conference on UV and Skin Cancer Prevention, Melbourne, Australia, 2015.

**Seckmeyer, G., Riechelmann, S., Schrempf, M., Stührmann, A., Niedzwiedz, A:** Solar simulators for a healthy Vitamin D synthethis, International Symposium Biologic Effects of Light, Homburg, Germany, 2015.

**Schrempf, M., Riechelmann, S., Wieczorek, A., Graw, H., Seckmeyer, G.:** Neue Methode zur Berechnung der Vitamin-D gewichteten UV-Exposition. 8. Biomet-Tagung, Dresden, Germany, 2014.

**Schrempf, M., Tohsing, K., Riechelmann, S., Schilke, H., Seckmeyer, G.:** Hochauflösende Bestimmung der hemisphärischen Leuchtdichte mit einer CCD Kamera. Poster, DACH, Innsbruck, Austria, 2013.

**Riechelmann, S., Schrempf, M., Seckmeyer, G.:** Spektrale Strahldichtemessungen: Einfluss des Oeffnungswinkels verwendeter Eingangsoptiken auf das Messergebnis. DACH, Innsbruck, Austria, 2013.

**Seckmeyer, G., Riechelmann, S., Schrempf, M., Tohsing, K., Klingebiel, M., McKenzie, R., Liley, B., Allen, M., Casale, G., Siani, A.-M.:** Requirements for the UV dosimetry of humans. International Radiation Symposium, Berlin, Germany, 2012.